

# GEOLOGY OF THE CALHOUN CRITICAL ZONE OBSERVATORY

by

BARRETT JORDAN

(Under the Direction of Paul Schroeder)

## ABSTRACT

The Calhoun Critical Zone Observatory (CCZO) is an interdisciplinary field site, located in Union, South Carolina that examines Critical Zone response to human interaction and the role the underlying bedrock has on Critical Zone structure. Currently, no detailed work has been done to map the bedrock or structural geology in the area. In order to advance this understanding, the present study used geologic mapping, petrography, X-ray Diffraction, and geochemical analysis to characterize the lithologies present at the CCZO. The field site was interpreted to contain a portion of the Central Piedmont Suture which bounds the Cat Square and Charlotte terranes present at the field site. The new interpretation of the Central Piedmont Suture lies farther west than previously described and provides new territory to investigate the history of the Appalachian orogeny.

INDEX WORDS: Calhoun Critical Zone Observatory, Geology, Mapping, Geochemistry, Central Piedmont Suture, Southern Piedmont, Cat Square terrane, Charlotte terrane, Appalachian orogeny, Union County, South Carolina

GEOLOGY OF THE CALHOUN CRITICAL ZONE OBSERVATORY

by

BARRETT JORDAN

BS, University of Georgia, 2018

A Thesis Submitted to the Graduate Faculty of The University of Georgia in Partial Fulfillment  
of the Requirements for the Degree

MASTER OF SCIENCE

ATHENS, GEORGIA

2020

© 2020

Barrett Jordan

All Rights Reserved

# GEOLOGY OF THE CAHOUN CRITICAL ZONE OBSERVATORY

by

BARRETT JORDAN

|                  |                    |
|------------------|--------------------|
| Major Professor: | Paul Schroeder     |
| Committee:       | Christian Klimczak |
|                  | Michael Roden      |

Electronic Version Approved:

Ron Walcott  
Interim Dean of the Graduate School  
The University of Georgia  
May 2020



## ACKNOWLEDGEMENTS

Thank you all to all the faculty in the University of Georgia: Department of Geology. This work is the result of countless hours in your offices and classrooms, and I appreciate the support I have received in excess within the department. In particular, I would like to thank my committee members Dr. Paul Schroeder, Dr. Mike Roden, and Dr. Christian Klimczak for their patience and guidance. To my family, thank you for your guidance and encouragement. And finally, this work would not have been complete without the hard work of my fearless field assistant Yogi.

## TABLE OF CONTENTS

|                                         | Page |
|-----------------------------------------|------|
| ACKNOWLEDGEMENTS .....                  | iv   |
| LIST OF TABLES .....                    | vii  |
| LIST OF FIGURES .....                   | viii |
| CHAPTER                                 |      |
| 1 INTRODUCTION .....                    | 1    |
| Calhoun Critical Zone Observatory ..... | 1    |
| Mapping in South Carolina .....         | 2    |
| Geography .....                         | 3    |
| Geologic History of the CCZO .....      | 3    |
| Cat Square Terrane .....                | 4    |
| Charlotte Terrane .....                 | 6    |
| The Central Piedmont Suture .....       | 7    |
| Hypothesis .....                        | 7    |
| 2 METHODS .....                         | 12   |
| Geologic Mapping .....                  | 12   |
| Petrology .....                         | 13   |
| Geochemistry .....                      | 14   |
| 3 RESULTS .....                         | 16   |
| Mapping Results .....                   | 16   |

|                                                      |    |
|------------------------------------------------------|----|
| Unit Descriptions .....                              | 16 |
| Granite Geochemistry .....                           | 23 |
| Tectonic Setting .....                               | 26 |
| 4 DISCUSSION .....                                   | 44 |
| Assignment and Interpretation of Terranes.....       | 44 |
| Interpretation of the Central Piedmont Suture .....  | 45 |
| Petrographic Interpretations.....                    | 46 |
| Structural Interpretations .....                     | 46 |
| Rare Earth Elements in CCZO Granites .....           | 47 |
| Lithologic Implications on Future CCZO Studies ..... | 47 |
| 5 SUMMARY .....                                      | 49 |
| REFERENCES .....                                     | 51 |
| APPENDICES                                           |    |
| A GEOLGOIC MAP .....                                 | 58 |
| B X-RAY DIFFRACTION DATA .....                       | 60 |
| C GEOCHEMICAL DATA .....                             | 65 |
| D STRUCTURAL MEASUREMENTS.....                       | 72 |
| E FIELD GUIDE.....                                   | 77 |
| F SAPMLE LOCATIONS .....                             | 80 |
| G ACT LABS RESUTLS .....                             | 83 |

## LIST OF TABLES

|                                    | Page |
|------------------------------------|------|
| Table 1: Granite Geochemistry..... | 38   |

## LIST OF FIGURES

|                                                                              | Page |
|------------------------------------------------------------------------------|------|
| Figure 1: Geologic Map Coverage in South Carolina .....                      | 8    |
| Figure 2: Regional Geology of the CCZO.....                                  | 9    |
| Figure 3: Geography of the CCZO .....                                        | 10   |
| Figure 4: Cross-section of CCZO Hills .....                                  | 10   |
| Figure 5: Paleogeography .....                                               | 11   |
| Figure 6: Field Picture of a Dike.....                                       | 28   |
| Figure 7: Biotite-Hornblende-Quartz Meta-Diorite (bhqd) .....                | 29   |
| Figure 8: Meta-Tonalite (tn) .....                                           | 30   |
| Figure 9: Meta-Tonalite in Thin Section .....                                | 31   |
| Figure 10: Biotite Meta-Granodiorite (bgd) .....                             | 32   |
| Figure 11: Biotite Meta-Granodiorite in Thin Section .....                   | 33   |
| Figure 12: Biotite Gneiss/Amphibolite (bgn) .....                            | 34   |
| Figure 13: Biotite Gneiss/Amphibolite in Thin Section .....                  | 35   |
| Figure 14: Meta-Granite (gr) .....                                           | 36   |
| Figure 15: Meta-Granite in Thin Section.....                                 | 37   |
| Figure 16: Harker Diagrams .....                                             | 39   |
| Figure 17: REE Element Geochemistry.....                                     | 40   |
| Figure 18: Upper Continental Crust Normalized REE Element Geochemistry ..... | 41   |
| Figure 19: Granite Tectonic Discrimination .....                             | 42   |

|                                           |    |
|-------------------------------------------|----|
| Figure 20: Petrogenetic Environment ..... | 43 |
| Figure 21: Terrane Boundaries .....       | 49 |

## CHAPTER 1

### INTRODUCTION

#### *1.1 Calhoun Critical Zone Observatory*

The Calhoun Critical Zone Observatory, located in Union, SC, is one of nine in a national network of interdisciplinary field sites organized under the direction of the U.S. National Science Foundation since 2013 (Fig. 1). These Critical Zone Observatories examine the structure, fluxes, and responses of components in the terrestrial sphere that reaches from the upper portion of the crust to the treetops, all of which are influenced by meteoric water (Banwart, 2012). Since the inception of this concept, it has been noted the coevolution of the Critical Zone occurs with humans with Banwart (2012) stating that “growth in human population and demand for wealth creates ever-increasing pressure on global soils, leading to soil losses and degradation worldwide. Critical Zone science studies the impact linkages between these pressures, the resulting environmental state of soils, and potential interventions to protect soil and reverse degradation.”

To further examine Critical Zone response to human activity, the CCZO was selected as a field site due to its unique land use history. The CCZO experienced heavy anthropogenic landscape change during the 20<sup>th</sup> century that led to massive erosion due to poor farming practices and subsequent recolonization of forest communities (Coughlan et al., 2017). This recent perturbation allowed for an ideal outdoor experimental area to tease apart factors of land use, geomorphology, climate, and underlying geologic variability into Critical Zone studies.

Many published studies out of the CCZO have sought to examine the changes in Critical Zone processes in these highly weathered soils by comparing sites that have different land use histories, hillslope positions, and watershed scales (e.g., Billings et al., 2018; Hodges et al., 2019; Wade et al., 2020). These studies were unable to consider the effects differing bedrock lithologies might have had on their results because the CCZO has not had a detailed geologic map prepared (Fig.1).

In addition to examining the relationship between humans and the Critical Zone, the CCZO was also directed to look at how changes in bedrock lithology affect Critical Zone development (Dietrich and Lohse, 2014). Despite this directive, no detailed work had been done to map the bedrock lithologies in the area, which was the motivation for the present study. The production of a geologic map would provide greater control on experimentation and more importantly, provide key insight to potential relationships between the Critical Zone structure and the surrounding bedrock lithologies.

### *1.2 Mapping in South Carolina*

Lack of a detailed geologic map was not only a concern at the CCZO, but also a concern for many quadrangles in South Carolina. At the present time, a significant part of South Carolina remained unmapped at the quadrangle scale (Fig. 1). To the west of the CCZO, one map named the Philson Crossroads quadrangle was produced by Horkowitz (1984). This map showed two distinct geologic terranes, or structurally bound allochthonous groups of rocks that share a distinct history from surrounding rocks (Howell, 1995). These two groups are the Cat Square terrane and the Charlotte terrane (Fig. 2).

Charlotte terrane lithologies mapped in Philson Crossroads had been used by multiple studies to examine the nature of volcanism in the peri-Gondwanan island Carolina which will be



detailed more in later sections (e.g. Dennis and Wright, 1997; Dennis and Shervais, 1991; West, 1998). The production of more detailed geologic maps in the surrounding area would not only aid in providing new areas to research the geologic history of the region, but it would also benefit the CCZO's goal to further understand interactions between the bedrock and the Critical Zone.

### *1.3 Geography*

The CCZO lies in the western portion of Sumter National Forest in Union, South Carolina (Fig. 3). This portion of South Carolina is a part of the Piedmont physiographic province defined by gently rolling hills on highly weathered saprolitic Ultisols that reached depths up to 100 ft (Fig. 4; Thornbury, 1965). At the field site, fluvial systems showed dendritic patterns often originating from highly developed gullies and interfluves (Richter et al., 2014). Floodplains in the area were well developed occurring adjacent to higher order streams. Interfluves displayed the highest degree of weathering and saprolitization while fluvial channels frequently revealed bedrock mirroring their transport-limited and weathering-limited local environments respectively (St. Clair et al., 2015).

### *1.4 Geologic History of the CCZO*

The geologic history of the CCZO spans across a billion years of Earth history and involved the formation and break up of two separate super-continents, Rodinia and Pangea (Hatcher et al., 2010). During the formation of Rodinia, the Grenvillian orogeny occurred from 1.3–1.0 Ga along proto-Laurentia's margin. This mountain belt (although at much different paleolatitudes) followed a similar strike to the present-day Appalachians (Thomas, 2006). Subsequent rifting of Rodinia in the Neoproterozoic developed the Iapetus Ocean basin in between Laurentia and Gondwana around 565 Ma (Merschat, 2009). This ocean basin accumulated mixed sediments from both Laurentia and Gondwana (as evidenced through zircon

geochronology) and would serve as the protolith for the Cat Square terrane (Huebner et al., 2018).

Along the Gondwanan margin, the newly formed oceanic crust was subducted under the continent forming a volcanic island arc around the Neoproterozoic–Paleozoic boundary. Here, the island Carolina developed with major eruptive events at 633 Ma and 528 Ma (Fig. 5; Wortman et al., 2000). The middle Paleozoic marked the closure of the Iapetus Ocean leading to the collision between Carolina and Laurentia in the late Ordovician (Pollock et al., 2011). Gondwana thrust over Laurentia zippering from north to south with some dextral strike slip component through the late Paleozoic forming the Appalachian Mountains (Secor et al., 1986; Hatcher, 2010). The extensive thrusting formed nappes along the Laurentian border emplacing several exotic terranes sutured onto Laurentia (Fig. 5; Griffin, 1972; Williams and Hatcher, 1983).

By the end of the Mesozoic, the collisional tectonics ended and extension would cause Pangea to rift apart to the Tethys Ocean around 200–183 Ma which would later develop to the Atlantic Ocean (Frizon de Lamotte, 2015; Hibbard, 2002). This extension left behind several joint sets, still observable in the field today (Mersch, 2005). In recent history, intensive weathering exposed the high pressure and high temperature metamorphic rocks from the interior of the Appalachian Mountains.

### *1.5 Cat Square Terrane*

The Cat Square Terrane was formed from the accretion of the Iapetus Ocean basin during the late Silurian and Devonian (Hatcher and Mersch, 2006). Sediments collected in the ocean basin share a complex history with the surrounding environments. The oldest detrital zircons in the Cat Square were dated using U/Pb to the Grenvillian orogeny sharing both Laurentian and

Gondwanan affinity (Huebner et al., 2018). A younger pulse of zircons was observed from the Ordovician-Silurian which serves as the maximum age of the Cat Square terrane (Huebner et al., 2018). If the rocks were older than the Ordovician-Silurian, they would not have been able to incorporate these detrital zircons.

These volcanogenic and weathered sediments were thrust and buried onto the Laurentian margin undergoing high grade metamorphism during the orogeny. This resulted in the formation of a sequence of metasedimentary rocks including paragneiss, amphibolites, pelitic schists, calc-silicates, and orthogneisses intruded by anatectic peraluminous granitoids during the Silurian-Devonian (Mersch and Hatcher, 2007). Gneisses were described as the most abundant unit appearing as a metagraywacke with a “K-feldspar plagioclase-biotite-quartz” composition having “abundant quartzofeldspathic leucosome(s)” (Huebner, 2018). Granites in the Cat Square terrane have been described as medium-grey slightly foliated rocks with K-feldspar, quartz, biotite and minor muscovite mineral assemblages (Griffitts and Overstreet, 1952).

These rocks generally form lenticular structures that follow the strike of the Appalachian (and Grenvillian) Mountains which is perpendicular to the vergence of Gondwana (Fig. 2; Griffitts and Overstreet, 1952; Secor et al., 1986a). The overall structural fabric of the Cat Square terrane is NE trending with gently dipping sillimanite-grade migmatitic rocks that were deformed into recumbent nappes (Hatcher, 2006). Two major fault systems bound the Cat Square terrane (Fig. 2). To the north, the Cat Square meets the Tugaloo terrane at the Brindle Creek Fault, and to the south, the Cat Square meets the Charlotte Terrane at the Central Piedmont Suture (Mersch et al., 2005). Rocks of the Cat Square terrane were crosscut by NE trending silicified breccias related to faulting during the Mesozoic opening of the Atlantic Ocean (Secor et al., 1986).

### *1.6 Charlotte Terrane*

The Charlotte terrane was formed from the accretion of Carolina onto the Laurentian margin. Initially, the mafic volcanic protolith that would become the Charlotte terrane was erupted off the coast of Gondwana in an island arc setting where oceanic crust from the Iapetus Ocean was subducted under Gondwanan crust (Pollock et al., 2011). The subduction zone led to the formation of two major arc systems, the Hyco magmatic arc, ~633–612 Ma, and the Albemarle arc, 555–528 Ma which are separated by the volcanoclastic Virgilina sequence (Hibbard et al., 2007). Rifting separated Carolina from Gondwana around ~545 Ma to form the Rheic ocean and began the convergence of Carolina and Laurentia (Hibbard et al., 2013). Although not precisely dated, Carolina is thought to have converged with Laurentia in the Devonian producing several plutons in the process (Pollock et al., 2011). In the southern portion of Laurentia, Gondwana would converge during the Alleghanian orogeny between ~315–268 Ma exposing Carolina to high pressures and temperatures (Dallmeyer et al., 1986).

These metamorphic conditions altered the mafic volcanic rocks of Carolina into those seen in the Charlotte terrane today. Locally, this terrane was described to contain rocks including meta-diorite, meta-gabbro, hornblende-gabbros, and meta-clinopyroxenites that typically formed zoned complexes ~10 km in diameter. The weakly foliated meta-diorites make up the majority of the rocks in the terrane while the meta-gabbros and meta-clinopyroxenites are subordinate (Dennis and Shervais, 1996). These meta-plutonic rocks are a slight departure from other rocks in the Carolina superterrane, of which the Charlotte terrane is a part. Other parts of the Carolina superterrane were described as containing more metamorphosed volcanic ash which produced expansive slate belts in the Carolinas (Griffin, 1974).

The structural fabric is slightly different between the Cat Square terrane and Charlotte terrane. The Charlotte terrane trends slightly more north and has a steeper dip than the Cat Square terrane (West, 1998). However, the Charlotte terrane rocks still reside in a nappe tectonic regime and display recumbent folds with some reclined folding (Griffin, 1972). Rocks of the Charlotte terrane were also crosscut by NE trending silicified breccias related to faulting during the Mesozoic opening of the Atlantic Ocean (Secor et al., 1986).

### *1.7 The Central Piedmont Suture*

The Central Piedmont Suture lies along the interface between the Cat Square and Charlotte terranes extending from Georgia through the Carolinas (Fig. 2; Huebner, 2017). Historically, the suture had been interpreted as both a low angle normal fault and a thrust fault but has been more commonly referred to as a thrust fault system (Dennis, 1991; West, 1998). The Central Piedmont Suture has a dextral component as well (Mersch, 2009). In South Carolina, the fault has been readily identified through a sharp lithologic contact between the mafics of the Carolina superterrane abutted next to the felsic gneisses of the Cat Square terrane (Horkowitz, 1984).

### *1.8 Hypothesis*

From background research on the Appalachian orogeny, the present study sought to confirm that the CCZO would display both the Cat Square terrane as well as the Charlotte terrane joined by the Central Piedmont Suture. Additionally, it hoped to find evidence of thrust tectonics with the Charlotte terrane overriding the Cat Square terrane.

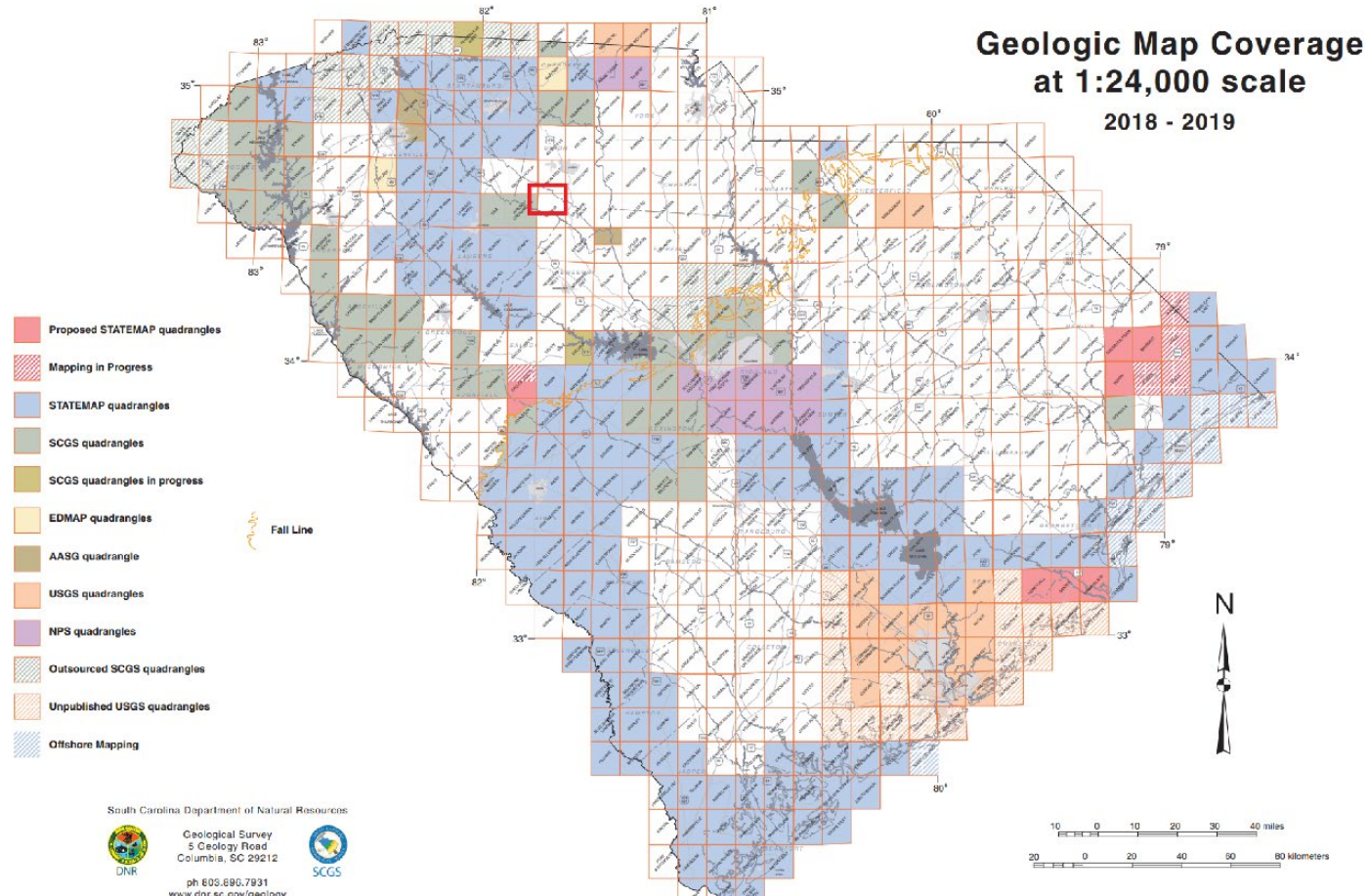


Figure 1: In South Carolina, areas in white do not have a quadrangle scale map produced. The CCZO and the mapped region are located in the red rectangle overlapping with the Sedalia, Union West, and Cross Anchor quadrangles (modified from SCDNR, 2018).

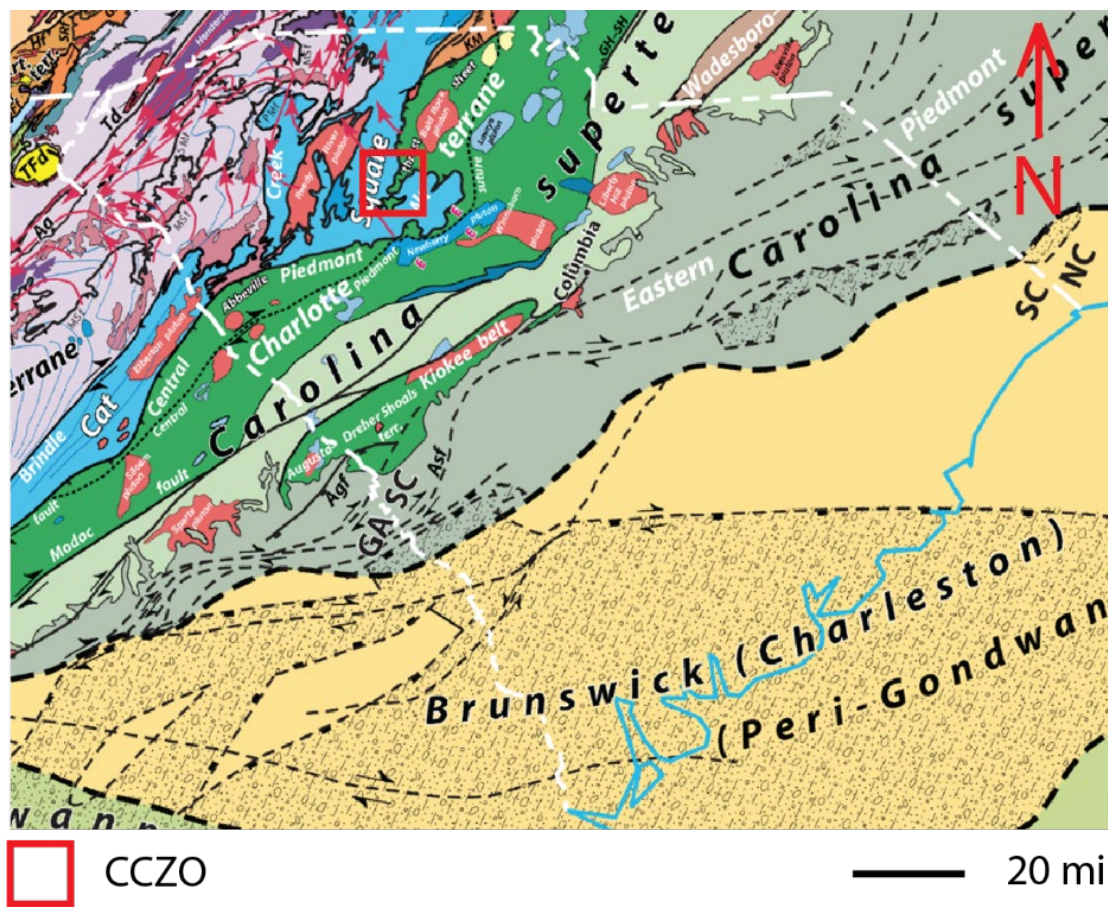


Figure 2: Regional geology of South Carolina with field area highlighted in red. The boundary between the light blue Cat Square and green Charlotte terrane represents the Central Piedmont Suture (adapted from Hatcher et al. 2007).



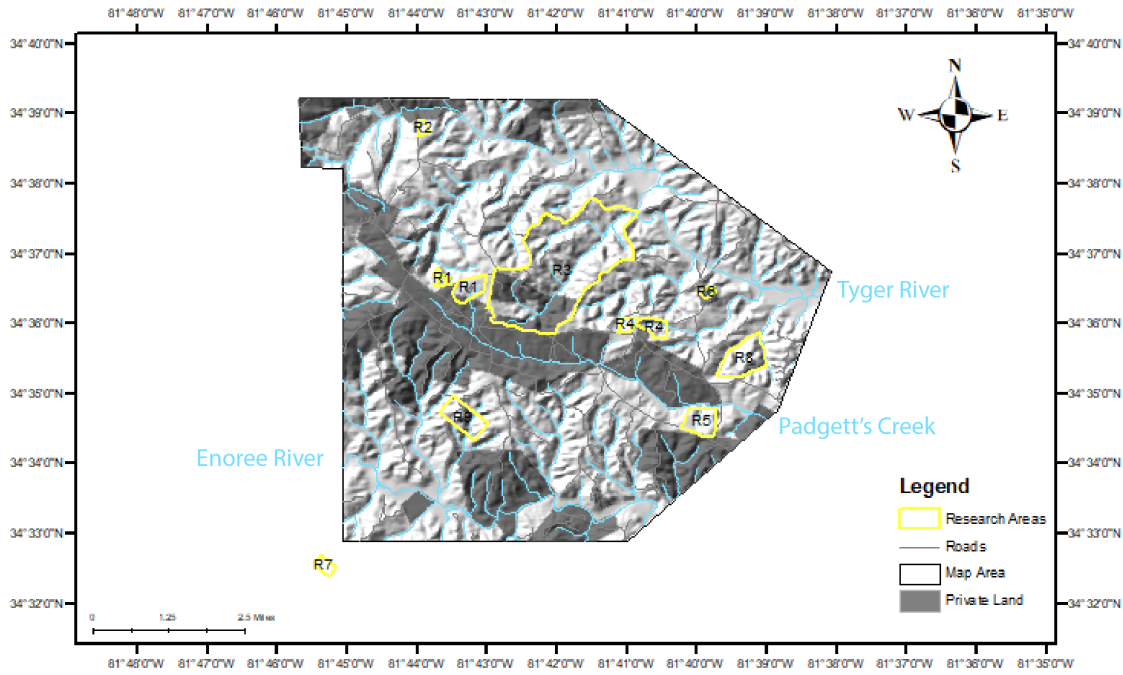


Figure 3: The field area is bound to the north by the Tyger River and to the south by the Enoree River. Within this, several research areas of the CCZO are located except for R7 that was previously mapped by Horkowitz (1984). The field site was mostly contained in the Sumter National Forest apart from private land.

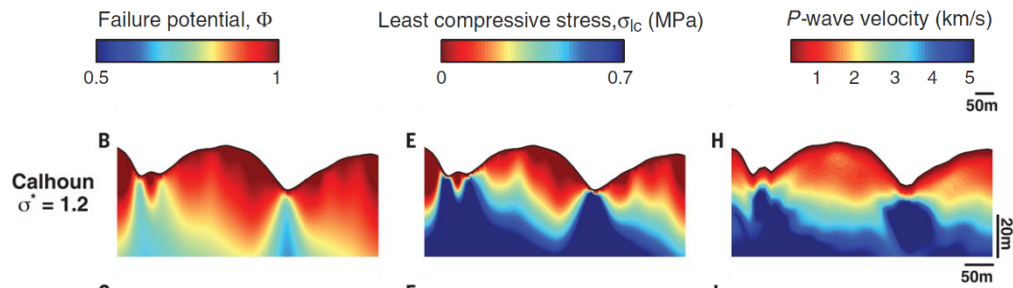


Figure 4: A typical cross section of the landscape within the CCZO. Cold areas of the figure show more competent rock. Outcrop preferentially occurred in low lying areas where water accumulates to remove overlying sediments (reprinted from St. Clair et al., 2015).



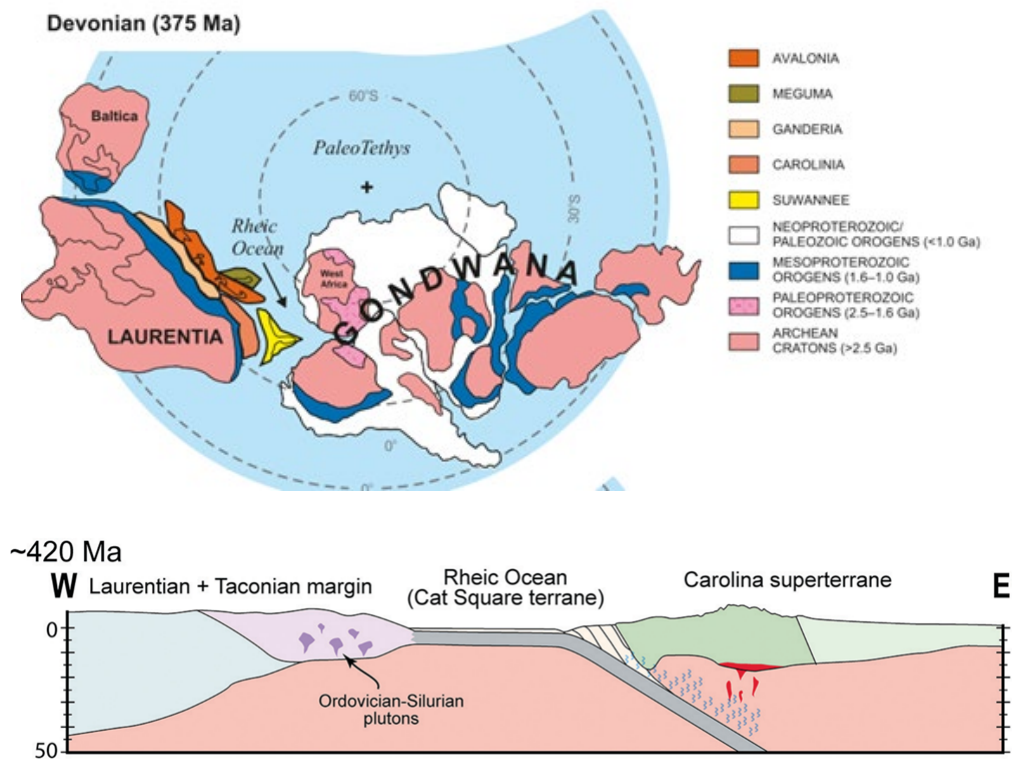


Figure 5: During the Paleozoic, ocean basins between Carolina and Laurentia began to close as exotic terranes, shown above in between Laurentia and Gondwana, began to accrete onto the Laurentian margin. Part of Carolina depicted above in dark pink would develop into the Charlotte terrane (adapted from Pollock et al., 2011).

## CHAPTER 2

### METHODS

#### *2.1 Geologic Mapping*

Reconnaissance mapping of the greater area was performed during the winter 2019 by observing the road cut geology along major and forest service roads in order to build a basic understanding of the field site. Although the CCZO mainly resides within the Sedalia quadrangle, the adjacent Philson Crossroads quadrangle was visited to verify previously described lithologies and verify existing map boundaries. Representative hand samples were taken from the field to build a rock library and descriptions were made for all present lithologies.

The following summer, detailed geologic mapping was performed beginning by extending the contacts of the Philson Crossroads quadrangle into the CCZO field site. Field data was collected at a watershed scale by walking along streambeds and gullies where there was the highest likelihood of exposure. Interfluves were then walked to search for float especially in complex areas or watersheds with low exposure within the stream beds.

At each rock sighting, the lithology and structure were characterized. First, the general texture of the rock was examined before fresh unweathered surfaces were exposed when available. After exposure, bulk mineral assemblages were recorded, and least altered samples were labeled for later thin section production. Labels were applied with a system based off their watershed identifier and then assigned a number (e.g. the first rock found in Holcombe's Branch was assigned the label HB01) and recorded in a sample index. On outcrops with preserved structures, visual assessment was used to determine the degree weathering to gauge the

likelihood that the surface rock was bedrock and not a detached block. Only locations interpreted with a high degree of confidence were sampled using a Brunton compass to record structural features like foliation, brittle fracture planes, and fold axes/limbs.

Throughout the majority of the field site, fresh outcrop was not available for analysis and saprolitic textures were relied upon for lithologic identification and structural analysis. The overall color, physical texture, presence of quartz and micas, as well as the presence of gneissic banding preserved in the saprolite were used as important indicators of potential lithologies. Low confidence was placed on lithologic identification from saprolite but was critical to use in conjunction with float to identify approximate lithologic contacts in interfluvial areas.

While the effects of saprolitization obfuscate mineralogical determinations, they also provided a higher confidence in structural measurements. The saprolite was generally assumed to be weathered in place and resistant minerals provided clear visual evidence of original shape preferred mineral orientations and foliation in the parent rock. Evidence of mass wasting was searched for before recording structural measurements in saprolite to reduce the possibility of making measurements in a slump or landslide.

These data were recorded in on watershed scale maps, in a field notebook, and location with a handheld GPS. Upon returning from field work, all data were copied into a master spreadsheet for later use in ArcGIS software included in the supplemental materials.

## *2.2 Petrology*

In order to produce detailed mineralogical descriptions of each lithology, 15 of the least altered hand samples were sent to Quality Thin Sections for standard (30  $\mu\text{m}$  thickness) thin section preparation. Samples were selected focusing on the western portion of the field site where more complex field relationships would benefit from petrographic determination.

Petrographic analysis was performed using a Nikon Eclipse LV100N polarized light microscope with an attached camera. For each thin section, approximate mineral abundances were produced through visual determination. When present, composition of plagioclase feldspars was estimated using the Michel-Levy method. Mineral grain boundaries were described to observe deformational history, and major fabrics and textures were recorded. Additionally, the degree of chemical weathering was noted based on the presence of sericite in the sample.

Because not every lithology was competent enough to produce a thin section, X-ray diffraction was also implemented to characterize mineral assemblages. Each sample was powdered using a mortar and pestle and ~5 g of were weighed out. The powder was then milled down to 10  $\mu\text{m}$  using a McCrone Mill. Then, a 10% by weight internal standard of zincite was added before powdered mounts were pressed. Samples were externally calibrated with a corundum sample (NIST 1976b) before analysis on a Bruker D8 Advanced X-ray Diffractometer using Co-radiation. Diffraction peaks were compared against data in the International Centre for Diffraction Data (ICDD) powder diffraction file (PDF4) using the EVA software suite by Bruker.

### *2.3 Geochemistry*

Geochemical characterization of two granitic bodies at the field site were performed. Samples were collected using a composite sampling methodology where multiple hand samples across the lithologic unit were crushed and mixed together before a 5 g portion was separated. These composite samples were then sent off to Activation Laboratories in Ontario, Canada for their 4-LITHO geochemical characterization of major oxides and trace elements. This method uses a lithium metaborate/tetraborate fusion approach analyzed by induction coupled plasma

(ICP) and ICP-mass spectroscopy (ICP-MS). Calibration is performed using USGS and CANMET reference materials, with totals running between 98.5 and 101.0 %.

The geochemical results were compared with literature data from the Cat Square (n=24) and Charlotte terrane (n=28) compiled from Huebner, 2017 as well as Butler and Fullagar, 1978. These data were processed and analyzed in R using the GeoChemical Data toolkit and Tidyverse packages (Janoušek, 2006; Wickman et al., 2019).

## CHAPTER 3

### RESULTS

#### *3.1 Mapping Results*

The CCZO field site revealed five different major lithologic groups. Towards the western portion of the field site, two mafic rock types were found including a meta-diorite and a meta-tonalite unit. In all portions of the field site, felsic meta-granodiorite and meta-granite units were observed. Additionally, a biotite gneiss/amphibolite unit was found throughout the field site that contained subordinate units of chlorite schist and quartzite. These units were bound to the north and south by alluvium (See Appendix A).

Structurally, few measurable structures were observed in the field site due to the high degree of weathering and poor exposure. However, foliations predominantly had NE strikes around 40° with a dip of 25° SE and did not appear to be uniform throughout the area. Folding was not observed regularly on outcrop scales only appearing in context of large portions of the mapped area. Dikes were observed, but only appeared infrequently (Fig. 6). These dikes were not continuous and were often only observable at one location. Throughout the field site, conjugate joint sets were observed with small apertures.

#### *3.2 Unit Descriptions*

##### *Biotite-Hornblende-Quartz Meta-Diorite (bhqd)*

This unit was located along the western boundary of the field site and covered an area of 0.65 mi<sup>2</sup> within the mapped region. Outcrops were normally found in streambeds where preservation was poor showing a high degree of saprolitization and preventing petrographic

analysis (Fig. 7a). Instead, this unit was identified in the context of the adjacent map (Horkowitz, 1984).

Although the biotite-hornblende-quartz meta-diorite unit never appeared as competent rock on an outcrop scale, there were larger spans of saprolite surrounded by float in the mapped region (Fig. 7b, c). The saprolite had a dark red-brown color with a slight shimmer from the biotite and a sandy texture. Float appeared as spheroidal highly altered boulders with oxidation rinds.

In hand sample the rock appeared as dark grey with a shiny luster. Minerals were medium grained and phaneritic. Cleavage was easily distinguished for both the biotite and hornblende although the dark color made the determination more difficult. Less weathered samples were competent requiring effort to split with a hammer. For weathered samples, the unit produced a distinctive black and white appearance with chemical alteration of the mafic minerals and feldspars. The feldspars specifically altered to a bright white chalky clay (Fig. 7a).

Previous descriptions of this unit note major phases of “hornblende, biotite, plagioclase, quartz, K-spar and epidote” with minor amounts of “sphene, apatite, zircon, and Fe-Ti opaques” (Horkowitz, 1984). Plagioclase was reported to have an average calcic andesine composition (An 38–46) (Horkowitz, 1984). Important mineral features include the presence of “warped pericline twins” as well as “anhedral quartz grains” that show “undulose extinction,” a crystallographic response to high strain that causes misalignment of crystallographic domains throughout the mineral (Horkowitz, 1984; Passchier and Trouw, 2005).

X-ray diffraction revealed a mineralogy of albite, pyroxene, talc, and a montmorillonite-chlorite structure. Peaks were relatively sharp for albite but appeared broader for the other mineral phases (See Appendix B).

### *Meta-Tonalite (tn)*

Located in the extreme northwest portion of the field site and covered an area of 0.19 mi<sup>2</sup>. Exposure consisted of clusters of small boulders approximately 10–40 cm in diameter. In the small stream bed, these clusters would extend intermittently for 2–3 m stretches. Boulders showed varying degrees of weathering with most having fresh rough edges. Soils in the area were of a similar characteristic to the biotite-hornblende-quartz meta-diorite unit having a dark red-brown and sandy texture.

In hand sample, the meta-tonalite appeared as a black very fine-grained rock (Fig. 8). Occasionally, the rocks would have a bright orange oxidation rind. Individual minerals were barely distinguishable to the point of almost being aphanitic, however, individual cleavage of both hornblende and pyroxene were distinguishable as well as the characteristic conchoidal fracture in quartz (Fig. 8).

Thin sections analysis showed the tonalite unit has major phases of quartz (40%), plagioclase (35%), and hornblende (25%) with trace amounts of orthopyroxene (Figs. 9a, b). Quartz in the sample was fine to medium grained, anhedral, and exhibited undulose extinction. Frequent fractures were present within the grains and dihedral angles were present along grain boundaries (Fig. 9c). These boundaries were also subject to grain boundary migration (Fig. 9d). Plagioclase was fine to medium grained, anhedral, and showed regular albite and polysynthetic twinning. The maximum identified composition was An(55). Hornblende was dominantly fine grained with infrequent medium grains, and it was subhedral to anhedral. The tonalite displayed a seriate-interlobate texture (Fig. 9b).



### *Biotite Meta-Granodiorite (bgd)*

This unit was located along the western and southern portion of the field site and covered an area of 5.2 mi<sup>2</sup> within the mapped region. Outcrops were moderately to well preserved in both streambeds and higher order gullies with some continuous sections spanning 5–10 m in the southern portion of the mapped area.

Several large microcline porphyroblasts and slight schistosity without migmatic textures distinguished the biotite meta-granodiorite from all other granitoids in the mapped area (Fig. 10a). On an outcrop scale, the biotite meta-granodiorite unit was slightly darker grey than the meta-granite outcrops and lighter grey than the biotite gneiss units (Figs. 10b). Soils appeared yellow-brown to red-brown and sandy with shiny micas and were not a distinguishing indicator.

In hand sample, the rock was medium grey with a medium grained matrix and very coarse grained porphyroblast of 3–4 cm (Fig. 10a). Early stages of both foliation and schistosity were evident in leucosome-like bands as well as minor shape preferred orientation in biotite (Figs. 10b, c). However, these features and the porphyroblasts were not always present from hand sample to hand sample.

Thin sections that did not sample the microcline porphyroblasts had major phase abundances of feldspar (40%), quartz (30%), biotite (15%), hornblende (10%), clinopyroxene (5%), and trace amounts of zircon and epidote (Figs. 11a, b). Feldspars were predominantly fine to coarse grained anhedral An(33) plagioclase (35%) that showed albite twinning and occasional fracture. Fine to medium grained anhedral microcline (5%) was also present with characteristic microcline twinning with grains exhibiting occasional fracture as well. Myrmekite was common while sericite was a rare texture in thin section (Fig. 11c). Quartz was fine to medium grained, anhedral, showed undulose extinction, developed subgrains, and rare dihedral angles along grain

boundaries. Additionally, the grains were frequently fractured and contained regular biotite inclusions. Biotite and hornblende were both fine to medium grained and anhedral while clinopyroxene, zircon, and epidote were fine grained and euhedral.

Overall, the rock had a seriate interlobate texture and was protomylonitic (Fig. 11d). Grains were slightly inequigranular with frequent fractures and highly deformed grain boundaries. Slight chemical weathering was evident in the formation of sericite in the feldspars.

X-ray diffraction data was consistent with the thin section mineralogy showing mostly quartz (38.8%), microcline (24.5%), albite (20.3%), and biotite (16.3%). Differences in modal mineralogy may be due to the inclusion of microcline porphyroblasts in the powdered sample (See Appendix B). All peaks in the pattern were sharp.

#### *Biotite Gneiss/Amphibolite*

This light grey lithology was located in the northeastern part of the field site and covered an area of 16.7 mi<sup>2</sup> within the mapped region (Fig. 12a). Outcrops were normally found in streambeds and gullies with variable preservation. Expansive outcrops on the scale of 10s of meters were observed in low-order streams while abundant boulders are found in gullies.

On an outcrop scale, the gneissic unit shows distinctive foliation with poorly formed leucosome and melanosomes (Fig. 12a). Folds were rarely observed on mesoscopic scales, but the rock was ptygmatic on rare occasions. Outcrops varied in color from dark grey for the biotite gneiss portions to dark black for amphibolitic lenses (Figs. 12b, c). These amphibolite lenses stretched for 3–5 m in length while the biotite gneiss portions were more expansive reaching over 10 m in sections. This lithology was not always competent readily breaking apart easily with a hammer. Soils were composed of two types. The first soil was generally yellow to red-

brown and sandy while the other appeared in small regions of dark red-brown soils lacking a quartz component.

In hand sample, leucosomes were subordinate to the melanosomes and appeared as medium to coarse grained continuous plagioclase foliations 1–2 cm in thickness. Melanosomes were medium-grey and showed well defined schistosity due to the abundance of biotite with variable thicknesses on the order of 2–10 cm (Fig. 12a). Two minor units appeared within the biotite gneiss/amphibolite unit that were not expansive enough to include on the scale of the map. These included a garnet quartzite and a chlorite schist.

In thin section, the biotite gneiss showed major phases of feldspar (40%), quartz (30%), and biotite (17.5%) and hornblende (12.5%) with trace amounts of zircon and chlorite (Fig. 13a, b). Feldspars ranged from fine to coarse grained with both An(30) plagioclase (30%) and microcline (15%) present which exhibit their respective twins. The feldspars both exhibited frequent fracture as well as alteration to sericite, and myrmekite was common in the sample. Quartz was fine to coarse grained and anhedral with frequent fracture (Fig 13c). It frequently showed well developed subgrains along grain boundaries. Grain fracture was present in the quartz as well (Fig 13d). Both biotite and hornblende were fine to medium grained and anhedral.

The rock displayed a seriate interlobate texture. Grains were slightly inequigranular with frequent fractures and highly deformed grain boundaries. Chemical weathering was evident in the formation of sericite in the feldspars (Fig. 13d).

These mineralogical observations were also observed in diffraction data in different abundances. Hornblende (51.7%), labradorite (39%), quartz (6.6%), and microcline (2.6%) were all observed in the pattern. However, no biotite was observed. Differences between the XRD and

thin section abundances may be due to the heterogeneity of the sample. For all mineral phases, the pattern showed sharp peaks (See Appendix B).

### *Meta-Granite*

This unit was located throughout the field site and covered an area of 4.0 mi<sup>2</sup> within the mapped region. Outcrops were normally found in stream beds where samples showed good preservation. Spheroidally weathered boulders were also prevalent in interfluvial areas.

Outcrops of this unit were expansive ranging from 1–3 m boulder fields all the way to 5–10 m continuous units. These rocks had the brightest color of any lithology typically appearing as a white-grey with fine grained slightly aligned biotite visible (Fig. 14a). Both jointing and foliation were observed within the outcrop (Figs. 14b, c). The meta-granite was competent requiring force to break apart. The soil produced by this lithology was a light red-brown to yellow brown sandy soil.

In hand sample, the meta-granite was light grey with abundant mafic minerals showing slight shape preferred orientation. Hematite staining and weathering rinds were common leaving behind orange-brown tints along the surface of hand samples. The meta-granite was readily distinguished from other granitoid units within the field area by its lighter grey appearance and lack of microcline porphyroblasts (Fig. 14a).

Thin sections of the meta-granite revealed a composition of quartz (45%), feldspar (35%), biotite (15%), and phengite (5%) with trace amounts of zircon, tourmaline and opaques (Figs. 15a, b). Quartz was fine to medium grained, anhedral, and showed undulose extinction with the presence of subgrains. These grains were frequently fractured and contained rare inclusions of biotite and feldspar as well as pressure dissolution along grain boundaries (Fig. 15c). Feldspar was composed of both An(70) plagioclase (25%) and microcline (10%).

Plagioclase was fine to medium grained, anhedral, and showed albite twinning. Microcline was fine to medium grained, anhedral, and showed common tartan twinning. Feldspars showed minor amounts of alteration to sericite and myrmekite was common (Fig. 15d). Biotite and muscovite were both fine grained, subhedral to anhedral, and exhibited birdseye extinction. Zircons were very fine grained, subhedral and showed poor zoning.

Meta-granites at the field site exhibited an inequigranular polygonal texture that was protomylonitic. Grains were frequently fractured with common, and incipient weathering was expressed with the presence of sericite in feldspars (Fig. 15d). X-ray diffraction data was consistent showing abundant quartz, plagioclase, microcline and biotite.

### *Alluvium*

This unit was located along the northern and southern bounds of the mapped region adjacent to the Tyger and Enoree rivers. The alluvium unit covered an area of 3.9 mi<sup>2</sup> and was frequently associated in the field by the presence of bamboo.

### *3.3 Granite Geochemistry*

#### *Cat Square Terrane*

A compilation of Cat Square granites in the southern Piedmont showed that major elements are not consistent between samples (Table 1). SiO<sub>2</sub> and Al<sub>2</sub>O<sub>3</sub> were the most abundant by weight percent (%) ( $\bar{x}_{\text{SiO}_2} = 68.30\%$  and  $\bar{x}_{\text{Al}_2\text{O}_3} = 15.50\%$ ). But the large standard errors mean they vary greatly within the sample set ( $\text{SEM}_{\text{SiO}_2} = 0.88$  and  $\text{SEM}_{\text{Al}_2\text{O}_3} = 0.33$ ). This variance was clearly displayed in the large range of SiO<sub>2</sub> and Al<sub>2</sub>O<sub>3</sub> values displayed on the Harker diagrams (Fig. 11).

Abundances of minor elements showed more consistent abundances between the sample set. Cations that substitute in feldspars decreased in abundance from K<sub>2</sub>O to Na<sub>2</sub>O to CaO with

standard errors half the size of the major elements ( $\bar{x}_{K_2O} = 4.48 \%$ ,  $\bar{x}_{Na_2O} = 3.06 \%$ ,  $\bar{x}_{CaO} = 2.24 \%$ ;  $SEM_{K_2O} = 0.13$ ,  $SEM_{Na_2O} = 0.10$ ,  $SEM_{CaO} = 0.20$ ). MnO, TiO<sub>2</sub>, and P<sub>2</sub>O<sub>5</sub> were consistent across all samples ( $SEM_{MnO} = 0.01$ ,  $SEM_{TiO_2} = 0.05$ ,  $SEM_{P_2O_5} = 0.02$ ). The only exception shown was FeO which had a similar standard error as Al<sub>2</sub>O<sub>3</sub> ( $SEM_{FeO} = 0.29$ ;  $SEM_{Al_2O_3} = 0.33$ ).

Geochemical relationships were evaluated using the non-parametric Spearman's Ranked Correlation because elemental abundances were not normally distributed. A  $\rho$  of 1 indicates a perfect positive relationship while a  $\rho$  of -1 indicates a perfect negative relationship. The oxides Al<sub>2</sub>O<sub>3</sub>, MgO, CaO, TiO<sub>2</sub>, P<sub>2</sub>O<sub>5</sub> and FeO versus SiO<sub>2</sub> all plotted with negative trends (Fig. 11). Al<sub>2</sub>O<sub>3</sub> had the most statistically significant negative relationship to SiO<sub>2</sub> ( $\rho = -0.8210$ ,  $S = 3685.60$ ,  $p = 1.59e-06$ ). Na<sub>2</sub>O and K<sub>2</sub>O showed no clear relationship with SiO<sub>2</sub> ( $\rho_{Na_2O} = -0.3856$ ,  $S_{Na_2O} = 2102.00$ ,  $p_{Na_2O} = 0.8613$ ;  $\rho_{K_2O} = 0.1676$ ,  $S_{K_2O} = 1684.8$ ,  $p_{K_2O} = 0.4447$ ).

Rare Earth Element (REE) in the Cat Square show abundant light REEs with a negative Eu anomaly (Fig. 17). These trends roughly follow the average composition of the upper continental crust staying within an order of magnitude above or below (Fig. 18). Only Ta showed a major departure in one sample with a ratio of 0.04 relative to the average continental crust. Nb, Ta and Sr consistently plotted as depleted relative to the average while La, Ce, Nd and Sm plotted as enriched. The heavy REEs Y, Tm, and Yb all plotted with high variance spanning between one and two orders of magnitude.

Classification of Cat Square granites using Frost and Frost (2008) showed consistent determinations despite large ranges of values (Fig. 19). When examining the ratio between iron and magnesium, granites plotted as intermediate between being ferroan and magnesian (Fig. 19a). The Modified Alkali Lime Index (MALI) further define the granites as alkali-calcic to calc-alkalic with the exception of two data points that plot as alkalic (Fig. 19b). All Cat Square

granites except one measured were peraluminous on the Aluminum Saturation Index (ASI) with values from 1 to 1.3 and silica saturated according to the Alkali Index (AI) vs Feldspathoid Silica Saturation Index (FSSI) (Figs. 19c, d).

### *Charlotte Terrane*

Charlotte terrane granites in the southern Piedmont contained major elements abundances that were relatively consistent between samples (Table 1). The most abundant elements, SiO<sub>2</sub> and Al<sub>2</sub>O<sub>3</sub>, had smaller standard errors as all samples had similar compositions ( $\bar{x}_{\text{SiO}_2} = 75.37\%$  and  $\bar{x}_{\text{Al}_2\text{O}_3} = 12.92\%$ ;  $\text{SEM}_{\text{SiO}_2} = 0.20$  and  $\text{SEM}_{\text{Al}_2\text{O}_3} = 0.09$ ). The SiO<sub>2</sub> values were consistently higher than the values for the Cat Square, and the Al<sub>2</sub>O<sub>3</sub> values were slightly lower. These similarities appeared in the small range of SiO<sub>2</sub> and Al<sub>2</sub>O<sub>3</sub> values displayed on the Harker diagrams (Fig. 11).

Minor elements in the Charlotte terrane showed high consistency within the sample set. Cations that substitute in feldspars decreased in abundance from K<sub>2</sub>O to Na<sub>2</sub>O to CaO with equally small standard errors as the major elements ( $\bar{x}_{\text{K}_2\text{O}} = 4.47\%$ ,  $\bar{x}_{\text{Na}_2\text{O}} = 4.29\%$ ,  $\bar{x}_{\text{CaO}} = 0.41\%$ ;  $\text{SEM}_{\text{K}_2\text{O}} = 0.08$ ,  $\text{SEM}_{\text{Na}_2\text{O}} = 0.05$ ,  $\text{SEM}_{\text{CaO}} = 0.06$ ). The Charlotte terrane did not have elemental data for MnO and P<sub>2</sub>O<sub>5</sub>.

No statistically significant relationships were observed between SiO<sub>2</sub> and other oxides within the Charlotte terrane. Instead, the oxides showed a range of distribution irrespective of SiO<sub>2</sub> (Fig. 11). REE and trace element data were not well described in the Charlotte terrane literature and no analysis could be made.

Granites within the Charlotte terrane plotted as highly ferroan with most values being close to one (Fig. 19a). On the MALI plot, granites dominantly plotted within the alkali-calcic field (Fig. 19b). On the ASI plot, samples plotted in both the metaluminous and peraluminous

fields resulting in an intermediate composition (Fig. 19c). The AI vs FSSI plot characterized the Charlotte terrane granites as silica saturated and meta/peraluminous, however, on the FSSI plot all values plotted close to the peralkaline field (Fig. 19d).

### *CCZO*

CCZO granites showed similar oxide compositions as the Cat Square terrane. FeO, MnO, MgO, and TiO<sub>2</sub> were all nearly half the abundance of the Cat Square granites and had insignificantly more SiO<sub>2</sub> (Table 1). CCZO granites did not have a large enough sample size for any statistical analysis on among group variation (n=2).

REE and trace elements in the CCZO were relatively depleted compared to the average upper continental crust and showed a positive Eu anomaly (Figs. 17, 18). Only Rb, Ba, Th and Sr showed enriched values with all others being depleted, especially the HREEs who had concentrations nearly an order of magnitude below the average. Opposite of the Cat Square, the CCZO granites showed negative anomalies for La, Ce, Nd, and Sm, and they showed a positive anomaly for Sr (Fig. 18).

CCZO granites plotted close to the intermediate boundary between ferroan and magnesian with a slightly magnesian classification (Fig. 19a). The MALI plot showed these granites have a mixed determination between alkali-calcic and calc-alkalic (Fig. 19b). ASI plots revealed a slightly peraluminous composition (Fig. 19c). In the AI versus FSSI plot, both CCZO granites lie within the silica saturated and meta/peraluminous fields (Fig. 19d).

### *3.4 Tectonic Setting*

Tectonic determinations were made using REEs which are enriched in specific tectonic regimes (Cabanis and Lecolle, 1989). Both Cat Square and CCZO granites plotted in the



orogenic field due to their high La abundances relative to Y and Nb. One outlier within the Cat Square terrane plotted in the anorogenic field (Fig. 20).



Figure 6: Quartz dikes (black) were often seen in steam beds crosscutting foliation (white) at the field site ranging in thickness up to 20 cm located NE of Holcombe's Branch.

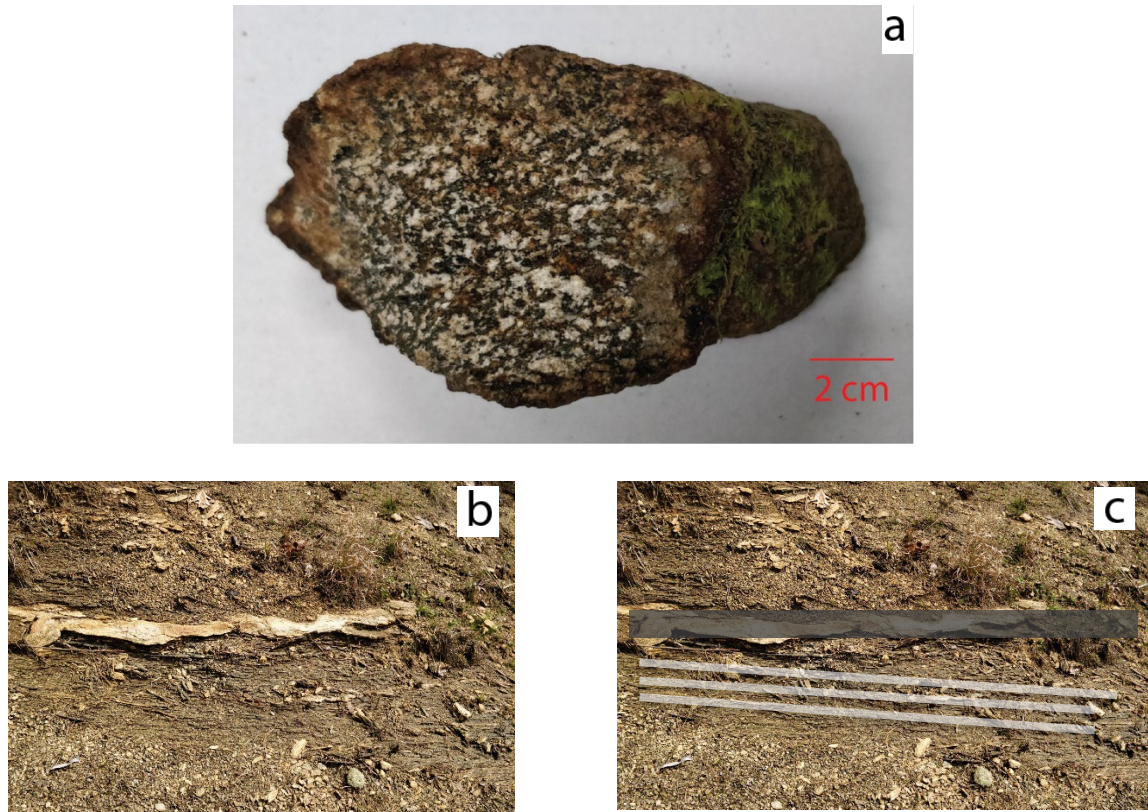


Figure 7: Biotite-hornblende-quartz meta-diorite was frequently weathered rarely preserving in hand sample. (a) The unique salt and pepper characteristic readily identified this lithology in the field. (b, c) Despite alteration, resistive unites like dikes (highlighted in black) and preferred orientations (highlighted in white) were easily identifiable.





Figure 8: Meta-tonalite (BR04) in hand sample. Oxidation rinds were typical with this lithology. Despite a very fine grain size, cleavage plains of amphiboles and pyroxene were observable.

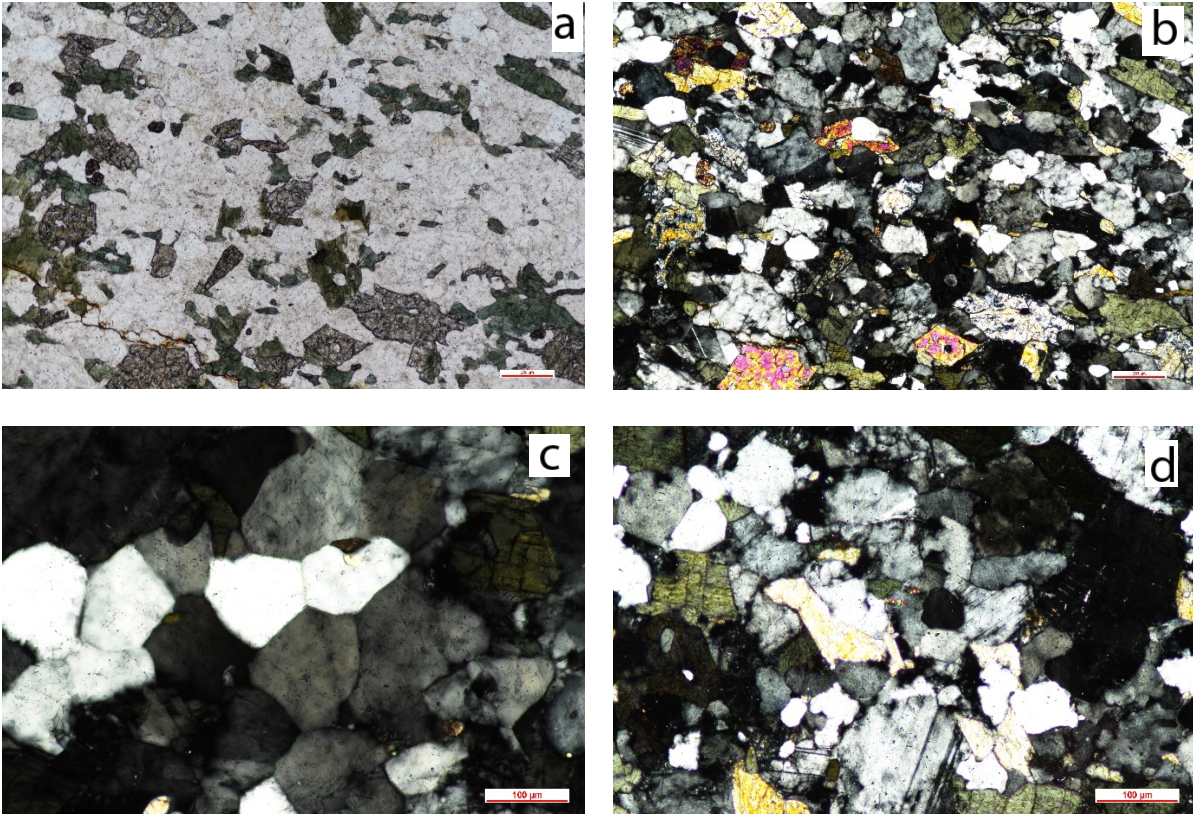


Figure 9: The meta-tonalite unit showed a primary igneous texture with subsequent alteration. (a) The thin section in plane polarized light shows the abundance of hornblende and pyroxenes. (b) The same region in cross polarized light. Anhedral grains compose most of the thin section. (c) The equilibrium texture of dihedral angles in quartz grains were regularly observed. (d) Subgrains were well developed in the meta-tonalite.



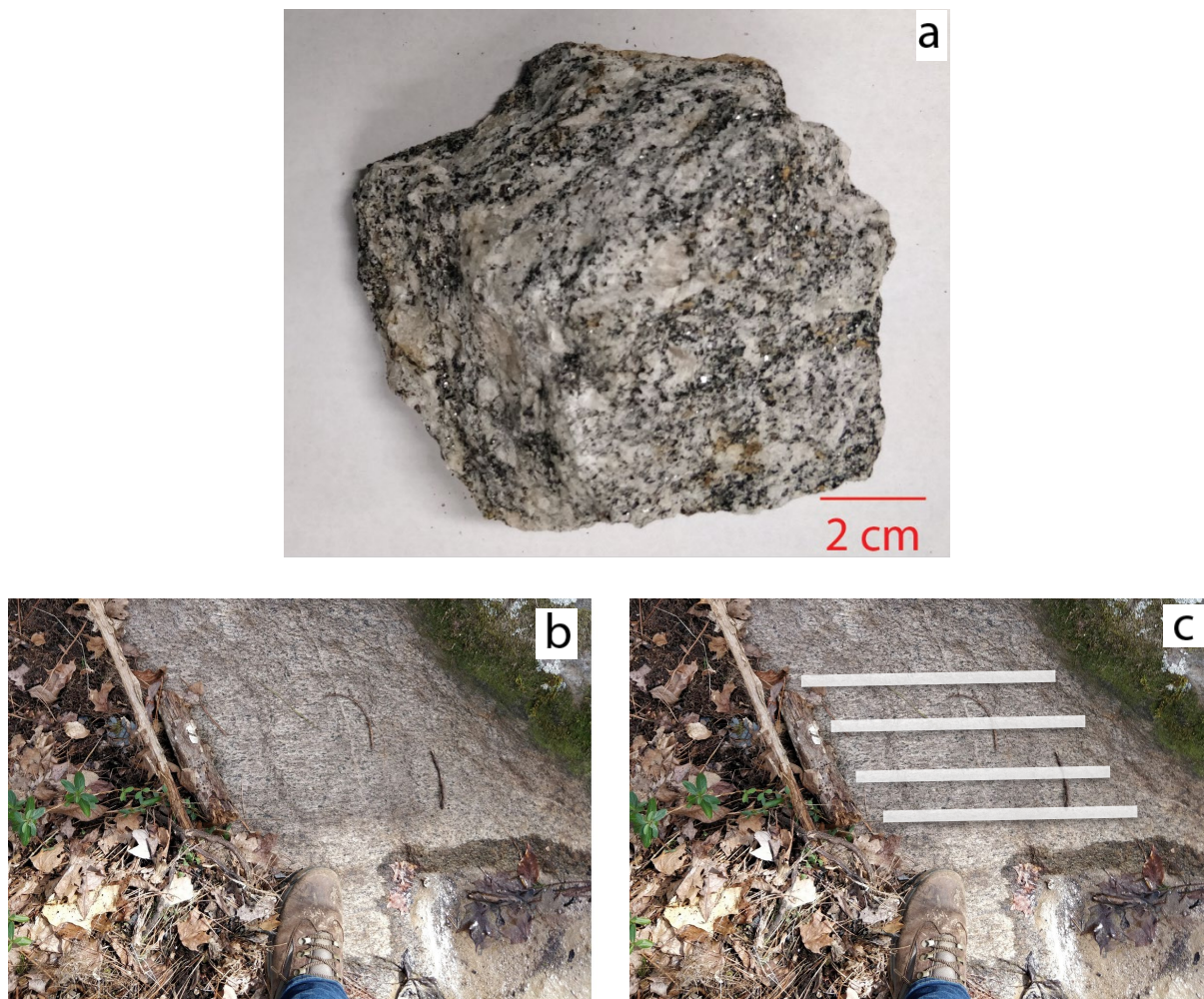


Figure 10: Biotite meta-granodiorite (SC04) was identified by its medium grey color, microcline porphyroblasts, and foliation. (a) In hand sample, well developed microcline porphyroblasts grew as large as 2 cm. (b, c) Foliation (white) was present throughout the biotite meta-granodiorite unit.

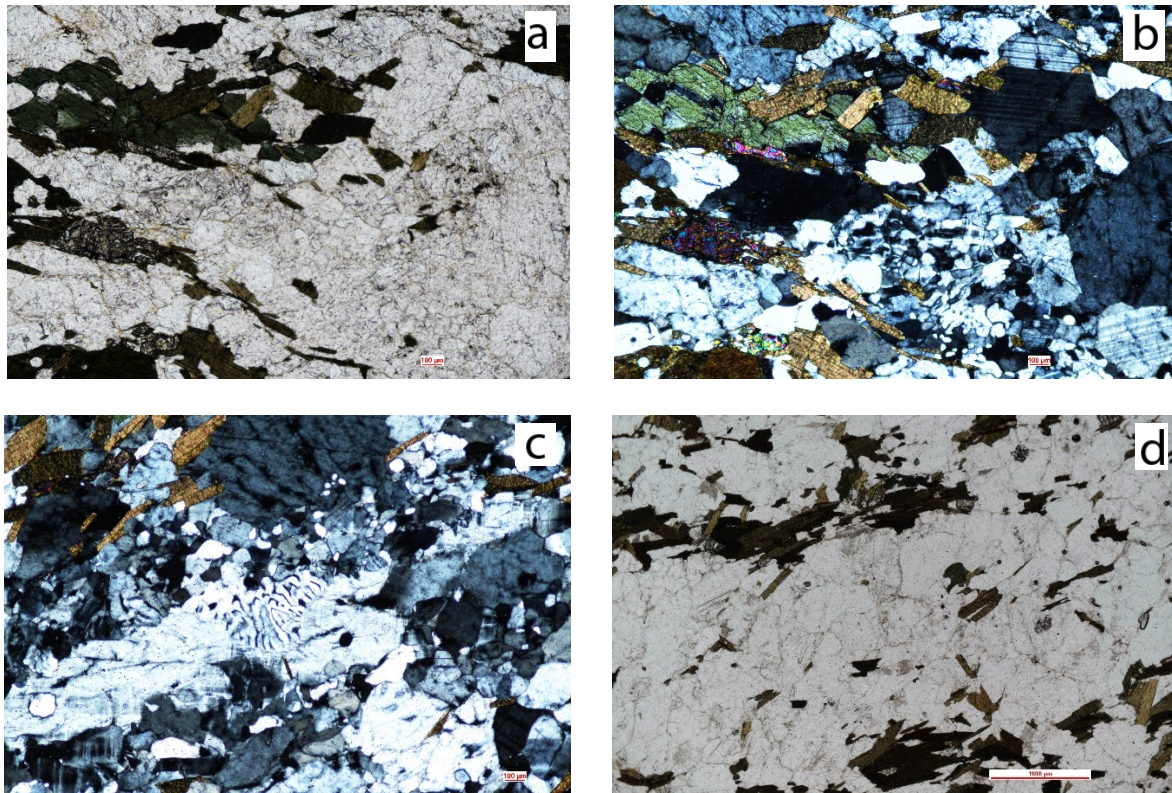


Figure 11: In thin section, incipient metamorphism was observable in this lithology. (a, b) Biotite meta-granodiorite plane polarized light, and cross polarized light. (c) The thin section frequently showed myrmekite. (d) Shape preferred mineral orientation of hornblende and biotites provide evidence of the protomylonitic texture.



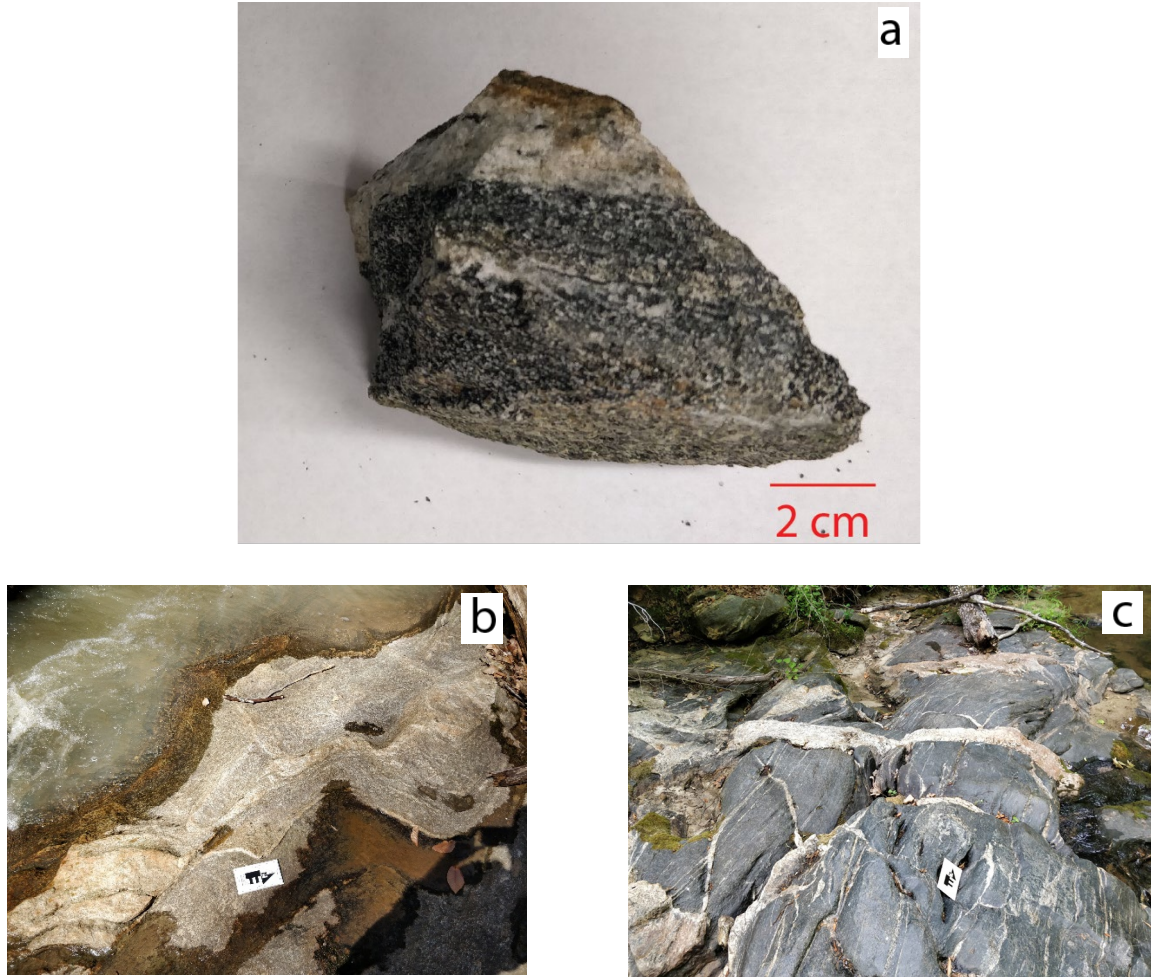


Figure 12: Biotite gneiss/amphibolite (HB21) was composed primarily of granitic gneiss with lenses of amphibolite scattered throughout the mapped area. (a) In hand sample, leucosomes and melanosomes were typically not folded or deformed. (b) Outcrops of gneiss were light to medium grey in color and rarely showed mesoscopic folding. (c) Amphibolite was typically convoluted or ptygmatic. Here prominent dikes were observed crosscutting the amphibolite.



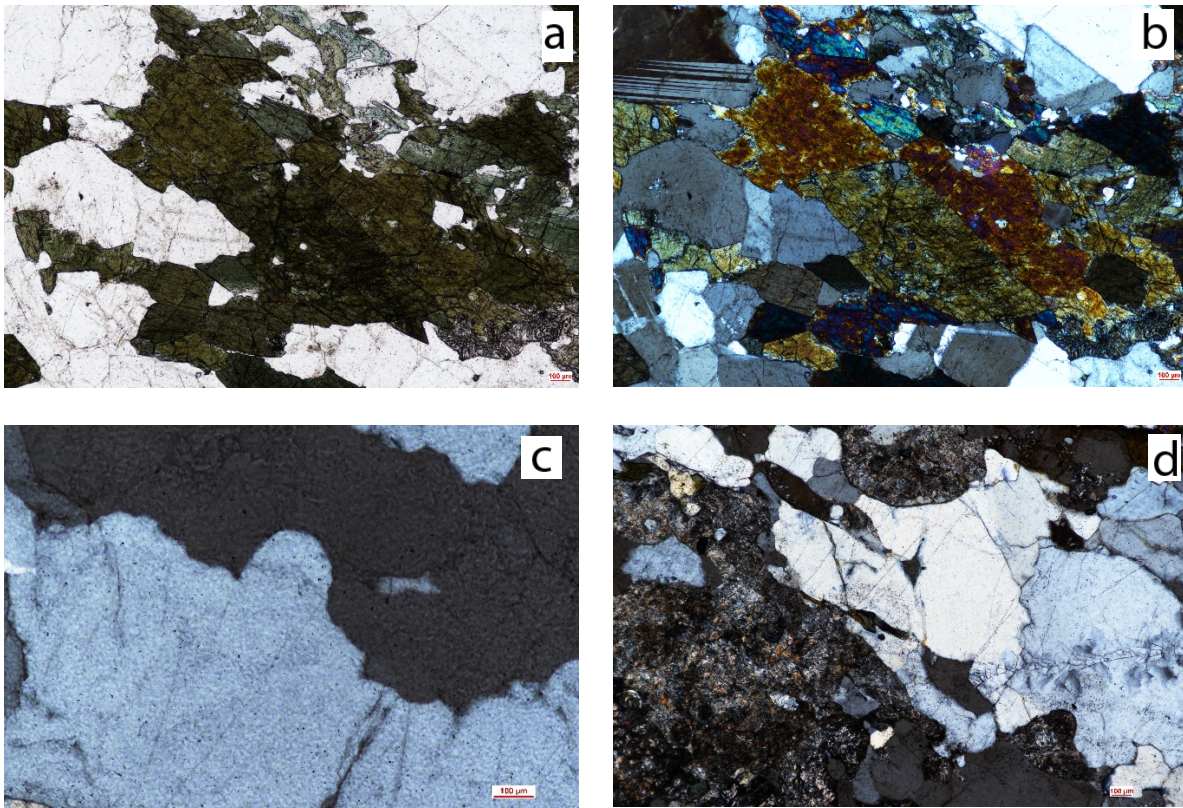


Figure 13: The gneissic portion of this unit showed highly altered grains. (a, b) Thin section in plane polarized light and cross polarized light. (c) Quartz grains displayed highly irregular grain boundaries and were typically anhedral. (d) Grain fracture was observed in several locations, and sericite was commonly observed.

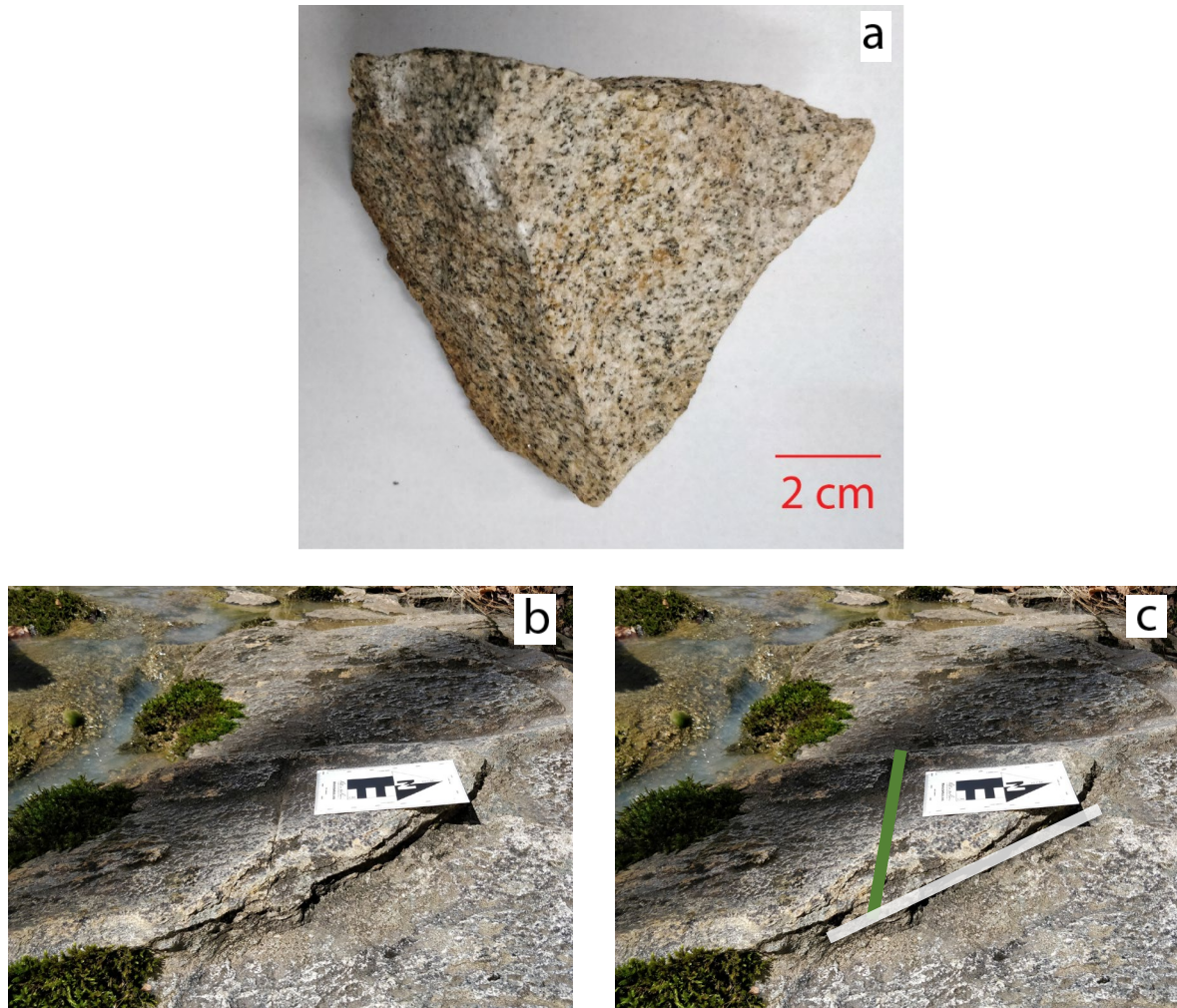


Figure 14: Meta-granite (PC04) was a highly competent unit at the field site forming expansive outcrops. (a) In hand sample, it could be distinguished from other granitoids by its bright and light grey appearance. (b) Joining (green) and foliation (white) were both observed in the meta-granite unit.



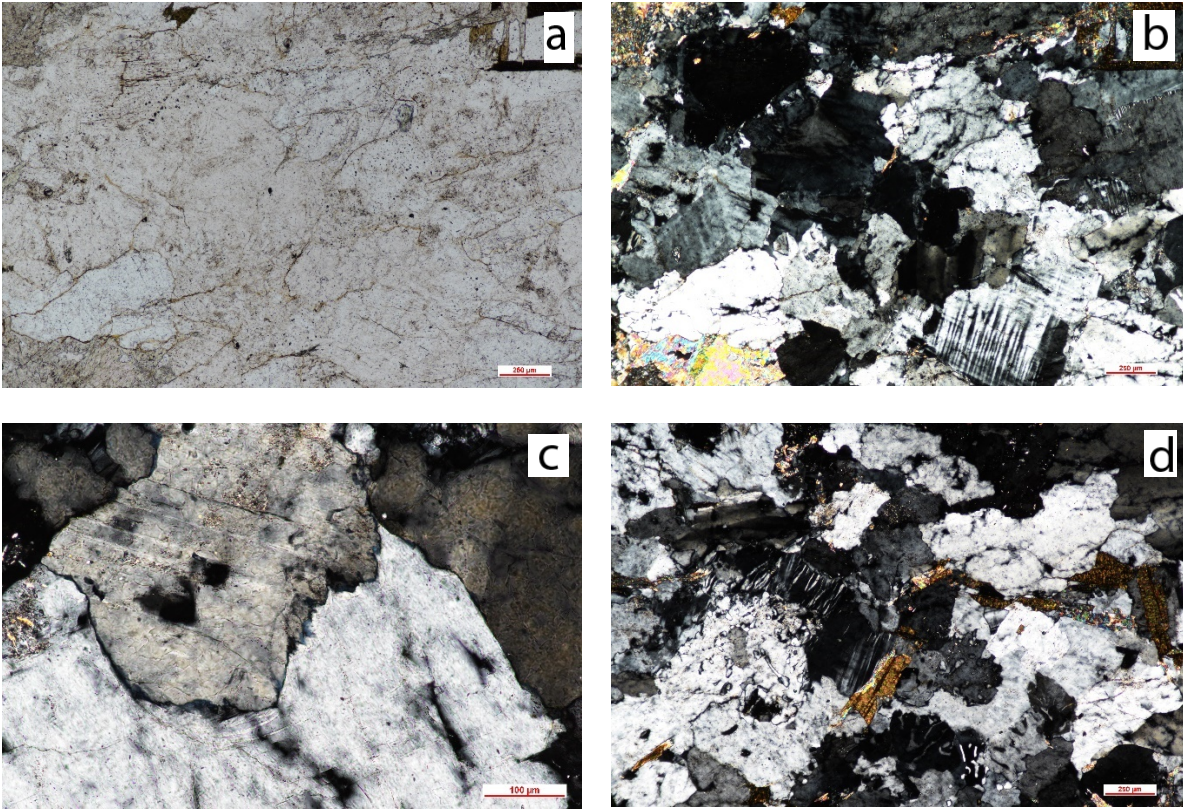


Figure 15: The CCZO meta-granite showed both biotite and muscovite unlike other granitoids in the field site. (a, b) The meta-granite in plane polarized light and in cross polarized light. (c) Pressure dissolution occurred along grain boundaries. (d) Myrmekite and grain boundary migration appeared throughout the thin sections.

Table 1: Mean weight percentages and standard error of the mean (SEM) of granites in the southern Piedmont. Charlotte terrane granites were reported to have higher SiO<sub>2</sub> than both Cat Square and CCZO granites. MgO and TiO<sub>2</sub> values are an order of magnitude different between the Charlotte terrane versus the Cat Square and CCZO granites. Data was compiled from Huebner et al., 2017 and Butler and Fullagar, 1978.

| Weight %          | SiO <sub>2</sub> | Al <sub>2</sub> O <sub>3</sub> | FeO  | MnO  | MgO  | CaO  | Na <sub>2</sub> O | K <sub>2</sub> O | TiO <sub>2</sub> | P <sub>2</sub> O <sub>5</sub> | n  |
|-------------------|------------------|--------------------------------|------|------|------|------|-------------------|------------------|------------------|-------------------------------|----|
| <b>Cat Square</b> | 68.30            | 15.50                          | 3.21 | 0.07 | 1.02 | 2.24 | 3.06              | 4.48             | 0.51             | 0.19                          | 23 |
| <b>CCZO</b>       | 70.48            | 15.01                          | 1.63 | 0.03 | 0.46 | 1.93 | 3.79              | 4.70             | 0.25             | 0.07                          | 2  |
| <b>Charlotte</b>  | 75.37            | 12.92                          | 1.08 | 0.18 | 0.04 | 0.41 | 4.29              | 4.47             | 0.06             | -                             | 28 |

| SEM               | SiO <sub>2</sub> | Al <sub>2</sub> O <sub>3</sub> | FeO  | MnO  | MgO  | CaO  | Na <sub>2</sub> O | K <sub>2</sub> O | TiO <sub>2</sub> | P <sub>2</sub> O <sub>5</sub> | n  |
|-------------------|------------------|--------------------------------|------|------|------|------|-------------------|------------------|------------------|-------------------------------|----|
| <b>Cat Square</b> | 0.88             | 0.33                           | 0.29 | 0.01 | 0.12 | 0.20 | 0.10              | 0.13             | 0.05             | 0.02                          | 23 |
| <b>CCZO</b>       | -                | -                              | -    | -    | -    | -    | -                 | -                | -                | -                             | 2  |
| <b>Charlotte</b>  | 0.20             | 0.09                           | 0.06 | -    | 0.01 | 0.06 | 0.05              | 0.08             | 0.01             | -                             | 28 |

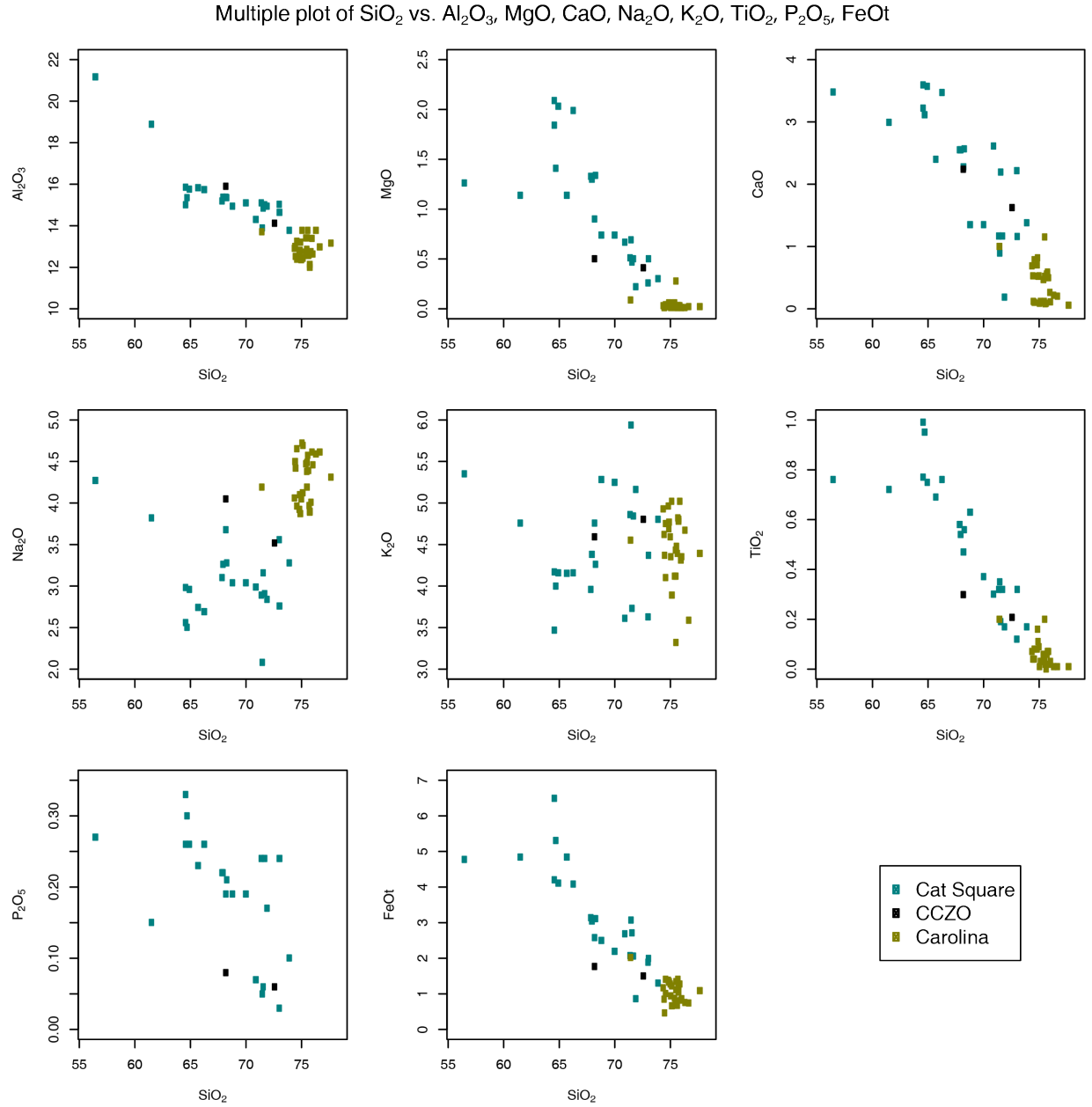


Figure 16: Elemental data plotted against  $\text{SiO}_2$  weight percent displayed a closer affinity between the CCZO and Cat Square granites than the CCZO and Charlotte terrane granites. Strong trends appeared between several oxide pairs with the exception of two elements susceptible to weathering,  $\text{Na}_2\text{O}$  and  $\text{K}_2\text{O}$ . No data was available for  $\text{P}_2\text{O}_5$  in the Charlotte terrane.

### Spider plot – REE chondrite (Anders & Grevesse 1989)

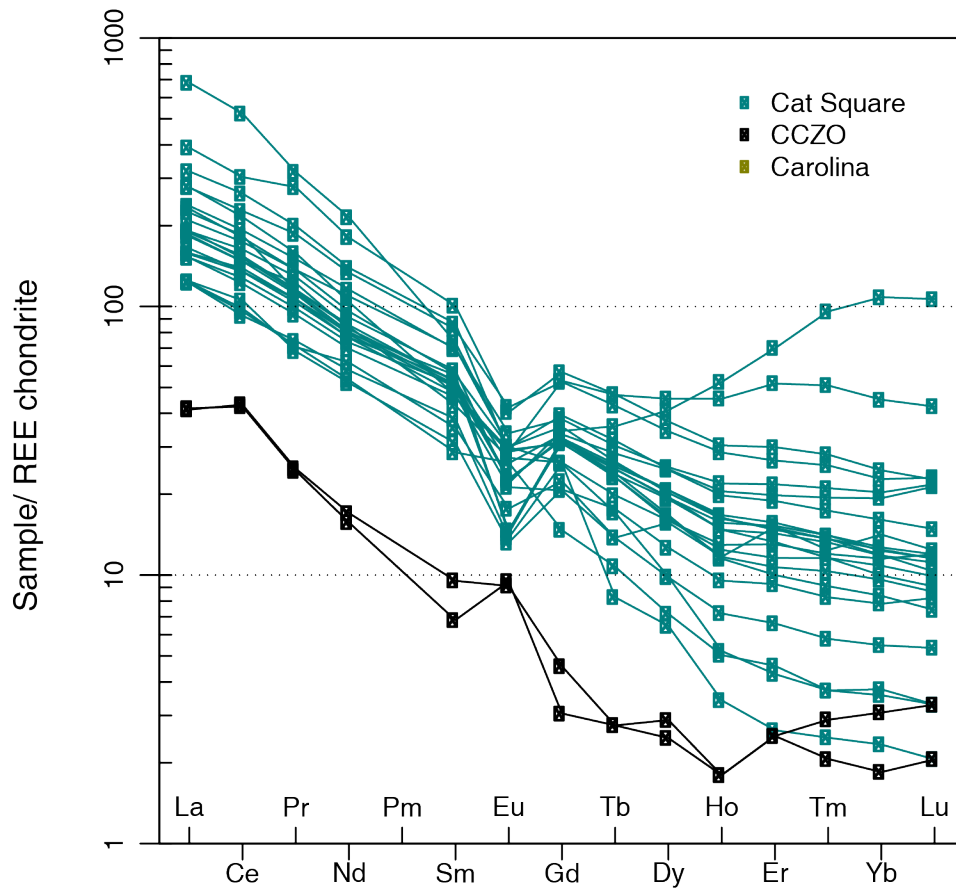


Figure 17: Chondrite normalized abundances of the Cat Square granites plotted much higher than the abundances of the CCZO granites. Additionally, Cat Square granites show a negative Eu anomaly while CCZO granites show a positive anomaly. No data was available for the Charlotte terrane granites for comparison.

# Spider plot – Upper Continental Crust (Taylor and McLennan 1995)

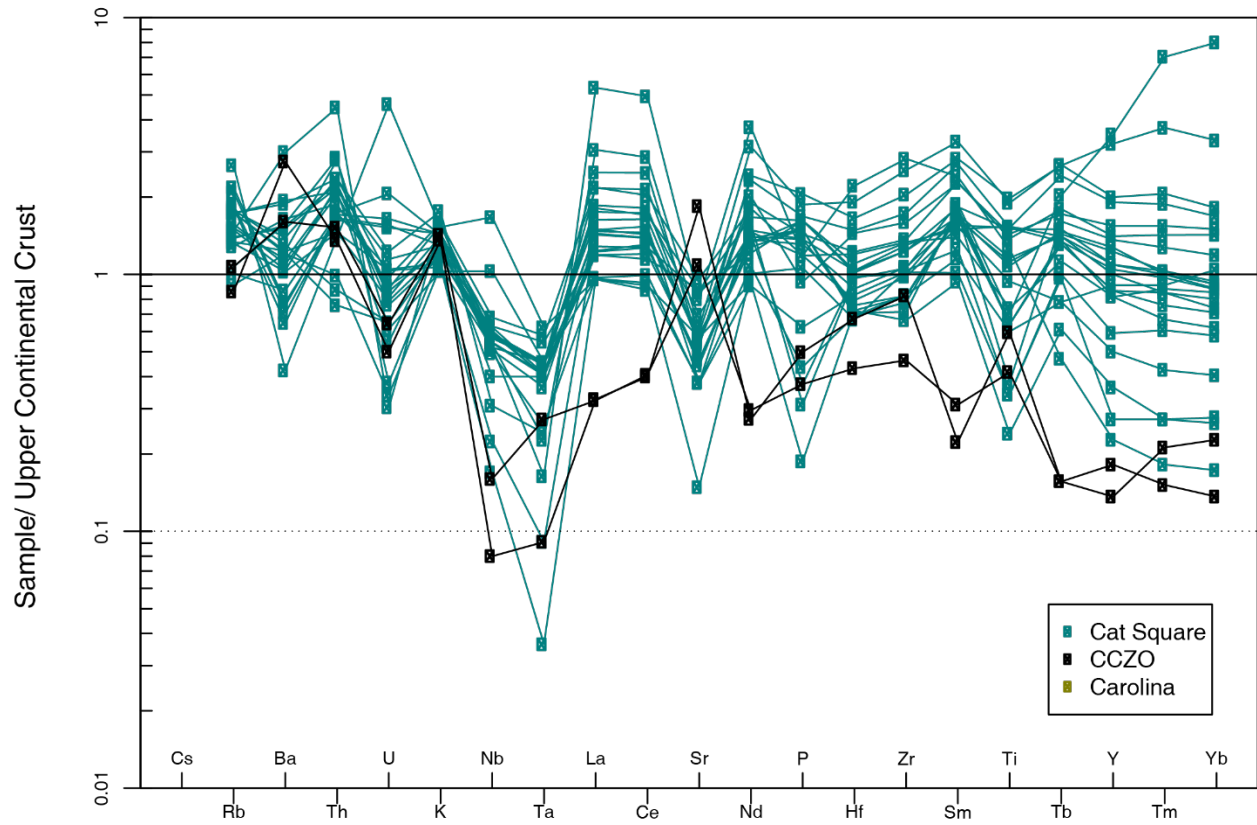


Figure 18: Abundances of Cat Square granite geochemistry closely resembles the average composition of the upper continental crust while CCZO granites show a low abundance of REEs relative to the upper continental crust.

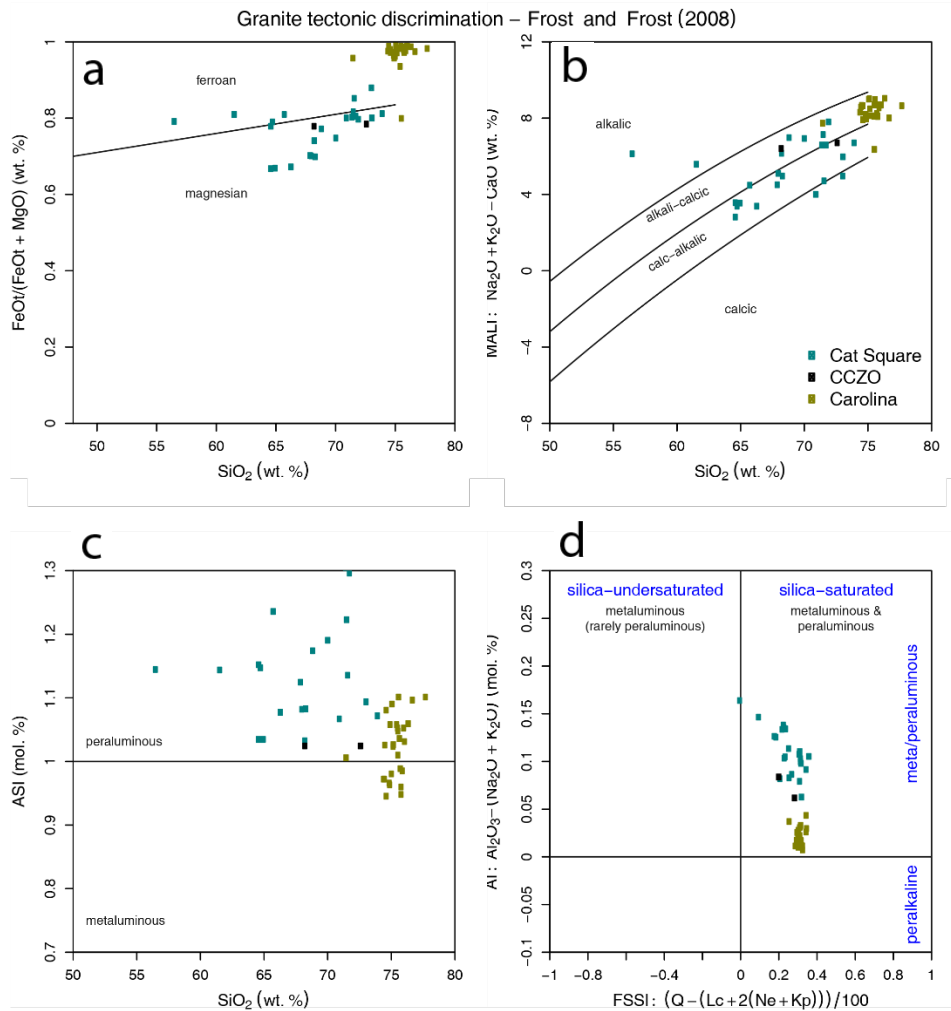


Figure 19: These plots reinforced similarities between the CCZO and Cat Square granites which were typically magnesian, peraluminous and silica saturated. (a) While most of the Cat Square granites plot as intermediate, Charlotte terrane granites plot as ferroan. (b) All three groups plot as calc-alkalic to alkali-calcic. (c) Cat Square and CCZO granites are peraluminous while Charlotte terrane granites are intermediate. (d) These granites are silica-saturated and prealuminous.



La/10 – Y/15 – Nb/8 (Cabanis + Lecolle 1989)

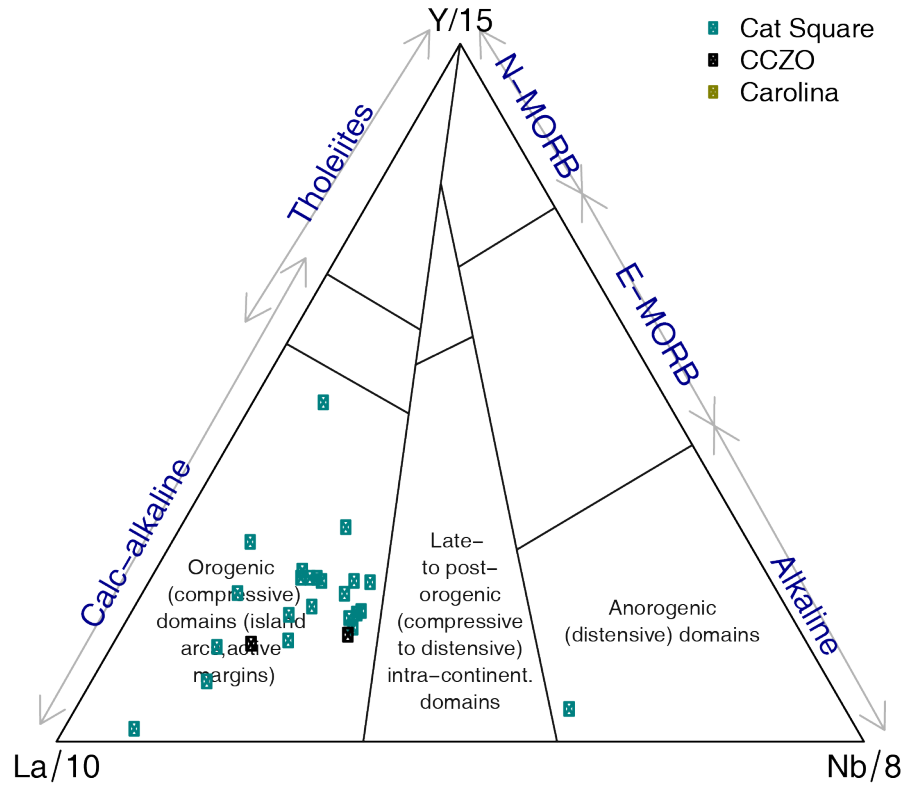


Figure 20: The plotted orogenic field that both the Cat Square and CCZO granites reside in was consistent with the regional history of the field site.

## CHAPTER 4

### DISCUSSION

#### *4.1 Assignment and Interpretation of Terranes*

In the mapped region, the biotite gneiss/amphibolite and the meta-granite units were attributed to the Cat Square terrane (Fig. 15). This determination was made off similarities between the structure and mineralogy of these rocks to literature descriptions found in Horkowitz (1984). Additionally, this interpretation was supported by previous regional scale mapping efforts which attributed lithologies found in the CCZO to the Cat Square terrane (Hatcher et al., 2007).

These units showed petrological and geochemical features that suggest a history of accreted ocean basin sediments which underwent high grade metamorphism. The meta-granite contained two types of micas, biotite and phengite. Clarke (1981) classified these two mica granites as S-types because they suggest a supracrustal source. One such supracrustal environment consistent with the site history would in the continent-continent collisional environment of the Appalachian orogeny. Here, accumulation of resistant minerals like quartz and feldspars could occur. This interpretation was also consistent with the geochemical data for the meta-granites at the CCZO which were peraluminous and silica saturated. These indicate a mature source from which the magma formed which leads to the possibility that the granites were crystalized from partial melting of the remnant ocean basin sediments. This scenario is further supported by the orogenic affinity displayed by the CCZO granites. Ultimately, the

observed lithologies and chemical analyses were consistent with literature descriptions of the Cat Square terrane.

The remaining biotite-hornblende-quartz meta-diorite, meta-tonalite, meta-granodiorite were all assigned to the Charlotte terrane (Fig. 21). These lithologies were parts of continuous units that crossed over from the Philson Crossroads quadrangle into the CCZO field site.

Researchers from the University of South Carolina have studied these rocks which they named the Wildcat Branch Complex extensively (Horkowitz, 1984; Allen and Shervais, 1991; Allen and Shervais, 1996). This previous body of work allowed for high degree of confidence in the present studies assignment of these lithologic units into the Charlotte terrane.

#### *4.2 Interpretation of the Central Piedmont Suture*

The Central Piedmont Suture was expected to lie within the boundaries of the field site from previous mapping efforts (Hatcher et al., 2007). No physical structure was identified that could be attributed to the thrust fault within the boundary of the field area. However, there was an indisputable sharp lithologic contact between the mafic and ultramafic Charlotte terrane rocks and the felsic Cat Square terrane rocks that require a structural boundary. As such, the Central Piedmont Suture was interpreted to lie along the lithologic contact between the Charlotte and Cat Square terranes. This mode of interpretation had been applied by multiple studies in the area where the lack of a clear fault boundary was not present at the interface between the two terranes (Horkowitz, 1984; Huebner et al., 2017).

Previously, the Central Piedmont Suture had been displayed on maps farther to the east (Hatcher et al., 2007). The present study revealed that this boundary lies farther west than previously thought. Additionally, the Central Piedmont Suture delineates the Wildcat Branch Complex which will allow for further investigations into the history of volcanism in Carolina.

### *4.3 Petrographic Interpretations*

Lithologies throughout the CCZO showed evidence of their history preserved in petrographic textures that were interpreted to reflect the history of the Appalachian orogeny. The primary igneous textures present in these lithologies showed clear evidence of subsequent deformation. First, evidence of syn-orogenic deformation was interpreted to have occurred during the collisional tectonics of the Appalachian orogeny. Grain boundaries in all samples were highly irregular frequently appearing as interlobate indicating recrystallization under strain (Fig.7; Gerald et al., 1983). The effects of minor strain were also evident in the protomylonitic texture of the meta-granodiorite unit (Fig. 11d). Here, tabular minerals began to show slight alignment. Rocks within the Cat Square, like the biotite gneiss/amphibolite, also showed evidence of strain through the presence of subgrains (Fig. 13d).

Evidence of potentially post-orogenic recovery was also observed throughout the thin sections which was interpreted to have occurred during the extensional tectonic regime during the rifting of Pangea. The grain boundaries in the meta-tonalite unit, for example, provided a clear example of dynamic recrystallization with the appearance of dihedral angles (Fig. 9c). Dihedral angles form as an equilibrium texture under high pressure and low shear during which the surface free energy of the crystals is minimized (Frost and Frost, 2019). Finally, the thin sections ubiquitously displayed grain fracture interpreted to have occurred more recently due to crosscutting relationships and lack of deformation (Fig. 13d).

### *4.4 Structural Interpretations*

While detailed structural analysis was outside of the scope of the present study, several qualitative observations assist in interpreting the field site. First, the highly irregular contact geometries between the Charlotte and Cat Square terranes are consistent with the regional nappe

tectonic regime (Fossen, 2016). Second, the isolated granitic body in the NW portion of the field site may be interpreted as a fenster with the overriding Charlotte terrane having eroded away. Additionally, the foliations observed trended NE which is consistent with regional trends and expected as it formed perpendicular to the vergence of Laurentia and Gondwana (Secor et al., 1986). In all, the limited structural data is internally consistent with the interpretation of the present study.

#### *4.4 Rare Earth Elements in CCZO Granites*

Although the CCZO granites share a closer affinity with the Cat Square granites than with the Charlotte terrane granites, the CCZO and Cat Square granites clearly separate out in their REE data. Most notably, the CCZO granites are highly depleted in total REE abundance in comparison to the Cat Square granites. Additionally, the Cat Square granites all show a negative Eu anomaly while the CCZO granites show a positive Eu anomaly. Perhaps the CCZO granites would share a closer similarity to the Charlotte terrane granites, but a more robust REE dataset from the Charlotte terrane would be needed to test this hypothesis.

#### *4.5 Lithologic Implications on Future CCZO Studies*

This study revealed new considerations which will help control lithologic influences in future studies at the CCZO. Because the CCZO hosts distinct mafic and felsic regions, lithology must be considered moving forward. Parity in lithologies should be maintained across field sites in order to remove the effects of differing parent materials, or studies should incorporate differing lithologies as a treatment to help explain variation in the landscape. This would be particularly important when attempting to characterize the effect different treatments (e.g. changing forest communities or land use history) would have on landscape evolution.

The CCZO showed two types of heterogeneity — one within lithologic units, and the other across lithologic units. Within unit heterogeneity was typified by the biotite gneiss/amphibolite unit. This unit showed distinct compositional zoning on the 3–10 m scale. Leucocratic and mafic foliations were observed side by side that clearly displayed the vast mineralogical differences. These foliations should be treated as chemically and physically distinct in the context of landscape evolution especially when considering preferential weathering of mafic regions. This effect should be considered within Research Watersheds 1, 3, 4, 6, and 8 at the CCZO (Fig. 3).

Across unit heterogeneity should be an important consideration for Research Watersheds 2, 5, and 7. Here, the Charlotte terrane lithologies would detract from direct comparisons to the Cat Square lithologies in other watersheds. The impact and importance of this effect was not quantified in the present study, and the degree to which chemical heterogeneity is observed within the CCZO may be minor as the majority of lithologies observed were granitoids. Future work should seek to characterize the importance geochemistry of the different granitoids to allow for greater control on future experimentation.

Research watersheds 2, 5, and 7 as well as all meta-granitoid units may have the distinct advantage of increased chemical homogeneity throughout its spatial extent. As such, more confidence may be placed in iso-chemical and iso-mineralogical starting conditions than in the biotite gneiss/amphibolite portion of the CCZO.

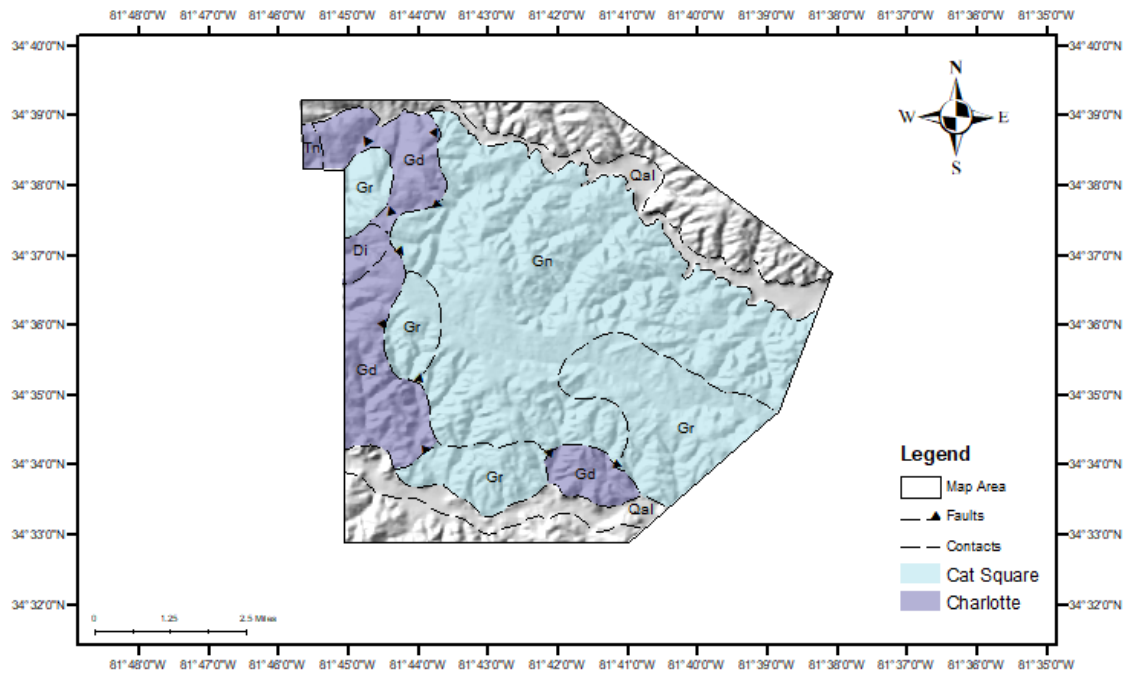


Figure 21: The Cat Square terrane composed the majority of the mapped region with smaller bodies of Charlotte terrane rocks lining the western portion of the field site. One granite body was detached from the rest of the Cat Square terrane interpreted to be a Fenster or “window” feature present in nappe tectonic regimes.

## CHAPTER 5

### SUMMARY

In order to provide a framework to understand the effect bedrock has on Critical Zone structure and processes, detailed geologic mapping was performed at the CCZO documenting the present lithologies and structural geology. The field site was found to host two distinct terranes, or genetically similar groups of rocks bound by faults. These were the Cat Square and the Charlotte terranes which were interpreted to mark the Central Piedmont Suture, a structural feature formed from the accretion of the peri-Gondwanan island Carolina onto the Laurentian margin in the Paleozoic.

Using petrography, these lithologies were examined to confirm their terrane assignment and investigate the history of the region through deformational features associated with various parts of the Appalachian orogeny. Dynamic recrystallization textures were preserved in the crystallography showing distinct syn-orogenic and post-orogenic features. Geochemical analysis further classified the nature of the granites at the CCZO as intermediate, silica-saturated, and peraluminous.

As a result of this study, research at the CCZO now can incorporate lithologic variation into consideration for future experiments allowing for meaningful investigation into the relationship between the bedrock and Critical Zone architectures. Additionally, geologists investigating the development of Carolina may now use the newly mapped areas to extend their sampling locations.



## REFERENCES

- Banwart, S., Menon, M., Bernasconi, S. M., Bloem, J., Blum, W. E. H., Souza, D. M. d., Davidsdotir, B., Duffy, C., Lair, G. J., Kram, P., Lamacova, A., Lundin, L., Nikolaidis, N. P., Novak, M., Panagos, P., Ragnarsdottir, K. V., Reynolds, B., Robinson, D., Rousseva, S., de Ruiter, P., van Gaans, P., Weng, L., White, T., and Zhang, B., 2012, Soil processes and functions across an international network of Critical Zone Observatories: Introduction to experimental methods and initial results: *Comptes Rendus Geoscience*, v. 344, no. 11, p. 758-772.
- Billings, S. A., Hirmas, D., Sullivan, P. L., Lehmeier, C. A., Bagchi, S., Min, K., Brecheisen, Z., Hauser, E., Stair, R., and Flournoy, R., 2018, Loss of deep roots limits biogenic agents of soil development that are only partially restored by decades of forest regeneration: *Elem Sci Anth*, v. 6, no. 1.
- Butler, J. R., and Fullagar, P. D., 1978, Petrochemical and geochronological studies of plutonic rocks in the southern Appalachians: III. Leucocratic adamellites of the Charlotte belt near Salisbury, North Carolina: *GSA Bulletin*, v. 89, no. 3, p. 460-466.
- Coughlan, M. R., Nelson, D. R., Lonneman, M., and Block, A. E., 2017, Historical land use dynamics in the highly degraded landscape of the Calhoun Critical Zone Observatory: *Land*, v. 6, no. 2, p. 32.

- Dallmeyer, R. D., Wright, J. E., Secor, J. D. T., and Snoke, A. W., 1986, Character of the Alleghanian orogeny in the southern Appalachians: Part II. Geochronological constraints on the tectonothermal evolution of the eastern Piedmont in South Carolina: GSA Bulletin, v. 97, no. 11, p. 1329-1344.
- Dennis, A. J., 1991, Is the central Piedmont suture a low-angle normal fault?: Geology, v. 19, no. 11, p. 1081-1084.
- Dennis, A. J., and Shervais, J. W., 1991, Arc rifting of the Carolina terrane in northwestern South Carolina: Geology, v. 19, no. 3, p. 226-229.
- Dennis, A. J., and Shervais, J. W., 1996, The Carolina Terrane in Northwestern South Carolina: Insights into the Development of an Evolving Island Arc: GSA Special Papers, v. 304.
- Dennis, A. J., and Wright, J. E., 1997, The Carolina terrane in northwestern South Carolina, USA: Late Precambrian-Cambrian deformation and metamorphism in a peri-Gondwanan oceanic arc: Tectonics, v. 16, no. 3, p. 460-473.
- Dennis, A. J., Cat Square terrane of the southern Appalachian Piedmont: correlation with northern Appalachian Salinic basins and magmatism, *in* Proceedings Geological Society of America Abstracts with Programs 2006, Volume 38, p. 73.
- Dietrich, W.E. and Lohse, K., 2014, Common questions of the US NSF–supported Critical Zone Observatories. A Guide Prepared By CZO PIs.
- Fossen, H., 2016, Structural geology, Cambridge University Press.
- Frizon de Lamotte, D., Fourdan, B., Leleu, S., Leparmentier, F., and de Clarens, P., 2015, Style of rifting and the stages of Pangea breakup: Tectonics, v. 34, no. 5, p. 1009-1029.
- Frost, B. R., and Frost, C. D., 2019, Essentials of igneous and metamorphic petrology, Cambridge University Press.

- Fullagar, P. D., Lemmon, R. E., and Ragland, P. C., 1971, Petrochemical and Geochronological Studies of Plutonic Rocks in the Southern Appalachians: I. The Salisbury Pluton: GSA Bulletin, v. 82, no. 2, p. 409-416.
- Gerald, J., Etheridge, M., and Vernon, R., 1983, Dynamic recrystallization in a naturally deformed albite: Texture, Stress, and Microstructure, v. 5, no. 4, p. 219-237.
- Griffin Jr, V. S., 1971, The Inner Piedmont belt of the southern crystalline Appalachians: Geological Society of America Bulletin, v. 82, no. 7, p. 1885-1898.
- Griffitts, W., and Overstreet, W., 1952, Granitic rocks of the western Carolina Piedmont: American Journal of Science, v. 250, no. 11, p. 777-789.
- Hatcher, R. D., and Mersch, A. J., 2006, The Appalachian Inner Piedmont: An exhumed strike-parallel, tectonically forced orogenic channel: Geological Society, London, Special Publications, v. 268, no. 1, p. 517-541.
- Hatcher, R. D., Bream, B. R., and Mersch, A. J., 2007, Tectonic map of the southern and central Appalachians: A tale of three orogens and a complete Wilson cycle: Geological Society of America Memoirs, v. 200, p. 595-632.
- Hatcher, R. D., Tollo, R., Bartholomew, M., Hibbard, J., and Karabinos, P., 2010, The Appalachian orogen: A brief summary: From Rodinia to Pangea: The Lithotectonic Record of the Appalachian Region: Geological Society of America Memoir, v. 206, p. 1-19.
- Hibbard, J. P., Stoddard, E. F., Secor, D. T., and Dennis, A. J., 2002, The Carolina Zone: overview of Neoproterozoic to Early Paleozoic peri-Gondwanan terranes along the eastern flank of the southern Appalachians: Earth-Science Reviews, v. 57, no. 3-4, p. 299-339.

- Hibbard, J. P., van Staal, C. R., and Miller, B. V., 2007, Links among Carolina, Avalonia, and Ganderia in the Appalachian peri-Gondwanan realm: Geological Society of America Special Papers, v. 433, p. 291-311.
- Hibbard, J., Pollock, J., and Bradley, P., 2013, One arc, two arcs, old arc, new arc: An overview of the Carolina terrane in central North Carolina, *in* Proceedings Carolina Geological Society Annual Meeting and Field Trip, p. 35-61.
- Hodges, C., Mallard, J., Markewitz, D., Barcellos, D., and Thompson, A., 2019, Seasonal and spatial variation in the potential for iron reduction in soils of the southeastern Piedmont of the US: Catena (Giessen), v. 180, p. 32-40.
- Horkowitz, J. P., 1984, Geology of the Philson crossroads 7 1/2 quadrangle, South Carolina: the nature of the boundary separating the inner Piedmont from the Carolina/Avalon terrane in central-northwestern South Carolina: University of South Carolina.
- Howell, D. G., 1995, Principles of terrane analysis: new applications for global tectonics, Chapman & Hall, Topics in the earth sciences: 8.
- Huebner, M. T., Hatcher, R. D., and Mersch, A. J., 2017, Confirmation of the southwest continuation of the Cat Square terrane, southern Appalachian Inner Piedmont, with implications for middle Paleozoic collisional orogenesis: American Journal of Science, v. 317, no. 2, p. 95-176.
- Janoušek, V., Farrow, C. M. & Erban, V., 2006, Interpretation of whole-rock geochemical data in igneous geochemistry: introducing Geochemical Data Toolkit (GCDkit), Journal of Petrology 47(6):1255-1259.

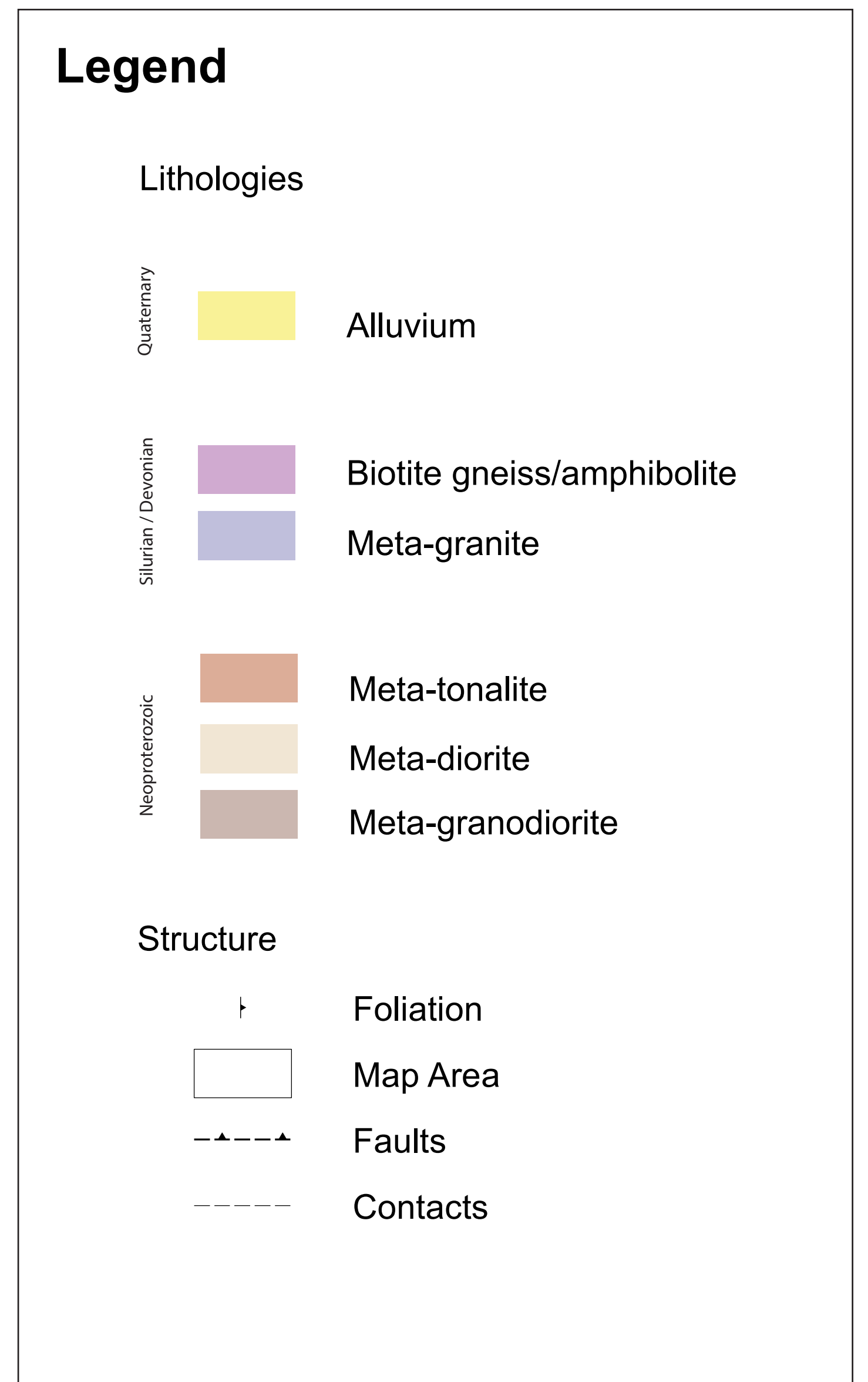
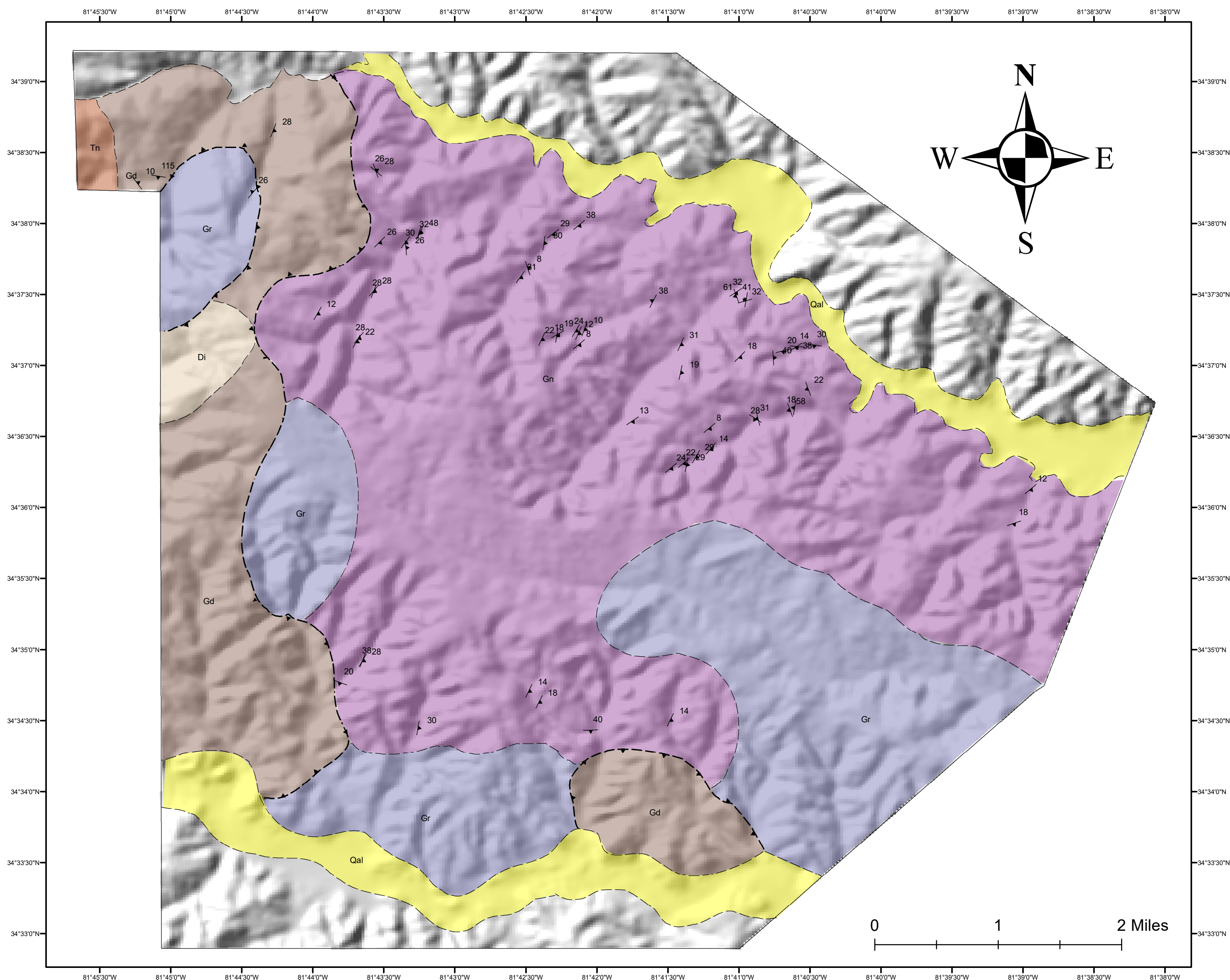
- Merschat, A. J., Hatcher Jr, R. D., and Davis, T. L., 2005, The northern Inner Piedmont, southern Appalachians, USA: kinematics of transpression and SW-directed mid-crustal flow: *Journal of Structural Geology*, v. 27, no. 7, p. 1252-1281.
- Merschat, A. J., and Hatcher, J. R. D., 2007, The Cat Square terrane: Possible Siluro-Devonian remnant ocean basin in the Inner Piedmont, southern Appalachians, USA, *in* Hatcher, J. R. D., Carlson, M. P., McBride, J. H., and Catalán, J. R. M., eds., 4-D Framework of Continental Crust, Geological Society of America.
- Merschat, A. J., 2009, Assembling the Blue Ridge and Inner Piedmont: Insights into the nature and timing of terrane accretion in the southern Appalachian orogen from geologic mapping, stratigraphy, kinematic analysis, petrology, geochemistry, and modern geochronology.
- Passchier, C. W., and Trouw, R. A., 2005, *Microtectonics*, Springer Science & Business Media.
- Phillips, W. J., 1974, The development of vein and rock textures by tensile strain crystallization: *Journal of the Geological Society*, v. 130, no. 5, p. 441-448.
- Pollock, J. C., Hibbard, J. P., and van Staal, C. R., 2011, A paleogeographical review of the peri-Gondwanan realm of the Appalachian orogen: *Canadian Journal of Earth Sciences*, v. 49, no. 1, p. 259-288.
- Richter, D. d., Bacon, A. R., Billings, S. A., Binkley, D., Buford, M., Callahan, M. A., Curry, A. E., Fimmen, R. L., Grandy, A. S., Heine, P. R., Hofmockel, M., Jackson, J. A., LeMaster, E., Li, J., Markewitz, D., Mobley, M. L., Morrison, M. W., Strickland, M. S., Waldrop, T., and Wells, C. G., 2014, Evolution of Soil, Ecosystem, and Critical Zone Research at the USDA FS Calhoun Experimental Forest: *USDA Forest Service Experimental Forests & Ranges*, p. 405.

- Secor, D. T., Snoke, A. W., and Dallmeyer, R. D., 1986, Character of the Alleghanian orogeny in the southern Appalachians: Part III. Regional tectonic relations: Geological Society of America Bulletin, v. 97, no. 11, p. 1345-1353.
- Secor, D. T., Snoke, A. W., Bramlett, K. W., Costello, O. P., and Kimbrell, O. P., 1986, Character of the Alleghanian orogeny in the southern Appalachians: Part I. Alleghanian deformation in the eastern Piedmont of South Carolina: Geological Society of America Bulletin v. 97, no. 11, p. 1319-1328.
- Sengebush, R. M., 2013, Basic Geologic Mapping, Fifth Edition by Richard J. Lisle, Peter Brabham, and John Barnes: United States, Geological Society of America, p. 196.
- South Carolina Department of Natural Resources, 2018, Geologic Map Coverage at 1:24,000 scale, [http://www.dnr.sc.gov/geology/images/Geologic\\_Map\\_Coverage\\_18-19.pdf](http://www.dnr.sc.gov/geology/images/Geologic_Map_Coverage_18-19.pdf) (Accessed March 2020).
- St. Clair, J., Moon, S., Holbrook, W. S., Perron, J. T., Riebe, C. S., Martel, S. J., Carr, B., Harman, C., Singha, K., and Richter, D. d., 2015, Geophysical imaging reveals topographic stress control of bedrock weathering: Science, v. 350, no. 6260, p. 534-538.
- Thomas, W. A., 2006, Tectonic inheritance at a continental margin: GSA today, v. 16, no. 2, p. 4-11.
- Thornbury, W. D., 1965, Regional geomorphology of the United States, New York, Wiley [1965].
- Wade, A. M., Richter, D. D., Cherkinsky, A., Craft, C. B., and Heine, P. R., Limited carbon contents of centuries old soils forming in legacy sediment, Netherlands, 2020 2020, Elsevier Science B.V., Amsterdam.

- West, T. E., 1998, Structural analysis of the Carolina-Inner Piedmont terrane boundary: Implications for the age and kinematics of the central Piedmont suture, a terrane boundary that records Paleozoic Laurentia-Gondwana interactions: *Tectonics*, v. 17, no. 3, p. 379-394.
- Wickham, H., Averick, M., Bryan, J., Chang, W., McGowan, L., François, R., Grolemund, G., Hayes, A., Henry, L., and Hester, J., 2019, Welcome to the Tidyverse: *Journal of Open Source Software*, v. 4, no. 43, p. 1686.
- Williams, H., and Hatcher Jr, R. D., 1983, Appalachian suspect terranes: Contributions to the tectonics geophysics of mountain chains: *Geological Society of America Memoir*, v. 158, p. 33-53.
- Wortman, G. L., Samson, S. D., and Hibbard, J. P., 2000, Precise U-Pb Zircon Constraints on the Earliest Magmatic History of the Carolina Terrane: *The Journal of Geology*, v. 108, no. 3, p. 321-338.

APPENDIX A:  
GEOLOGIC MAP



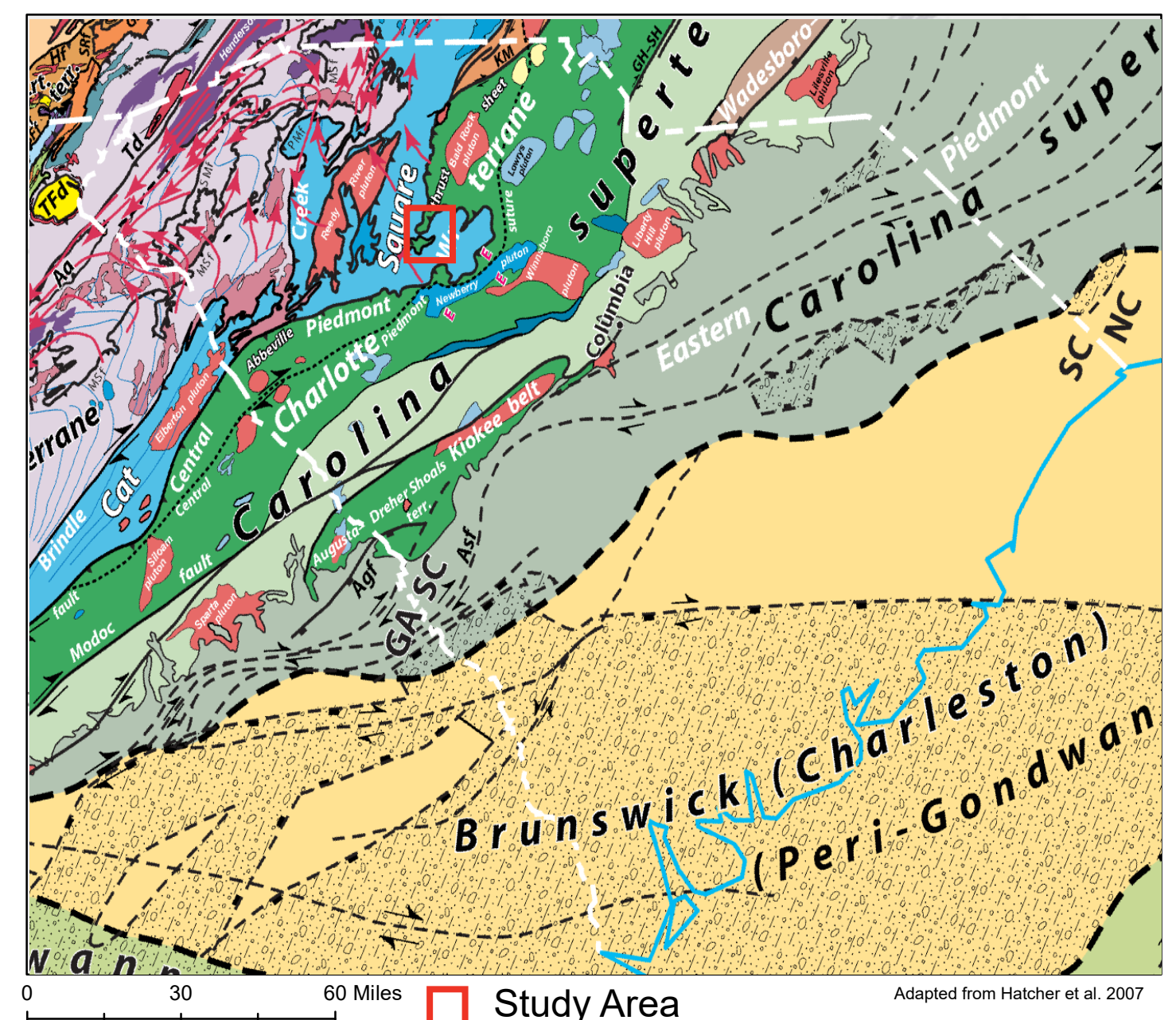


# Geology of the Calhoun Critical Zone Observatory

by Bear Jordan

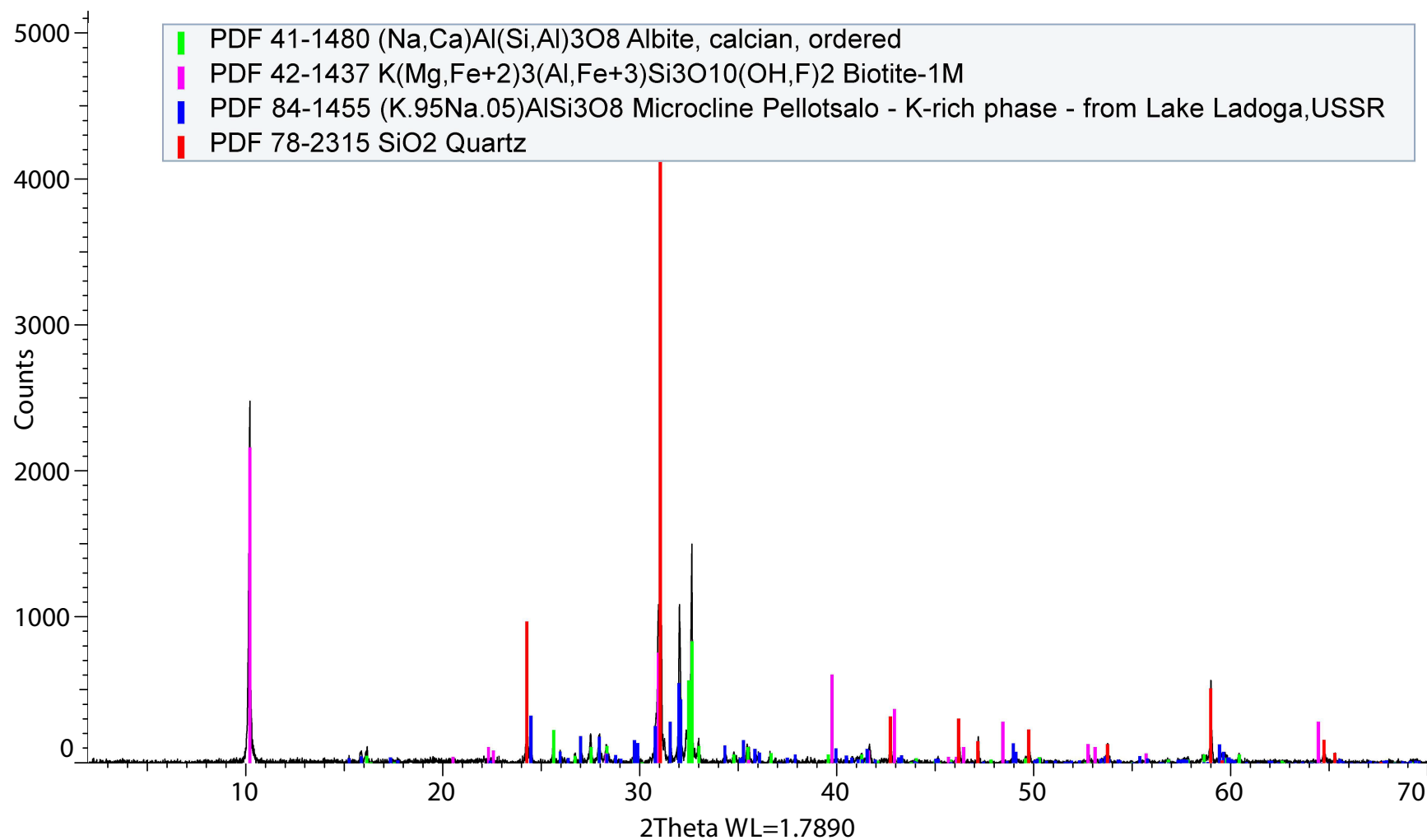
This map was produced in conjunction with the University of Georgia and the Calhoun Critical Zone Observatory. Further information about the mapped area can be found in "Geology of the Calhoun Critical Zone Observatory" by Bear Jordan.

Corresponding email: [bearjordan@gmail.com](mailto:bearjordan@gmail.com)



APPENDIX B:  
X-RAY DIFFRACTION DATA

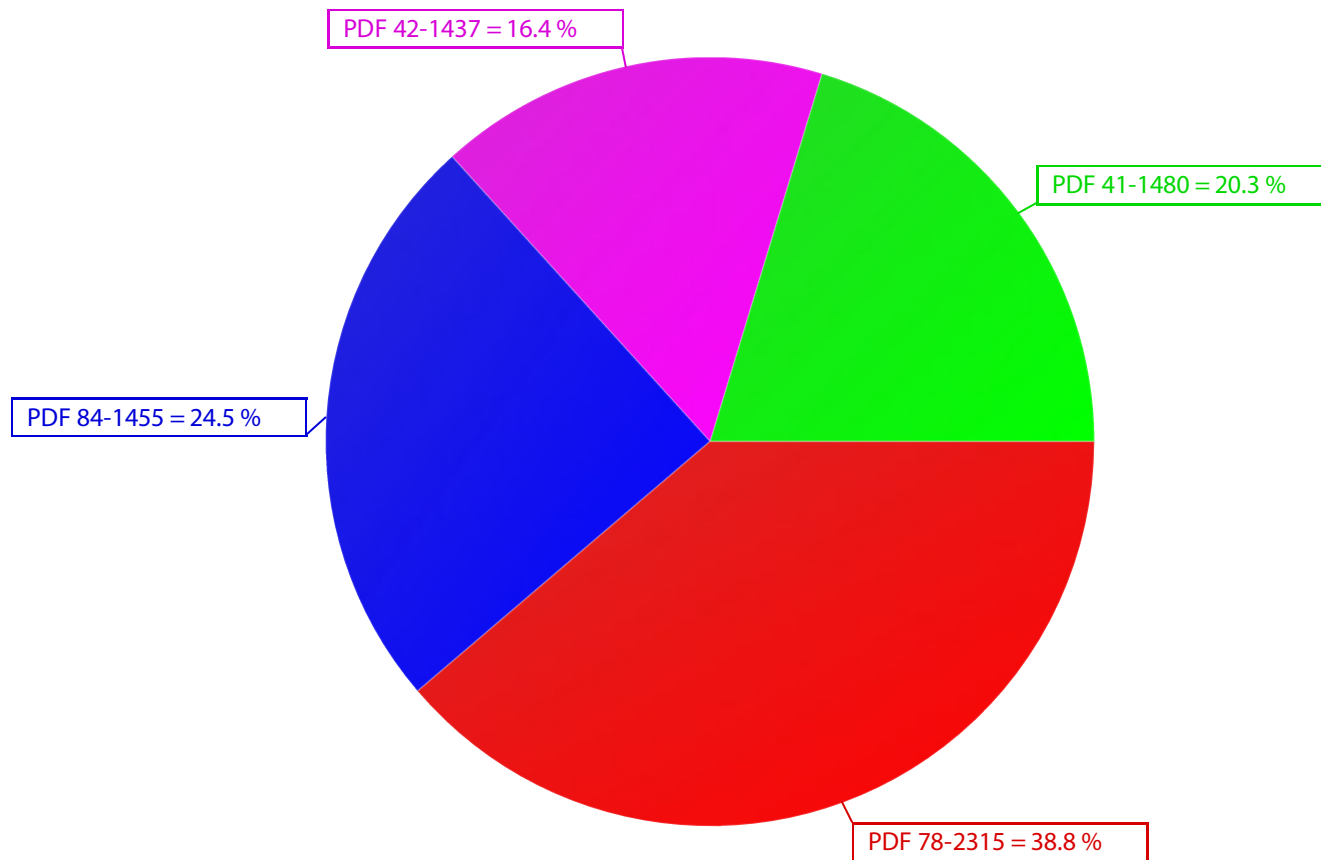
## Biotite Meta-Granodiorite



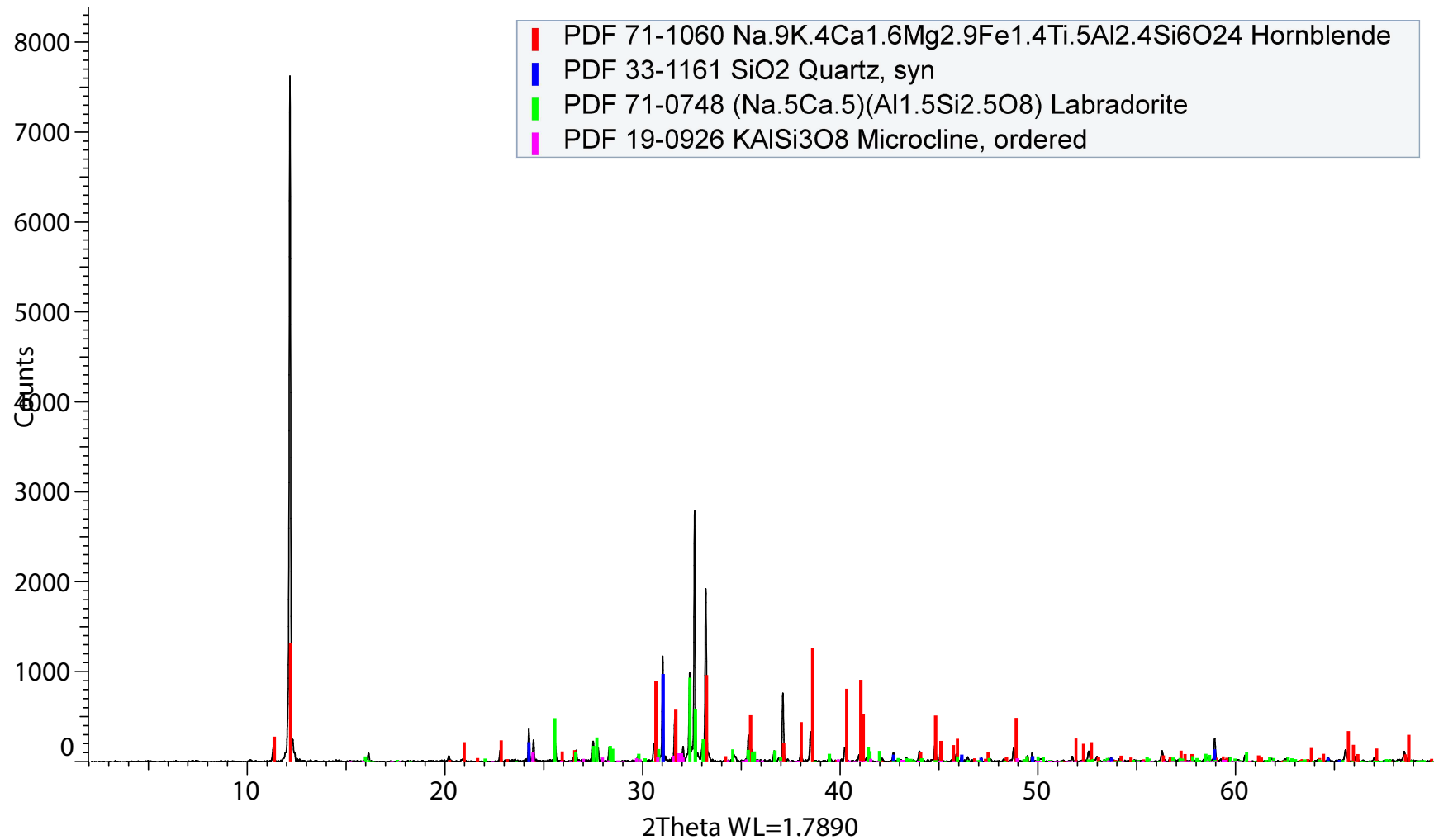
## Biotite Meta-Granodiorite

---

S-Q



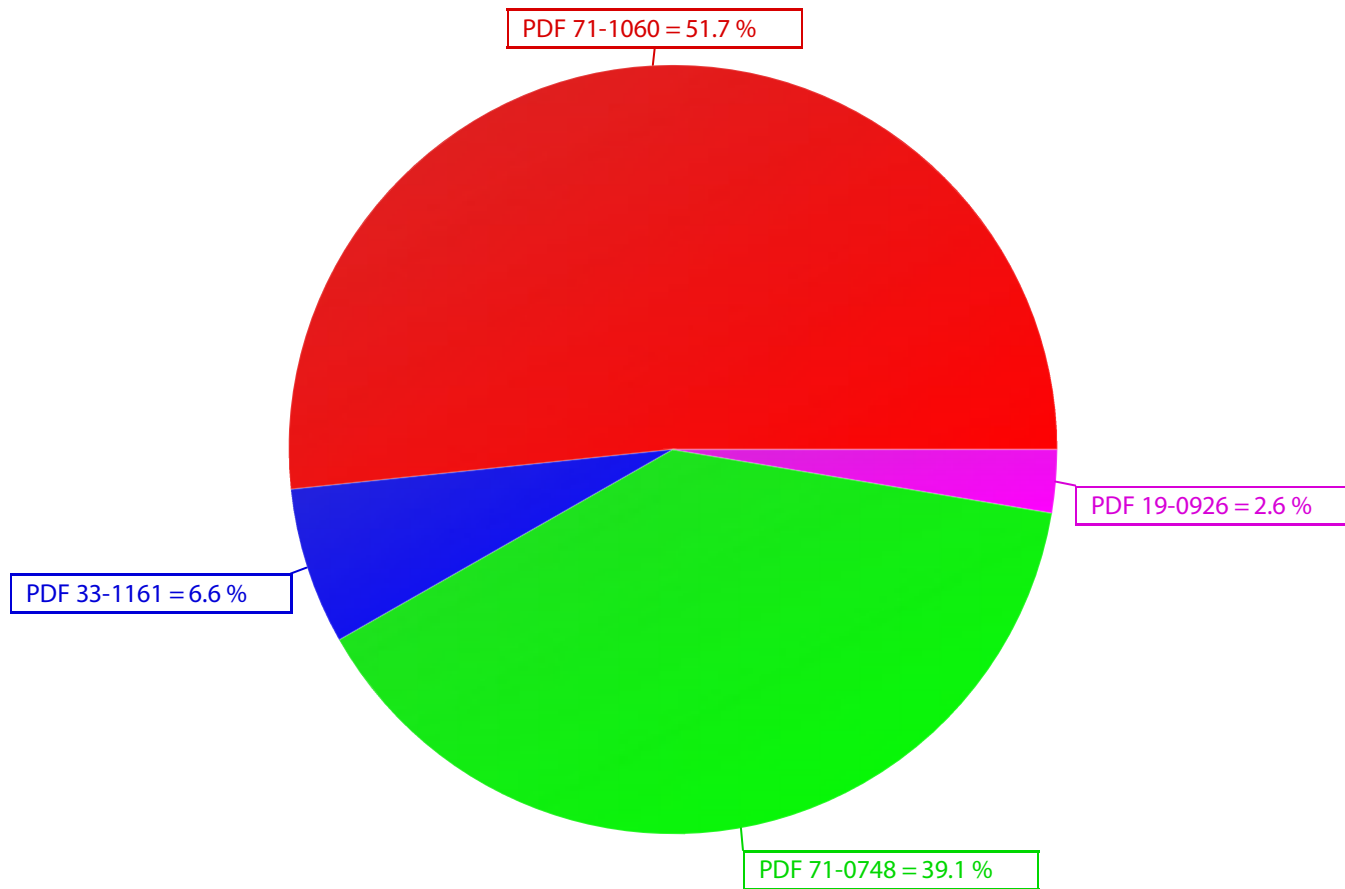
## Biotite Gneiss/Amphibolite



## Biotite Gneiss/Amphibolite

---

S-Q



APPENDIX C:  
GEOCHEMICAL DATA

| Terrane    | Granitoid    | Sample | Age | SiO2  | Al2O3 | Fe2O3 | MnO  | MgO  | CaO  | Na2O | K2O  | TiO2 | P2O5 |
|------------|--------------|--------|-----|-------|-------|-------|------|------|------|------|------|------|------|
| Carolina   | Gold Hill    | NC-318 | 368 | 75.6  | 12.7  | 1.24  | -    | 0.28 | 1.15 | 4.19 | 3.32 | 0.2  | -    |
| Carolina   | Salisbury    | 96     | 411 | 75.5  | 13.4  | 0.97  | 0.18 | 0.06 | 0.47 | 4.47 | 4.12 | 0.06 | -    |
| Carolina   | Southmont    | 744    | 486 | 74.47 | 12.9  | 1.3   | -    | 0.03 | 0.69 | 4.06 | 4.93 | 0.07 | -    |
| Carolina   | Southmont    | 928    | 486 | 74.69 | 12.38 | 1.56  | -    | 0.04 | 0.79 | 3.96 | 4.75 | 0.08 | -    |
| Carolina   | Southmont    | 930    | 486 | 75.09 | 12.35 | 1.41  | -    | 0.05 | 0.53 | 4.05 | 4.59 | 0.09 | -    |
| Carolina   | Southmont    | 931    | 486 | 74.96 | 12.82 | 1.47  | -    | 0.05 | 0.82 | 4.1  | 4.69 | 0.16 | -    |
| Carolina   | Southmont    | 932    | 486 | 75.8  | 12.62 | 1.56  | -    | 0.03 | 0.56 | 3.97 | 4.82 | 0.06 | -    |
| Carolina   | Southmont    | 743*   | 486 | 74.92 | 12.64 | 1.54  | -    | 0.04 | 0.7  | 3.92 | 4.96 | 0.08 | -    |
| Carolina   | Southmont    | 745*   | 486 | 71.54 | 13.71 | 2.25  | -    | 0.09 | 1    | 4.19 | 4.55 | 0.2  | -    |
| Carolina   | Southmont    | 746*   | 486 | 75.85 | 12.14 | 1.35  | -    | 0.03 | 0.59 | 3.89 | 4.78 | 0.07 | -    |
| Carolina   | Southmont    | 927*   | 486 | 75.85 | 11.99 | 1.17  | -    | 0.03 | 0.57 | 3.9  | 4.8  | 0.07 | -    |
| Carolina   | Southmont    | 929*   | 486 | 75.95 | 12.75 | 1.42  | -    | 0.03 | 0.5  | 4.01 | 5.02 | 0.07 | -    |
| Carolina   | Southmont    | 933*   | 486 | 75.22 | 12.72 | 1.35  | -    | 0.02 | 0.12 | 4.12 | 5.02 | 0.03 | -    |
| Carolina   | Southmont    | NC-62* | 486 | 75    | 13.2  | 1.49  | -    | 0.06 | 0.52 | 3.87 | 4.77 | 0.11 | -    |
| Carolina   | Yadkin       | 747    | 461 | 74.54 | 12.99 | 0.94  | -    | 0.01 | 0.53 | 4.5  | 4.62 | 0.04 | -    |
| Carolina   | Yadkin       | 748    | 461 | 74.68 | 13.26 | 1.12  | -    | 0.02 | 0.1  | 4.65 | 4.1  | 0.04 | -    |
| Carolina   | Yadkin       | 749    | 461 | 74.58 | 12.53 | 0.52  | -    | 0.01 | 0.12 | 4.42 | 4.37 | 0.04 | -    |
| Carolina   | Yadkin       | 750    | 461 | 75.25 | 12.43 | 0.73  | -    | 0.02 | 0.1  | 4.69 | 3.89 | 0.03 | -    |
| Carolina   | Yadkin       | 751    | 461 | 75.58 | 12.86 | 0.88  | -    | 0.01 | 0.12 | 4.38 | 4.43 | 0.03 | -    |
| Carolina   | Yadkin       | 752    | 461 | 75.73 | 12.57 | 0.75  | -    | 0.01 | 0.09 | 4.39 | 4.39 | 0    | -    |
| Carolina   | Yadkin       | 920    | 461 | 75.66 | 13.78 | 1.24  | -    | 0.02 | 0.08 | 4.57 | 4.48 | 0.02 | -    |
| Carolina   | Yadkin       | 921    | 461 | 76.75 | 12.97 | 0.83  | -    | 0.02 | 0.2  | 4.61 | 3.59 | 0.01 | -    |
| Carolina   | Yadkin       | 922    | 461 | 75.14 | 13.78 | 1.05  | -    | 0.01 | 0.09 | 4.72 | 4.35 | 0.01 | -    |
| Carolina   | Yadkin       | 923    | 461 | 76.41 | 13.78 | 0.84  | -    | 0.01 | 0.22 | 4.59 | 4.67 | 0.01 | -    |
| Carolina   | Yadkin       | 924    | 461 | 77.76 | 13.16 | 1.21  | -    | 0.02 | 0.06 | 4.31 | 4.39 | 0.01 | -    |
| Carolina   | Yadkin       | 925    | 461 | 76.06 | 13.39 | 0.91  | -    | 0.01 | 0.26 | 4.61 | 4.31 | 0.02 | -    |
| Carolina   | Yadkin       | 926    | 461 | 76.12 | 12.63 | 0.95  | -    | 0.01 | 0.11 | 4.46 | 4.35 | 0.03 | -    |
| Carolina   | Yadkin       | NC-97  | 461 | 75.6  | 13.4  | 1.49  | -    | 0.02 | 0.52 | 4.49 | 4.12 | 0.04 | -    |
| Cat Square | Anderson Mil | AMG    | 415 | 71    | 14.3  | 2.99  | 0.07 | 0.67 | 2.61 | 2.99 | 3.61 | 0.3  | 0.07 |
| Cat Square | Cherryville  | C-10   | 355 | 72    | 14.93 | 0.96  | 0.02 | 0.22 | 0.19 | 2.84 | 5.16 | 0.17 | 0.17 |
| Cat Square | Gray Court   | GC-1   | 357 | 74    | 13.78 | 1.44  | 0.03 | 0.3  | 1.38 | 3.28 | 4.8  | 0.17 | 0.1  |
| Cat Square | High Falls   | FRHF   | 372 | 68.3  | 15.38 | 2.86  | 0.06 | 0.9  | 2.28 | 3.68 | 4.76 | 0.47 | 0.19 |
| Cat Square | High Falls   | HF862  | 378 | 61.6  | 18.89 | 5.38  | 0.09 | 1.14 | 2.99 | 3.82 | 4.76 | 0.72 | 0.15 |



| Terrane    | Granitoid  | Sample  | Age | SiO2  | Al2O3 | Fe2O3 | MnO   | MgO  | CaO  | Na2O | K2O  | TiO2  | P2O5 |
|------------|------------|---------|-----|-------|-------|-------|-------|------|------|------|------|-------|------|
| Cat Square | High Falls | HFSP    | 399 | 56.56 | 21.17 | 5.31  | 0.08  | 1.26 | 3.48 | 4.27 | 5.35 | 0.76  | 0.27 |
| Cat Square | High Falls | IS370   | 378 | 65.8  | 15.83 | 5.38  | 0.12  | 1.14 | 2.4  | 2.74 | 4.15 | 0.69  | 0.23 |
| Cat Square | High Falls | S123    | 383 | 71.57 | 13.88 | 3.41  | 0.27  | 0.69 | 0.89 | 2.08 | 5.94 | 0.35  | 0.05 |
| Cat Square | Toluca     | CH117   | 383 | 71.65 | 14.85 | 3.01  | 0.1   | 0.47 | 2.19 | 3.16 | 3.73 | 0.19  | 0.06 |
| Cat Square | Toluca     | TOL-1   | 383 | 73.1  | 15.04 | 2.1   | 0.04  | 0.26 | 2.22 | 3.56 | 3.63 | 0.12  | 0.03 |
| Cat Square | Toluca     | TOL-10  | 383 | 70.1  | 15.1  | 2.43  | 0.02  | 0.74 | 1.35 | 3.04 | 5.25 | 0.37  | 0.19 |
| Cat Square | Toluca     | TOL-11  | 383 | 68.9  | 14.93 | 2.78  | 0.02  | 0.74 | 1.35 | 3.04 | 5.28 | 0.63  | 0.19 |
| Cat Square | Walker Top | B9WT    | 357 | 64.67 | 15.01 | 7.21  | 0.12  | 1.84 | 3.22 | 2.56 | 3.47 | 0.99  | 0.33 |
| Cat Square | Walker Top | GL-1    | 357 | 66.36 | 15.74 | 4.54  | 0.09  | 1.99 | 3.47 | 2.69 | 4.16 | 0.76  | 0.26 |
| Cat Square | Walker Top | GL-1B   | 357 | 65.03 | 15.77 | 4.56  | 0.09  | 2.03 | 3.57 | 2.96 | 4.16 | 0.75  | 0.26 |
| Cat Square | Walker Top | GL-2    | 357 | 64.66 | 15.85 | 4.67  | 0.09  | 2.09 | 3.59 | 2.98 | 4.17 | 0.77  | 0.26 |
| Cat Square | Walker Top | MV-19   | 408 | 67.96 | 15.18 | 3.48  | 0.06  | 1.33 | 2.55 | 3.1  | 3.96 | 0.58  | 0.22 |
| Cat Square | Walker Top | MV-19B  | 357 | 68.37 | 15.35 | 3.45  | 0.06  | 1.34 | 2.57 | 3.28 | 4.26 | 0.56  | 0.21 |
| Cat Square | Walker Top | MV-249  | 357 | 68.05 | 15.38 | 3.38  | 0.06  | 1.3  | 2.55 | 3.26 | 4.38 | 0.54  | 0.22 |
| Cat Square | Walker Top | MV-564  | 357 | 71.48 | 15.09 | 2.3   | 0.05  | 0.51 | 1.17 | 2.89 | 4.86 | 0.32  | 0.24 |
| Cat Square | Walker Top | MV-566  | 357 | 73.13 | 14.64 | 2.22  | 0.04  | 0.5  | 1.16 | 2.76 | 4.37 | 0.32  | 0.24 |
| Cat Square | Walker Top | MV-566B | 357 | 71.79 | 15.01 | 2.29  | 0.05  | 0.5  | 1.17 | 2.91 | 4.84 | 0.32  | 0.24 |
| Cat Square | Walker Top | RP281   | 357 | 64.81 | 15.35 | 5.9   | 0.09  | 1.41 | 3.11 | 2.5  | 4    | 0.95  | 0.3  |
| CCZO       | CCZO       | BR02    | -   | 68.28 | 15.89 | 1.96  | 0.035 | 0.5  | 2.24 | 4.05 | 4.59 | 0.298 | 0.08 |
| CCZO       | CCZO       | HC02    | -   | 72.67 | 14.12 | 1.66  | 0.028 | 0.41 | 1.62 | 3.52 | 4.8  | 0.208 | 0.06 |

| Terrane    | Granitoid     | Sample  | Age | V  | Cr   | Cu   | Zn   | Rb  | Sr  | Y  | Zr  | Nb   |
|------------|---------------|---------|-----|----|------|------|------|-----|-----|----|-----|------|
| Cat Square | Anderson Mill | AMG     | 415 | 35 | 3    | 1.1  | 60.4 | 148 | 133 | 20 | 158 | 13   |
| Cat Square | Cherryville   | C-10    | 355 | 6  | 3.2  | 1.37 | 54.6 | 298 | 52  | 6  | 197 | 41.8 |
| Cat Square | Gray Court    | GC-1    | 357 | 11 | 2.1  | 3.9  | 39.4 | 204 | 132 | 13 | 194 | 12.3 |
| Cat Square | High Falls    | FRHF    | 372 | 44 | 13.3 | 4    | 61   | 194 | 337 | 11 | 186 | 10   |
| Cat Square | High Falls    | HF862   | 378 | 63 | 14.9 | 2    | 91   | 155 | 190 | 34 | 303 | 14.6 |
| Cat Square | High Falls    | HFSP    | 399 | 67 | 30   | -    | 84   | 194 | 208 | 42 | 329 | 17   |
| Cat Square | High Falls    | IS370   | 378 | 63 | 21.7 | 17   | 91   | 144 | 187 | 31 | 260 | 14.7 |
| Cat Square | High Falls    | S123    | 383 | 31 | -    | -    | 41   | 198 | 133 | 77 | 201 | 7.7  |
| Cat Square | Toluca        | CH117   | 383 | 13 | 8    | 37   | 40   | 113 | 204 | 30 | 190 | 5.6  |
| Cat Square | Toluca        | TOL-1   | 383 | 8  | 0.5  | -    | 31.2 | 102 | 199 | 8  | 126 | 4.24 |
| Cat Square | Toluca        | TOL-10  | 383 | 37 | 9.7  | 2.35 | 46.8 | 157 | 244 | 18 | 254 | 14.4 |
| Cat Square | Toluca        | TOL-11  | 383 | 44 | 2.9  | 8.08 | 90.2 | 165 | 280 | 5  | 536 | 13   |
| Cat Square | Walker Top    | B9WT    | 357 | 78 | 33.1 | 13   | 110  | 150 | 184 | 71 | 388 | 25.7 |
| Cat Square | Walker Top    | GL-1    | 357 | 94 | 73.6 | 10   | 71   | 200 | 297 | 23 | 247 | 14.7 |
| Cat Square | Walker Top    | GL-1B   | 357 | 96 | 58.3 | 10   | 63   | 195 | 304 | 24 | 235 | 14.1 |
| Cat Square | Walker Top    | GL-2    | 357 | 97 | 61.3 | 9    | 64   | 195 | 305 | 24 | 253 | 14.3 |
| Cat Square | Walker Top    | MV-19   | 408 | 64 | 50.1 | 2    | 61   | 167 | 195 | 22 | 157 | 13.5 |
| Cat Square | Walker Top    | MV-19B  | 357 | 62 | 42.3 | 4    | 51   | 176 | 202 | 27 | 203 | 13.6 |
| Cat Square | Walker Top    | MV-249  | 357 | 61 | 32.2 | 4    | 49   | 170 | 204 | 28 | 235 | 12.7 |
| Cat Square | Walker Top    | MV-564  | 357 | 19 | 3.9  | 1    | 56   | 244 | 162 | 19 | 156 | 15.6 |
| Cat Square | Walker Top    | MV-566  | 357 | 22 | 8.6  | 1    | 65   | 209 | 155 | 18 | 136 | 15.1 |
| Cat Square | Walker Top    | MV-566B | 357 | 19 | 6.2  | 2    | 58   | 234 | 163 | 19 | 148 | 15.7 |
| Cat Square | Walker Top    | RP281   | 357 | 75 | 31   | 20   | 77   | 120 | 217 | 44 | 484 | 13.4 |
| CCZO       | CCZO          | BR02    | -   | 28 | -    | 20   | 40   | 96  | 644 | 3  | 157 | 2    |
| CCZO       | CCZO          | HC02    | -   | 21 | -    | 40   | 40   | 120 | 381 | 4  | 88  | 4    |

| Terrane    | Granitoid     | Sample  | Age | Ba   | La    | Ce    | Pr    | Nd    | Sm    | Eu   | Gd   | Tb   |
|------------|---------------|---------|-----|------|-------|-------|-------|-------|-------|------|------|------|
| Cat Square | Anderson Mill | AMG     | 415 | 564  | 28.9  | 59.3  | 6.3   | 28    | 5.2   | 0.99 | 4.4  | 0.5  |
| Cat Square | Cherryville   | C-10    | 355 | 233  | 28.71 | 55.74 | 6.64  | 26.17 | 5.61  | 0.77 | 5.11 | 0.62 |
| Cat Square | Gray Court    | GC-1    | 357 | 355  | 29.15 | 63.59 | 6.07  | 23.48 | 4.56  | 0.74 | 4.1  | 0.64 |
| Cat Square | High Falls    | FRHF    | 372 | 1066 | 65.4  | 130   | 14.1  | 47    | 6.89  | 1.19 | 4.06 | 0.5  |
| Cat Square | High Falls    | HF862   | 378 | 851  | 55.7  | 116   | 13.4  | 52.3  | 10.2  | 1.89 | 7.48 | 1.1  |
| Cat Square | High Falls    | HFSP    | 399 | 1036 | 65.1  | 137   | 16.6  | 60.5  | 12.1  | 2.36 | 10.3 | 1.55 |
| Cat Square | High Falls    | IS370   | 378 | 905  | 49    | 105   | 12.2  | 49.4  | 10.3  | 1.68 | 7.73 | 1.15 |
| Cat Square | High Falls    | S123    | 383 | 765  | 44.7  | 98.5  | 11.5  | 41.2  | 8.48  | 1.23 | 6.77 | 1.3  |
| Cat Square | Toluca        | CH117   | 383 | 477  | 42.8  | 88.7  | 10.9  | 37.3  | 7.77  | 1.46 | 6.57 | 1.03 |
| Cat Square | Toluca        | TOL-1   | 383 | 661  | 28.78 | 57.88 | 6.36  | 24.12 | 4.21  | 1.47 | 2.89 | 0.39 |
| Cat Square | Toluca        | TOL-10  | 383 | 832  | 52.56 | 111   | 10.2  | 38.07 | 6.29  | 1.53 | 5.16 | 0.72 |
| Cat Square | Toluca        | TOL-11  | 383 | 1642 | 160   | 316   | 28.24 | 97.36 | 10.81 | 1.68 | 5.14 | 0.3  |
| Cat Square | Walker Top    | B9WT    | 357 | 679  | 74.8  | 159   | 17.8  | 63.1  | 12.7  | 1.61 | 10.4 | 1.7  |
| Cat Square | Walker Top    | GL-1    | 357 | 719  | 38.6  | 81.5  | 9.48  | 34.6  | 6.99  | 1.64 | 6.07 | 0.86 |
| Cat Square | Walker Top    | GL-1B   | 357 | 676  | 54.3  | 109   | 12.2  | 43.4  | 8.24  | 1.68 | 7.01 | 0.96 |
| Cat Square | Walker Top    | GL-2    | 357 | 664  | 35.7  | 73.4  | 8.31  | 31.5  | 6.75  | 1.61 | 6.18 | 0.9  |
| Cat Square | Walker Top    | MV-19   | 408 | 572  | 44.2  | 93.1  | 10.3  | 38.6  | 7.71  | 1.28 | 6.24 | 0.9  |
| Cat Square | Walker Top    | MV-19B  | 357 | 603  | 43.3  | 88.9  | 9.92  | 35.6  | 7.36  | 1.27 | 6.26 | 0.92 |
| Cat Square | Walker Top    | MV-249  | 357 | 628  | 44.9  | 91.4  | 10.1  | 36.4  | 7.54  | 1.26 | 6.36 | 0.94 |
| Cat Square | Walker Top    | MV-564  | 357 | 429  | 35.7  | 77    | 8.78  | 33.2  | 7.51  | 0.82 | 6.11 | 0.84 |
| Cat Square | Walker Top    | MV-566  | 357 | 389  | 37.1  | 83.8  | 9.49  | 36    | 8.16  | 0.8  | 6.23 | 0.87 |
| Cat Square | Walker Top    | MV-566B | 357 | 416  | 36.8  | 81.3  | 9.21  | 34.7  | 7.82  | 0.82 | 6.31 | 0.84 |
| Cat Square | Walker Top    | RP281   | 357 | 869  | 91.7  | 183   | 24.8  | 81.7  | 14.8  | 2.26 | 11.2 | 1.71 |
| CCZO       | CCZO          | BR02    | -   | 1512 | 9.8   | 25.6  | 2.18  | 7.1   | 1     | 0.53 | 0.6  | 0.1  |
| CCZO       | CCZO          | HC02    | -   | 882  | 9.7   | 26    | 2.22  | 7.7   | 1.4   | 0.51 | 0.9  | 0.1  |

| Terrane    | Granitoid     | Sample  | Age | Dy   | Ho   | Er   | Tm   | Yb   | Lu   | Hf    | Ta   | Pb   |
|------------|---------------|---------|-----|------|------|------|------|------|------|-------|------|------|
| Cat Square | Anderson Mill | AMG     | 415 | 3.8  | 0.65 | 2.4  | 0.3  | 2.3  | 0.3  | 4     | 1    | 17   |
| Cat Square | Cherryville   | C-10    | 355 | 2.39 | 0.29 | 0.68 | 0.09 | 0.58 | 0.08 | 3.86  | 1.37 | 48.6 |
| Cat Square | Gray Court    | GC-1    | 357 | 3.07 | 0.53 | 1.47 | 0.2  | 1.27 | 0.2  | 4.83  | 0.57 | 39.5 |
| Cat Square | High Falls    | FRHF    | 372 | 2.38 | 0.4  | 1.05 | 0.14 | 0.89 | 0.13 | 4.6   | 0.88 | 32   |
| Cat Square | High Falls    | HF862   | 378 | 6.12 | 1.22 | 3.46 | 0.51 | 3.3  | 0.53 | 8.4   | 1    | 35   |
| Cat Square | High Falls    | HFSP    | 399 | 8.32 | 1.59 | 4.24 | 0.62 | 3.7  | 0.56 | 8.6   | 1.27 | 35   |
| Cat Square | High Falls    | IS370   | 378 | 6.01 | 1.14 | 3.15 | 0.47 | 3.14 | 0.52 | 7.1   | 1    | 30   |
| Cat Square | High Falls    | S123    | 383 | 9.98 | 2.91 | 11.1 | 2.32 | 17.6 | 2.59 | 5.6   | 0.53 | 51   |
| Cat Square | Toluca        | CH117   | 383 | 5.98 | 1.1  | 3    | 0.42 | 2.61 | 0.36 | 5.7   | 0.2  | 39   |
| Cat Square | Toluca        | TOL-1   | 383 | 1.74 | 0.28 | 0.73 | 0.09 | 0.61 | 0.08 | 4.19  | 0.08 | 29.3 |
| Cat Square | Toluca        | TOL-10  | 383 | 3.87 | 0.72 | 2.07 | 0.29 | 1.87 | 0.29 | 6.96  | 0.97 | 32.5 |
| Cat Square | Toluca        | TOL-11  | 383 | 1.57 | 0.19 | 0.42 | 0.06 | 0.38 | 0.05 | 12.84 | 0.36 | 25.7 |
| Cat Square | Walker Top    | B9WT    | 357 | 11   | 2.52 | 8.21 | 1.23 | 7.31 | 1.03 | 9.6   | 1    | 27   |
| Cat Square | Walker Top    | GL-1    | 357 | 4.65 | 0.82 | 2.27 | 0.32 | 1.92 | 0.27 | 6     | 0.89 | 28   |
| Cat Square | Walker Top    | GL-1B   | 357 | 4.91 | 0.9  | 2.38 | 0.33 | 2.02 | 0.28 | 5.9   | 1    | 26   |
| Cat Square | Walker Top    | GL-2    | 357 | 4.71 | 0.87 | 2.42 | 0.34 | 2.06 | 0.29 | 6.4   | 1    | 20   |
| Cat Square | Walker Top    | MV-19   | 408 | 4.74 | 0.82 | 2.11 | 0.28 | 1.62 | 0.22 | 4.4   | 0.89 | 39   |
| Cat Square | Walker Top    | MV-19B  | 357 | 5.03 | 0.93 | 2.49 | 0.34 | 2    | 0.28 | 5.1   | 0.9  | 32   |
| Cat Square | Walker Top    | MV-249  | 357 | 5.03 | 0.91 | 2.34 | 0.33 | 1.93 | 0.25 | 6     | 0.8  | 32   |
| Cat Square | Walker Top    | MV-564  | 357 | 3.89 | 0.69 | 1.84 | 0.28 | 1.76 | 0.24 | 4.2   | 0.9  | 25   |
| Cat Square | Walker Top    | MV-566  | 357 | 4.06 | 0.64 | 1.59 | 0.22 | 1.36 | 0.18 | 4.1   | 0.88 | 27   |
| Cat Square | Walker Top    | MV-566B | 357 | 3.97 | 0.65 | 1.7  | 0.25 | 1.56 | 0.21 | 4     | 1.2  | 24   |
| Cat Square | Walker Top    | RP281   | 357 | 9.06 | 1.69 | 4.76 | 0.68 | 3.99 | 0.55 | 11.1  | 0.5  | 27   |
| CCZO       | CCZO          | BR02    | -   | 0.6  | 0.1  | 0.4  | 0.07 | 0.5  | 0.08 | 3.9   | 0.2  | 27   |
| CCZO       | CCZO          | HC02    | -   | 0.7  | 0.1  | 0.4  | 0.05 | 0.3  | 0.05 | 2.5   | 0.6  | 32   |

| Terrane    | Granitoid     | Sample  | Age | Th   | U     |
|------------|---------------|---------|-----|------|-------|
| Cat Square | Anderson Mill | AMG     | 415 | 15.6 | 2.9   |
| Cat Square | Cherryville   | C-10    | 355 | 14.9 | 12.87 |
| Cat Square | Gray Court    | GC-1    | 357 | 18.6 | 5.77  |
| Cat Square | High Falls    | FRHF    | 372 | 22.5 | 1.53  |
| Cat Square | High Falls    | HF862   | 378 | 24.1 | 2.29  |
| Cat Square | High Falls    | HFSP    | 399 | 25.3 | 2.74  |
| Cat Square | High Falls    | IS370   | 378 | 20.1 | 2.53  |
| Cat Square | High Falls    | S123    | 383 | 25.2 | 3.44  |
| Cat Square | Toluca        | CH117   | 383 | 18.5 | 2.93  |
| Cat Square | Toluca        | TOL-1   | 383 | 10.6 | 0.95  |
| Cat Square | Toluca        | TOL-10  | 383 | 23.3 | 2.47  |
| Cat Square | Toluca        | TOL-11  | 383 | 47.8 | 0.85  |
| Cat Square | Walker Top    | B9WT    | 357 | 29.9 | 1.72  |
| Cat Square | Walker Top    | GL-1    | 357 | 9.31 | 1.82  |
| Cat Square | Walker Top    | GL-1B   | 357 | 15.6 | 2.21  |
| Cat Square | Walker Top    | GL-2    | 357 | 8.11 | 1.82  |
| Cat Square | Walker Top    | MV-19   | 408 | 23.6 | 2.13  |
| Cat Square | Walker Top    | MV-19B  | 357 | 21.9 | 2.41  |
| Cat Square | Walker Top    | MV-249  | 357 | 22.8 | 3.21  |
| Cat Square | Walker Top    | MV-564  | 357 | 17.4 | 4.26  |
| Cat Square | Walker Top    | MV-566  | 357 | 17.7 | 4.35  |
| Cat Square | Walker Top    | MV-566B | 357 | 18.3 | 4.61  |
| Cat Square | Walker Top    | RP281   | 357 | 30.4 | 1.06  |
| CCZO       | CCZO          | BR02    | -   | 14.5 | 1.4   |
| CCZO       | CCZO          | HC02    | -   | 16.3 | 1.8   |

APPENDIX D:  
STRUCTURAL MEASUREMENTS

| Measurement | Latitude | Longitdue | Strike | Dip | Dip Direction |
|-------------|----------|-----------|--------|-----|---------------|
| Joint       | 34.6131  | -81.6959  | 305    | 60  | E             |
| Joint       | 34.6131  | -81.6959  | 43     | 72  | E             |
| Joint       | 34.6131  | -81.6959  | 40     | 85  | E             |
| Joint       | 34.6131  | -81.6959  | 355    | 75  | E             |
| Joint       | 34.6191  | -81.6900  | 315    | 30  | E             |
| Joint       | 34.6191  | -81.6900  | 267    | 31  | W             |
| Joint       | 34.6114  | -81.6775  | 240    | 80  | W             |
| Joint       | 34.6114  | -81.6775  | 233    | 82  | W             |
| Joint       | 34.6112  | -81.6776  | 246    | 73  | W             |
| Joint       | 34.6106  | -81.6786  | 62     | 72  | E             |
| Joint       | 34.6106  | -81.6786  | 65     | 72  | E             |
| Joint       | 34.6105  | -81.6798  | 60     | 80  | E             |
| Joint       | 34.6055  | -81.6912  | 101    | 82  | W             |
| Joint       | 34.6055  | -81.6912  | 100    | 80  | W             |
| Joint       | 34.6052  | -81.6893  | 290    | 89  | E             |
| Joint       | 34.6038  | -81.6892  | 112    | 90  | -             |
| Joint       | 34.6038  | -81.6892  | 123    | 90  | -             |
| Joint       | 34.6056  | -81.6890  | 115    | 90  | -             |
| Joint       | 34.6059  | -81.6882  | 304    | 89  | E             |
| Joint       | 34.6067  | -81.6874  | 252    | 92  | W             |
| Joint       | 34.6068  | -81.6865  | 330    | 82  | E             |
| Joint       | 34.6068  | -81.6865  | 333    | 72  | E             |
| Joint       | 34.6068  | -81.6865  | 340    | 70  | E             |
| Joint       | 34.6068  | -81.6865  | 231    | 86  | W             |
| Joint       | 34.6068  | -81.6865  | 240    | 82  | W             |
| Joint       | 34.6068  | -81.6865  | 250    | 90  | -             |
| Joint       | 34.6226  | -81.6972  | 260    | 64  | W             |
| Joint       | 34.6190  | -81.7020  | 308    | 70  | E             |
| Joint       | 34.6190  | -81.7020  | 270    | 78  | S             |
| Joint       | 34.6190  | -81.7020  | 150    | 89  | W             |
| Joint       | 34.6190  | -81.7020  | 122    | 82  | W             |
| Joint       | 34.6190  | -81.7020  | 144    | 80  | W             |
| Joint       | 34.6190  | -81.7020  | 112    | 90  | -             |
| Joint       | 34.6245  | -81.6935  | 310    | 64  | E             |
| Joint       | 34.6180  | -81.6910  | 124    | 90  | -             |
| Joint       | 34.6371  | -81.7405  | 204    | 74  | W             |
| Joint       | 34.6387  | -81.7515  | 106    | 80  | W             |
| Joint       | 34.6387  | -81.7515  | 94     | 84  | W             |
| Joint       | 34.5857  | -81.7301  | 303    | 74  | E             |
| Joint       | 34.5795  | -81.7085  | 89     | 80  | E             |
| Joint       | 34.5795  | -81.7085  | 109    | 84  | W             |
| Joint       | 34.5795  | -81.7085  | 105    | 80  | W             |
| Joint       | 34.5749  | -81.7053  | 288    | 74  | E             |
| Joint       | 34.5749  | -81.7053  | 85     | 82  | E             |
| Joint       | 34.5719  | -81.6898  | 104    | 90  | -             |
| Joint       | 34.5719  | -81.6898  | 281    | 80  | E             |

| Measurement | Latitude | Longitude | Strike | Dip | Dip Direction |
|-------------|----------|-----------|--------|-----|---------------|
| Joint       | 34.5719  | -81.6898  | 197    | 77  | W             |
| Joint       | 34.6310  | -81.7060  | 54     | 90  | -             |
| Joint       | 34.6194  | -81.7280  | 100    | 88  | W             |
| Joint       | 34.6194  | -81.7280  | 190    | 82  | W             |
| Joint       | 34.6194  | -81.7280  | 67     | 90  | -             |
| Dike        | 34.6257  | -81.6839  | 240    | 89  | W             |
| Dike        | 34.6244  | -81.6827  | 190    | 40  | W             |
| Dike        | 34.6187  | -81.6765  | 280    | 38  | E             |
| Dike        | 34.6139  | -81.6754  | 310    | 59  | E             |
| Dike        | 34.6092  | -81.6867  | 70     | 76  | E             |
| Dike        | 34.6160  | -81.6947  | 210    | 70  | W             |
| Dike        | 34.6160  | -81.6947  | 140    | 82  | W             |
| Dike        | 34.5867  | -81.7295  | 260    | 74  | W             |
| Dike        | 34.5793  | -81.7302  | 320    | 82  | E             |
| Dike        | 34.5741  | -81.7208  | 166    | 82  | W             |
| Dike        | 34.6310  | -81.7060  | 236    | 74  | W             |
| Fold Arm    | 34.6131  | -81.6959  | 59     | 74  | E             |
| Fold Arm    | 34.6131  | -81.6959  | 56     | 66  | E             |
| Fold Arm    | 34.6131  | -81.6959  | 180    | 62  | W             |
| Fold Arm    | 34.6131  | -81.6959  | 195    | 70  | W             |
| Fold Arm    | 34.6160  | -81.6947  | 215    | 84  | W             |
| Fold Arm    | 34.6160  | -81.6947  | 224    | 81  | W             |
| Foliation   | 34.6100  | -81.6957  | 56     | 13  | E             |
| Foliation   | 34.6158  | -81.6900  | 12     | 19  | E             |
| Foliation   | 34.6176  | -81.6831  | 18     | 26  | E             |
| Foliation   | 34.6176  | -81.6831  | 45     | 18  | E             |
| Foliation   | 34.6191  | -81.6900  | 24     | 31  | E             |
| Foliation   | 34.6248  | -81.6838  | 160    | 61  | W             |
| Foliation   | 34.6251  | -81.6836  | 57     | 32  | E             |
| Foliation   | 34.6244  | -81.6827  | 254    | 41  | W             |
| Foliation   | 34.6244  | -81.6827  | 190    | 32  | W             |
| Foliation   | 34.6176  | -81.6791  | 356    | 40  | E             |
| Foliation   | 34.6182  | -81.6781  | 76     | 20  | E             |
| Foliation   | 34.6187  | -81.6765  | 57     | 38  | E             |
| Foliation   | 34.6187  | -81.6765  | 95     | 14  | W             |
| Foliation   | 34.6185  | -81.6762  | 130    | 20  | W             |
| Foliation   | 34.6185  | -81.6762  | 128    | 22  | W             |
| Foliation   | 34.6189  | -81.6745  | 97     | 30  | W             |
| Foliation   | 34.6139  | -81.6754  | 160    | 22  | W             |
| Foliation   | 34.6117  | -81.6770  | 190    | 18  | W             |
| Foliation   | 34.6114  | -81.6775  | 160    | 58  | W             |
| Foliation   | 34.6114  | -81.6775  | 158    | 40  | W             |
| Foliation   | 34.6114  | -81.6775  | 165    | 46  | W             |
| Foliation   | 34.6104  | -81.6813  | 166    | 28  | W             |
| Foliation   | 34.6103  | -81.6815  | 123    | 31  | W             |



| Measurement | Latitude | Longitude | Strike | Dip | Dip Direction |
|-------------|----------|-----------|--------|-----|---------------|
| Foliation   | 34.6045  | -81.6912  | 50     | 24  | E             |
| Foliation   | 34.6045  | -81.6912  | 30     | 14  | E             |
| Foliation   | 34.6055  | -81.6912  | 310    | 12  | E             |
| Foliation   | 34.6051  | -81.6897  | 50     | 22  | E             |
| Foliation   | 34.6052  | -81.6893  | 17     | 8   | E             |
| Foliation   | 34.6050  | -81.6893  | 10     | 29  | E             |
| Foliation   | 34.6056  | -81.6890  | 4      | 28  | E             |
| Foliation   | 34.6059  | -81.6882  | 30     | 29  | E             |
| Foliation   | 34.6067  | -81.6874  | 57     | 26  | E             |
| Foliation   | 34.6068  | -81.6865  | 50     | 10  | E             |
| Foliation   | 34.6068  | -81.6865  | 40     | 14  | E             |
| Foliation   | 34.6092  | -81.6867  | 50     | 8   | E             |
| Foliation   | 34.6197  | -81.7063  | 25     | 22  | E             |
| Foliation   | 34.6202  | -81.7045  | 10     | 18  | E             |
| Foliation   | 34.6202  | -81.7045  | 60     | 19  | E             |
| Foliation   | 34.6207  | -81.7023  | 30     | 24  | E             |
| Foliation   | 34.6204  | -81.7020  | 24     | 12  | E             |
| Foliation   | 34.6209  | -81.7013  | 20     | 10  | E             |
| Foliation   | 34.6190  | -81.7020  | 50     | 8   | E             |
| Foliation   | 34.6243  | -81.6936  | 207    | 38  | W             |
| Foliation   | 34.6371  | -81.7405  | 220    | 26  | W             |
| Foliation   | 34.6442  | -81.7378  | 21     | 28  | E             |
| Foliation   | 34.6382  | -81.7538  | 323    | 10  | E             |
| Foliation   | 34.6387  | -81.7515  | 99     | 115 | W             |
| Foliation   | 34.6396  | -81.7258  | 310    | 26  | E             |
| Foliation   | 34.6396  | -81.7258  | 341    | 28  | E             |
| Foliation   | 34.5820  | -81.7273  | 30     | 38  | E             |
| Foliation   | 34.5820  | -81.7273  | 21     | 28  | E             |
| Foliation   | 34.5793  | -81.7302  | 110    | 20  | W             |
| Foliation   | 34.5741  | -81.7208  | 10     | 30  | E             |
| Foliation   | 34.5784  | -81.7078  | 25     | 14  | E             |
| Foliation   | 34.5771  | -81.7066  | 27     | 18  | E             |
| Foliation   | 34.5737  | -81.7007  | 87     | 40  | E             |
| Foliation   | 34.5750  | -81.6912  | 53     | 29  | E             |
| Foliation   | 34.5750  | -81.6912  | 26     | 14  | E             |
| Foliation   | 34.6322  | -81.7207  | 18     | 32  | E             |
| Foliation   | 34.6227  | -81.7326  | 30     | 12  | E             |
| Foliation   | 34.6330  | -81.7020  | 50     | 38  | E             |
| Foliation   | 34.6330  | -81.7020  | 55     | 32  | E             |
| Foliation   | 34.6320  | -81.7050  | 53     | 29  | E             |
| Foliation   | 34.6310  | -81.7060  | 8      | 30  | E             |
| Foliation   | 34.6282  | -81.7080  | 342    | 8   | E             |
| Foliation   | 34.6270  | -81.7088  | 36     | 31  | E             |
| Foliation   | 34.6323  | -81.7206  | 24     | 48  | E             |
| Foliation   | 34.6310  | -81.7223  | 37     | 30  | E             |

| Measurement | Latitude | Longitdue | Strike | Dip | Dip Direction |
|-------------|----------|-----------|--------|-----|---------------|
| Foliation   | 34.6305  | -81.7222  | 355    | 26  | E             |
| Foliation   | 34.6310  | -81.7254  | 45     | 26  | E             |
| Foliation   | 34.6253  | -81.7260  | 21     | 28  | E             |
| Foliation   | 34.6254  | -81.7260  | 40     | 28  | E             |
| Foliation   | 34.6198  | -81.7278  | 40     | 28  | E             |
| Foliation   | 34.6194  | -81.7280  | 29     | 22  | E             |
| Foliation   | 34.6194  | -81.7280  | 44     | 52  | E             |
| Foliation   | 34.5980  | -81.6510  | 71     | 18  | E             |
| Foliation   | 34.6000  | -81.6500  | 330    | 24  | E             |
| Foliation   | 34.6020  | -81.6490  | 50     | 12  | E             |

APPENDIX E:  
FIELD GUIDE

# **Geology of the Calhoun Critical Zone Observatory: Field Guide**

By Bear Jordan

February 28, 2020

## Index

|                             |   |
|-----------------------------|---|
| Preface. . . . .            | 1 |
| Itinerary. . . . .          | 2 |
| Introduction. . . . .       | 3 |
| Geologic Map. . . . .       | 4 |
| Charlotte Terrane. . . . .  | 5 |
| Cat Square Terrane. . . . . | 6 |
| Structure. . . . .          | 7 |
| References. . . . .         | 8 |

## Preface

Thank you all for attending my field defense. Today is the result of 100s of hours of time in the field and in the offices of many professors, and I appreciate the support I have received in excess within the department. In particular, I would like to thank my committee members Dr. Paul Schroeder, Dr. Mike Roden, and Dr. Christian Klimczak for their patience and guidance.

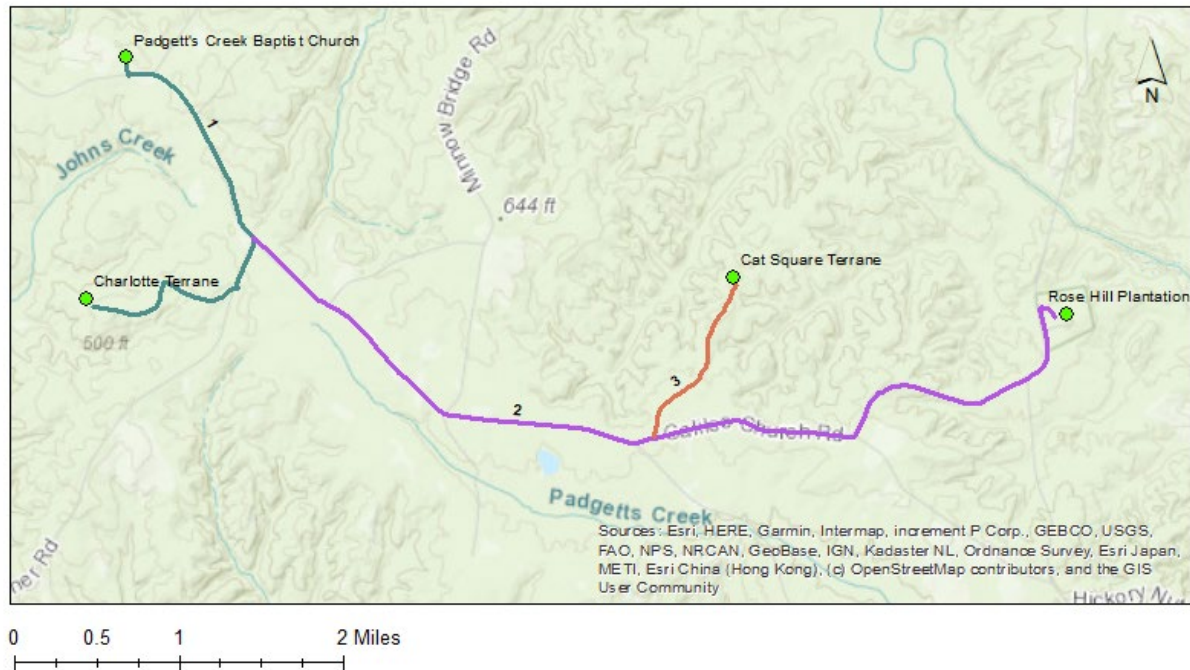
The purpose of this field trip is to explore and review field observations produced during the past two years in order to validate the geologic map I have produced. With that understanding, the explanations and observations given today will focus on ideas that are observable with boots, a hand lens, and a compass. Detailed petrographic and geochemical analysis will be reserved to present during my oral defense later this Spring. Thank you all once again, and I'm looking forward to sharing my work with you.

Sincerely,

A handwritten signature in black ink, appearing to read 'Bear Jordan', with a stylized, flowing script.

Bear Jordan

## Itinerary



### Goals

Stop 1: Examine type lithologies for the Charlotte Terrane

Stop 2: Eat lunch

Stop 3: Examine type lithologies of the Cat Square Terrane and observe structural trends

### Directions

1. Padgett's Creek to Charlotte Terrane  
Left onto Old Buncombe Rd  
First right onto Forest Service Road
2. Charlotte Terrane to Rose Hill  
Exit towards Old Buncombe Rd  
Left at fork to SR-S-44-64  
Right into Rose Hill Plantation
3. Rose Hill Plantation to Cat Square Terrane  
Exit towards Old Buncombe Rd  
Right turn on Galilee Baptist Rd

## Introduction

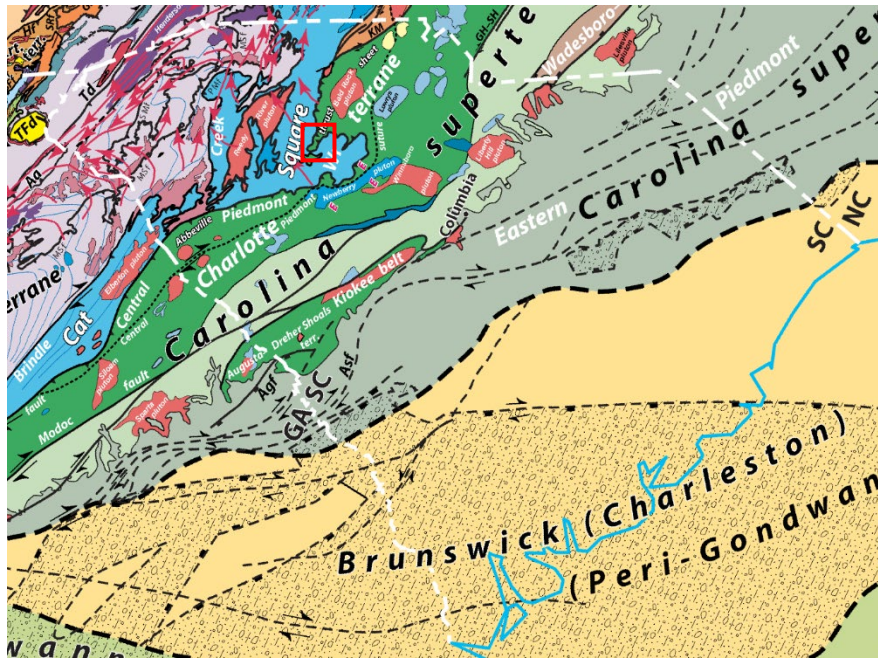


Figure 1: Regional geology of South Carolina with field site highlighted in red (adapted from Hatcher et al. 2007)

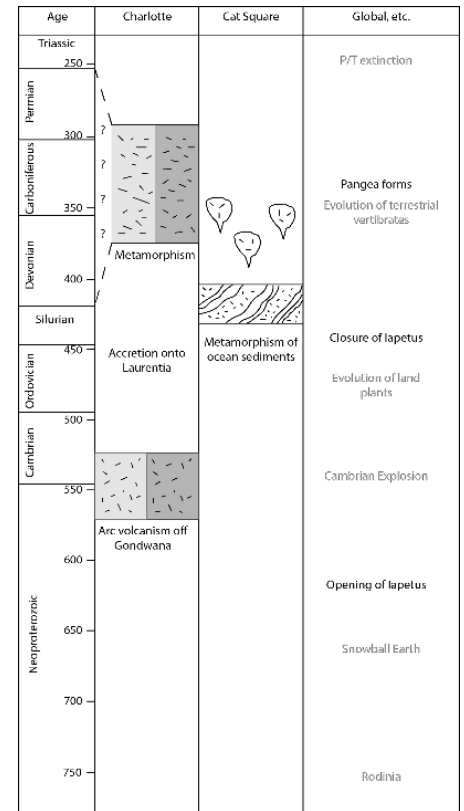


Figure 2: Correlated history of Cat Square and Charlotte Terranes (adapted from Pollock 2011)

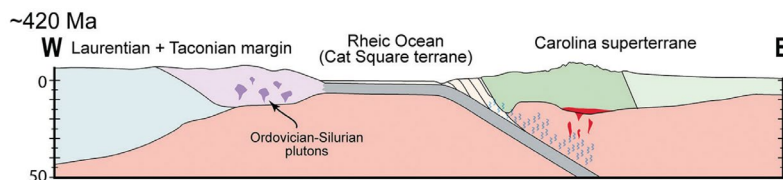
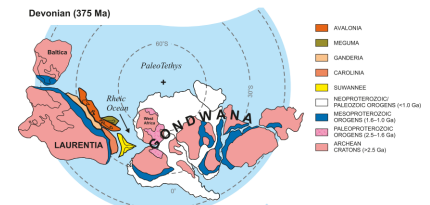
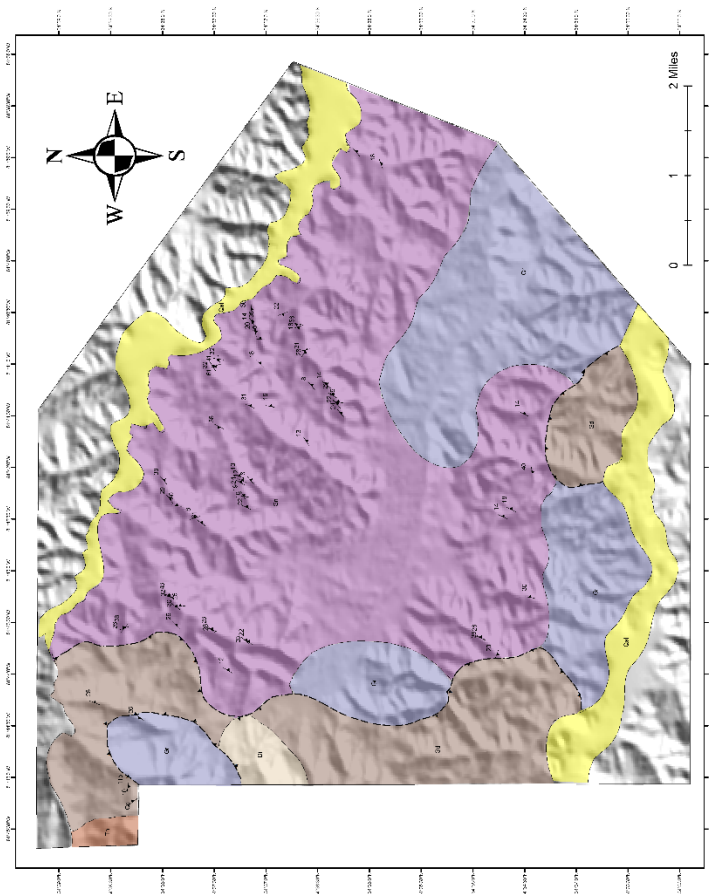
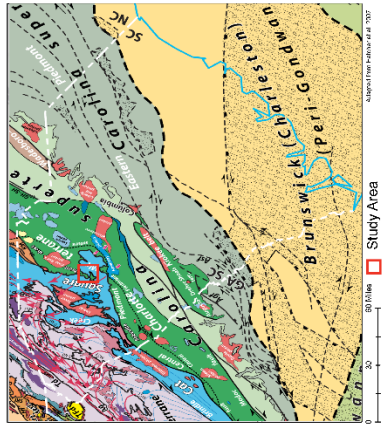
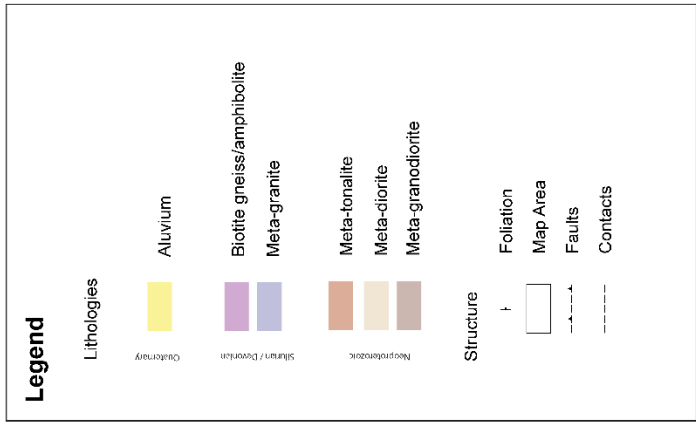


Figure 3: Tectonic setting for the formation of the Cat Square and Charlotte Terranes



The geologic history of the CCZO spans across a billion years of earth history involving the formation and break up of two super-continents. From 1.3-1.0 Ga, the Grenvillian orogeny occurred along proto-Laurentia's margin whose weathered sediments accumulated in the subsequent ocean basin formed during Neoproterozoic rifting (Thomas, 2006). As the new oceanic crust grew, it was subsequently subducted at the Gondwanan margin during the Neoproterozoic-Cambrian transition resulting in island arc volcanism forming Carolina (Pollock, 2011). These ocean basins closed in the middle Paleozoic as Gondwana and Laurentia began to converge. Gondwana thrust over Laurentia zippering from north to south with a dextral strike slip component accreting the ocean basin sediments and Carolina onto Laurentia and forming the Appalachian Mountains (Hatcher, 2010). By the end of the Mesozoic, Pangea would fully rift, developing the Atlantic Ocean and leaving behind dikes and joints. Over the past 60 Ma, extensive weathering has torn down the Appalachians to form the Piedmont and the modern setting in which we find the CCZO.

Geologic Map



Geology of the Calhoun Critical Zone Observatory

by Bear Jordan

This map was produced in conjunction with the University of Georgia and the Calhoun Critical Zone Observatory. Further information about the mapped area can be found in "Geology of the Calhoun Critical Zone Observatory" by Bear Jordan.

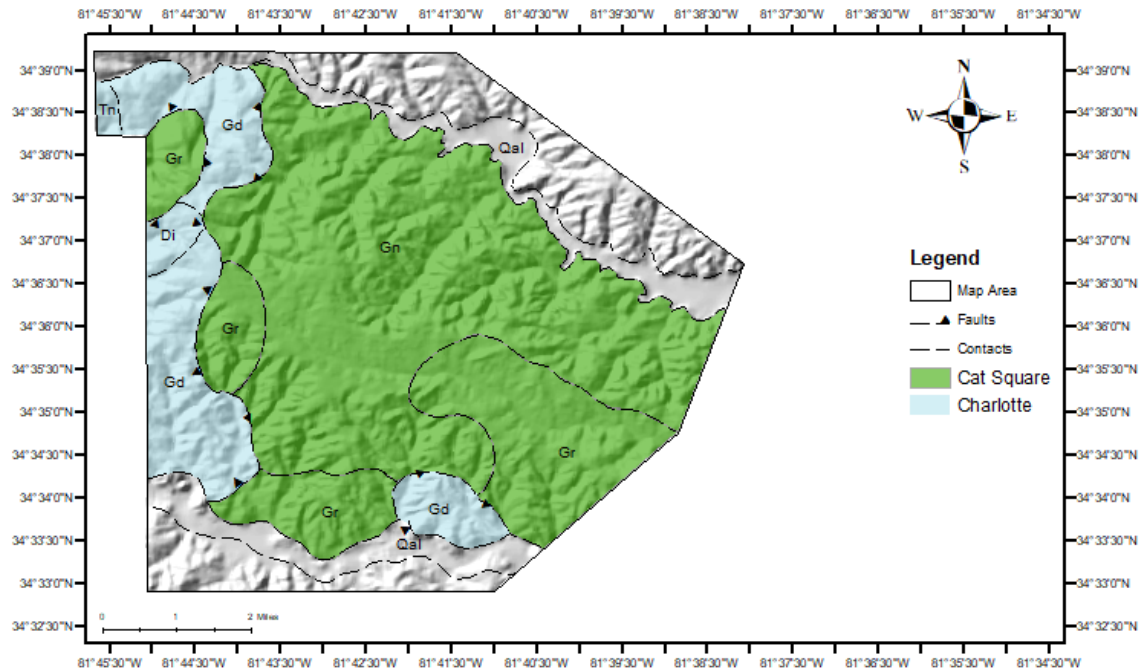
Corresponding email: [bearjordan@gmail.com](mailto:bearjordan@gmail.com)



Department of Geology  
Franklin College of Arts and Sciences  
UNIVERSITY OF GEORGIA

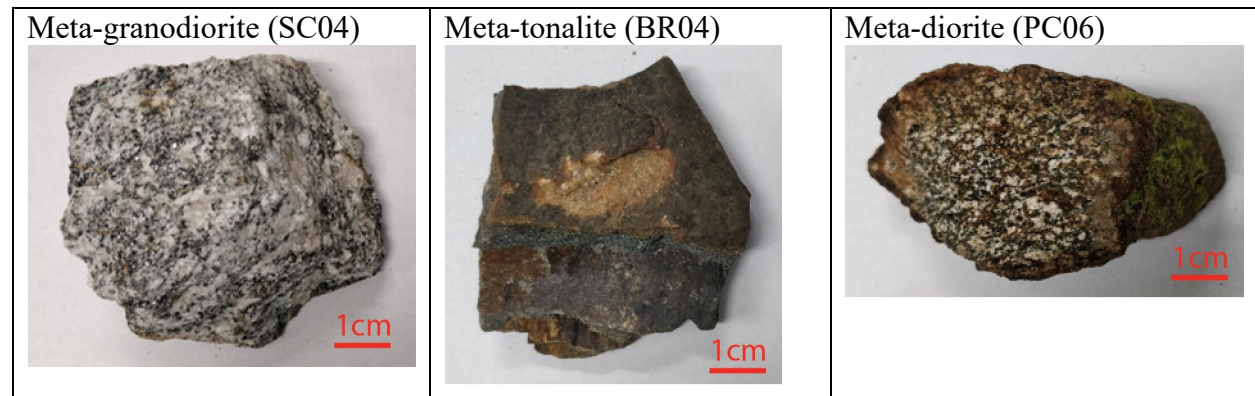


## Charlotte Terrane

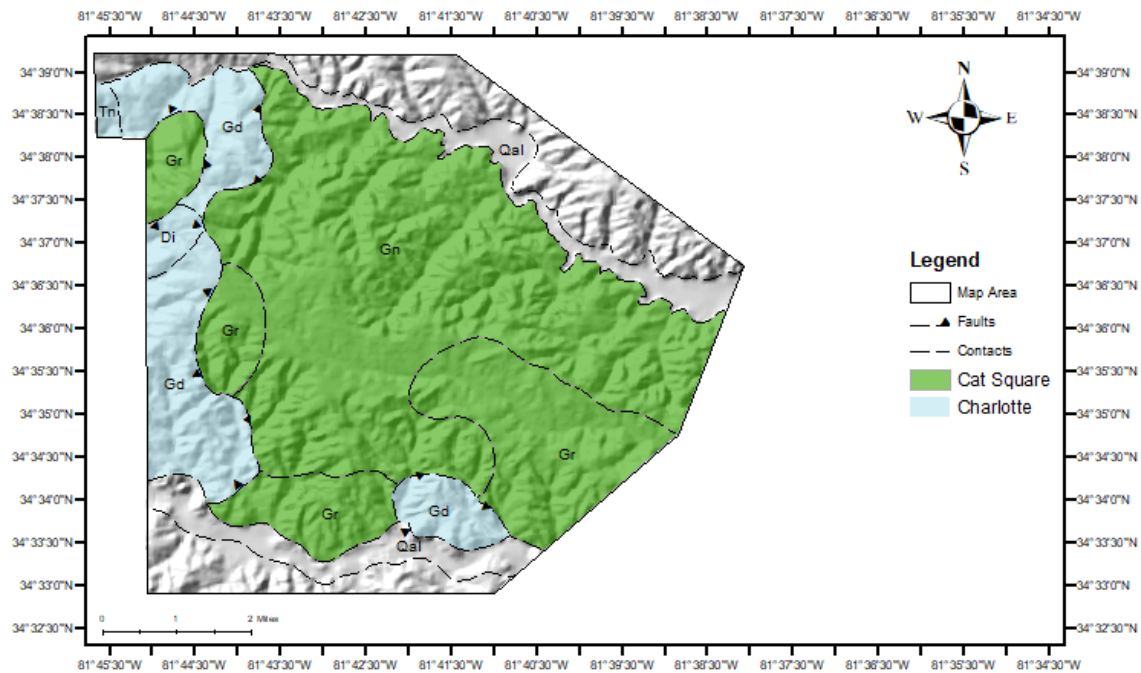


The Charlotte Terrane is observed along the western and southern boundaries of the field site. Both volcanic and plutonic rocks are present demonstrating various degrees of metamorphism presented in hand sample as incipient shape preferred orientation. Preservation is typically poor except for the meta-granodiorite units observed frequently as spheroidally weathered boulders in streambeds. The Charlotte Terrane's abundance of mafic and ultramafic rock types distinguishes it from the Cat Square Terrane.






### Hand Samples



## Cat Square Terrane



The Cat Square Terrane is mainly observed in the eastern portion of the field site with well preserved outcrops of gneiss and meta-granites in streambeds. Within the gneissic unit, rare inclusions of garnet quartzite and chlorite schists are observed. The extents of these regions are not large enough to include on the map.

|                                                                                                                    |                                                                                                                   |                                                                                                                      |
|--------------------------------------------------------------------------------------------------------------------|-------------------------------------------------------------------------------------------------------------------|----------------------------------------------------------------------------------------------------------------------|
| <p>Biotite gneiss (HB21)</p>    | <p>Meta-granite (PC04)</p>     | <p>Amphibolite lens (HB08)</p>  |
| <p>Garnet quartzite (HB02)</p>  | <p>Chlorite schist (HB23)</p>  |                                                                                                                      |



## Structure



On display at this outcrop within Holcombe's Branch is an extensive record of deformational events that preserve the CCZO's long geologic history. To reiterate, this outcrop shows scars from the Pangean supercontinental cycle consistent with regional structural trends.

Least recent

M1 – Development of foliation (pictured in alternating light and dark bands)

D1 – Folding

D2 – Jointing

Most recent

## References

- Hatcher, R. D. and A. J. Merschat (2006). "The Appalachian Inner Piedmont: An exhumed strike-parallel, tectonically forced orogenic channel." Geological Society, London, Special Publications **268**(1): 517-541.
- Hatcher, R. D., et al. (2010). "The Appalachian orogen: A brief summary." From Rodinia to Pangea: The Lithotectonic Record of the Appalachian Region: Geological Society of America Memoir **206**: 1-19.
- Pollock, J. C., et al. (2011). "A paleogeographical review of the peri-Gondwanan realm of the Appalachian orogen." Canadian Journal of Earth Sciences **49**(1): 259-288.
- Thomas, W. A. (2006). "Tectonic inheritance at a continental margin." GSA today **16**(2): 4-11.

APPENDIX F:  
SAMPLE LOCATIONS

| Latitude | Longitude | ID           |
|----------|-----------|--------------|
| 34.6098  | -81.6939  | HB01         |
| 34.6095  | -81.695   | HB02, HB02-S |
| 34.61    | -81.6957  | HB03, HB03-S |
| 34.61    | -81.6966  | HB04         |
| 34.6088  | -81.6932  | HB05         |
| 34.6113  | -81.6967  | HB06         |
| 34.6131  | -81.6959  | HB07         |
| 34.6176  | -81.692   | HB08         |
| 34.6168  | -81.6896  | HB09         |
| 34.6153  | -81.6898  | HB10         |
| 34.6233  | -81.6849  | HB11         |
| 34.6244  | -81.6827  | HB12         |
| 34.6244  | -81.6827  | HB13         |
| 34.6237  | -81.6794  | HB14         |
| 34.6187  | -81.6765  | HB15         |
| 34.6159  | -81.6726  | HB15         |
| 34.6189  | -81.6745  | HB16         |
| 34.6133  | -81.6837  | HB18         |
| 34.6198  | -81.7054  | ORT01        |
| 34.618   | -81.691   | HB21         |
| 34.6324  | -81.7426  | BR01         |
| 34.6371  | -81.7405  | BR02         |
| 34.6408  | -81.7575  | BR04         |
| 34.6395  | -81.7564  | BR05         |
| 34.6396  | -81.7565  | BR06         |
| 34.6177  | -81.749   | PC02         |
| 34.6212  | -81.7484  | PC03         |
| 34.6063  | -81.753   | PC05         |
| 34.6053  | -81.7591  | PC06         |
| 34.6097  | -81.7523  | PC07         |
| 34.5944  | -81.7509  | PC08         |
| 34.5956  | -81.7654  | PC09         |
| 34.5944  | -81.7618  | PC10         |
| 34.5951  | -81.7395  | HC01         |
| 34.5925  | -81.7388  | HC02         |
| 34.5867  | -81.7468  | HC03         |
| 34.5857  | -81.7301  | HC04         |
| 34.5866  | -81.7297  | HC05, HC06   |
| 34.5867  | -81.7295  | HC07         |
| 34.582   | -81.7273  | HC08         |
| 34.5719  | -81.7093  | RH01         |
| 34.5749  | -81.7053  | RH02         |
| 34.5737  | -81.7011  | RH03, RH04   |
| 34.5802  | -81.6964  | RH05         |

|         |          |            |
|---------|----------|------------|
| 34.5718 | -81.6898 | RH06       |
| 34.5719 | -81.6898 | RH07       |
| 34.5719 | -81.6898 | RH08       |
| 34.5762 | -81.6768 | RH09       |
| 34.57   | -81.6798 | RH10, RH11 |
| 34.6312 | -81.725  | SC01       |
| 34.6264 | -81.7286 | SC02       |
| 34.6264 | -81.7288 | SC03       |
| 34.629  | -81.7305 | SC05       |

APPENDIX G:  
ACT LABS RESULTS



**Final Report**  
**Activation Laboratories**

Report Number: A19-15874

Report Date: 28/11/2019

|                 |         |         |          |
|-----------------|---------|---------|----------|
| Analyte Symbol  | SiO2    | Al2O3   | Fe2O3(T) |
| Unit Symbol     | %       | %       | %        |
| Detection Limit | 0.01    | 0.01    | 0.01     |
| Analysis Method | FUS-ICP | FUS-ICP | FUS-ICP  |
| BR02            | 68.28   | 15.89   | 1.96     |
| HC02            | 72.67   | 14.12   | 1.66     |

|                 |         |         |         |
|-----------------|---------|---------|---------|
| Analyte Symbol  | CaO     | Na2O    | K2O     |
| Unit Symbol     | %       | %       | %       |
| Detection Limit | 0.01    | 0.01    | 0.01    |
| Analysis Method | FUS-ICP | FUS-ICP | FUS-ICP |
| BR02            | 2.24    | 4.05    | 4.59    |
| HC02            | 1.62    | 3.52    | 4.8     |

|                 |      |         |
|-----------------|------|---------|
| Analyte Symbol  | LOI  | Total   |
| Unit Symbol     | %    | %       |
| Detection Limit |      | 0.01    |
| Analysis Method | GRAV | FUS-ICP |
| BR02            | 0.36 | 98.28   |
| HC02            | 0.24 | 99.33   |

|                 |         |         |         |
|-----------------|---------|---------|---------|
| Analyte Symbol  | Sc      | Be      | V       |
| Unit Symbol     | ppm     | ppm     | ppm     |
| Detection Limit | 1       | 1       | 5       |
| Analysis Method | FUS-ICP | FUS-ICP | FUS-ICP |
| BR02            | 3       | 2       | 28      |
| HC02            | 3       | 2       | 21      |

|                 |        |        |        |
|-----------------|--------|--------|--------|
| Analyte Symbol  | Ni     | Cu     | Zn     |
| Unit Symbol     | ppm    | ppm    | ppm    |
| Detection Limit | 20     | 10     | 30     |
| Analysis Method | FUS-MS | FUS-MS | FUS-MS |
| BR02            | < 20   | 20     | 40     |
| HC02            | < 20   | 40     | 40     |

|                 |        |        |         |
|-----------------|--------|--------|---------|
| Analyte Symbol  | As     | Rb     | Sr      |
| Unit Symbol     | ppm    | ppm    | ppm     |
| Detection Limit | 5      | 2      | 2       |
| Analysis Method | FUS-MS | FUS-MS | FUS-ICP |
| BR02            | < 5    | 96     | 644     |
| HC02            | < 5    | 120    | 381     |

|                 |        |        |        |
|-----------------|--------|--------|--------|
| Analyte Symbol  | Nb     | Mo     | Ag     |
| Unit Symbol     | ppm    | ppm    | ppm    |
| Detection Limit | 1      | 2      | 0.5    |
| Analysis Method | FUS-MS | FUS-MS | FUS-MS |
| BR02            | 2      | < 2    | 0.5    |

**Final Report**  
**Activation Laboratories**

Report Number: A19-15874

Report Date: 28/11/2019

|                 |         |         |          |
|-----------------|---------|---------|----------|
| Analyte Symbol  | SiO2    | Al2O3   | Fe2O3(T) |
| Unit Symbol     | %       | %       | %        |
| Detection Limit | 0.01    | 0.01    | 0.01     |
| Analysis Method | FUS-ICP | FUS-ICP | FUS-ICP  |
| HC02            | 4       | < 2     | < 0.5    |

|                 |        |        |         |
|-----------------|--------|--------|---------|
| Analyte Symbol  | Sb     | Cs     | Ba      |
| Unit Symbol     | ppm    | ppm    | ppm     |
| Detection Limit | 0.5    | 0.5    | 2       |
| Analysis Method | FUS-MS | FUS-MS | FUS-ICP |
| BR02            | < 0.5  | 2.5    | 1512    |
| HC02            | < 0.5  | 1.3    | 882     |

|                 |        |        |        |
|-----------------|--------|--------|--------|
| Analyte Symbol  | Pr     | Nd     | Sm     |
| Unit Symbol     | ppm    | ppm    | ppm    |
| Detection Limit | 0.05   | 0.1    | 0.1    |
| Analysis Method | FUS-MS | FUS-MS | FUS-MS |
| BR02            | 2.18   | 7.1    | 1      |
| HC02            | 2.22   | 7.7    | 1.4    |

|                 |        |        |        |
|-----------------|--------|--------|--------|
| Analyte Symbol  | Tb     | Dy     | Ho     |
| Unit Symbol     | ppm    | ppm    | ppm    |
| Detection Limit | 0.1    | 0.1    | 0.1    |
| Analysis Method | FUS-MS | FUS-MS | FUS-MS |
| BR02            | 0.1    | 0.6    | 0.1    |
| HC02            | 0.1    | 0.7    | 0.1    |

|                 |        |        |        |
|-----------------|--------|--------|--------|
| Analyte Symbol  | Yb     | Lu     | Hf     |
| Unit Symbol     | ppm    | ppm    | ppm    |
| Detection Limit | 0.1    | 0.01   | 0.2    |
| Analysis Method | FUS-MS | FUS-MS | FUS-MS |
| BR02            | 0.5    | 0.08   | 3.9    |
| HC02            | 0.3    | 0.05   | 2.5    |

|                 |        |        |        |
|-----------------|--------|--------|--------|
| Analyte Symbol  | Tl     | Pb     | Bi     |
| Unit Symbol     | ppm    | ppm    | ppm    |
| Detection Limit | 0.1    | 5      | 0.4    |
| Analysis Method | FUS-MS | FUS-MS | FUS-MS |
| BR02            | 0.5    | 27     | < 0.4  |
| HC02            | 0.7    | 32     | < 0.4  |

**Final Report**  
**Activation Laboratories**

Report Number: A19-15874

Report Date: 28/11/2019

|                 |         |         |
|-----------------|---------|---------|
| Analyte Symbol  | MnO     | MgO     |
| Unit Symbol     | %       | %       |
| Detection Limit | 0.001   | 0.01    |
| Analysis Method | FUS-ICP | FUS-ICP |
| BR02            | 0.035   | 0.5     |
| HC02            | 0.028   | 0.41    |

|                 |         |         |
|-----------------|---------|---------|
| Analyte Symbol  | TiO2    | P2O5    |
| Unit Symbol     | %       | %       |
| Detection Limit | 0.001   | 0.01    |
| Analysis Method | FUS-ICP | FUS-ICP |
| BR02            | 0.298   | 0.08    |
| HC02            | 0.208   | 0.06    |

Analyte Symbol  
Unit Symbol  
Detection Limit  
Analysis Method  
BR02  
HC02

|                 |        |        |
|-----------------|--------|--------|
| Analyte Symbol  | Cr     | Co     |
| Unit Symbol     | ppm    | ppm    |
| Detection Limit | 20     | 1      |
| Analysis Method | FUS-MS | FUS-MS |
| BR02            | < 20   | 4      |
| HC02            | < 20   | 3      |

|                 |        |        |
|-----------------|--------|--------|
| Analyte Symbol  | Ga     | Ge     |
| Unit Symbol     | ppm    | ppm    |
| Detection Limit | 1      | 1      |
| Analysis Method | FUS-MS | FUS-MS |
| BR02            | 19     | < 1    |
| HC02            | 20     | 1      |

|                 |         |         |
|-----------------|---------|---------|
| Analyte Symbol  | Y       | Zr      |
| Unit Symbol     | ppm     | ppm     |
| Detection Limit | 1       | 2       |
| Analysis Method | FUS-ICP | FUS-ICP |
| BR02            | 3       | 157     |
| HC02            | 4       | 88      |

|                 |        |        |
|-----------------|--------|--------|
| Analyte Symbol  | In     | Sn     |
| Unit Symbol     | ppm    | ppm    |
| Detection Limit | 0.2    | 1      |
| Analysis Method | FUS-MS | FUS-MS |
| BR02            | < 0.2  | 1      |

**Final Report**  
**Activation Laboratories**

Report Number: A19-15874

Report Date: 28/11/2019

|                 |         |         |
|-----------------|---------|---------|
| Analyte Symbol  | MnO     | MgO     |
| Unit Symbol     | %       | %       |
| Detection Limit | 0.001   | 0.01    |
| Analysis Method | FUS-ICP | FUS-ICP |
| HC02            | < 0.2   | 1       |

|                 |        |        |
|-----------------|--------|--------|
| Analyte Symbol  | La     | Ce     |
| Unit Symbol     | ppm    | ppm    |
| Detection Limit | 0.1    | 0.1    |
| Analysis Method | FUS-MS | FUS-MS |
| BR02            | 9.8    | 25.6   |
| HC02            | 9.7    | 26     |

|                 |        |        |
|-----------------|--------|--------|
| Analyte Symbol  | Eu     | Gd     |
| Unit Symbol     | ppm    | ppm    |
| Detection Limit | 0.05   | 0.1    |
| Analysis Method | FUS-MS | FUS-MS |
| BR02            | 0.53   | 0.6    |
| HC02            | 0.51   | 0.9    |

|                 |        |        |
|-----------------|--------|--------|
| Analyte Symbol  | Er     | Tm     |
| Unit Symbol     | ppm    | ppm    |
| Detection Limit | 0.1    | 0.05   |
| Analysis Method | FUS-MS | FUS-MS |
| BR02            | 0.4    | 0.07   |
| HC02            | 0.4    | 0.05   |

|                 |        |        |
|-----------------|--------|--------|
| Analyte Symbol  | Ta     | W      |
| Unit Symbol     | ppm    | ppm    |
| Detection Limit | 0.1    | 1      |
| Analysis Method | FUS-MS | FUS-MS |
| BR02            | 0.2    | 6      |
| HC02            | 0.6    | < 1    |

|                 |        |        |
|-----------------|--------|--------|
| Analyte Symbol  | Th     | U      |
| Unit Symbol     | ppm    | ppm    |
| Detection Limit | 0.1    | 0.1    |
| Analysis Method | FUS-MS | FUS-MS |
| BR02            | 14.5   | 1.4    |
| HC02            | 16.3   | 1.8    |